TOWARDS THERAPEUTIC AUTOMATA AND HYPOXIA ACTIVATED SINGLET OXYGEN GENERATORS

A DISSERTATION SUBMITTED TO
THE GRADUATE SCHOOL OF ENGINEERING AND SCIENCE
OF BILKENT UNIVERSITY
IN PARTIAL FULFILLMENT OF THE REQUIREMENTS FOR
THE DEGREE OF
DOCTOR OF PHILOSOPHY
IN
CHEMISTRY

By
Seylan AYAN
August 2019

TOWARDS THERAPEUTIC AUTOMATA AND HYPOXIA ACTIVATED SINGLET OXYGEN GENERATORS

By Seylan AYAN
August 2019

We certify that we have read this dissertation and that in our opinion it is fully adequate, in scope and in quality, as a thesis for the degree of Doctor of Philosophy.

_____
Engin Umut AKKAYA (Advisor)

_____
Dönüş TUNCEL

_____
Salih ÖZÇUBUKÇU

_____
Sündüs ERBAŞ ÇAKMAK

_____
Safacan KÖLEMEN

Approved for the Graduate School of Engineering and Science:

_____
Ezhan KARAŞAN
Director of the Graduate School

ABSTRACT

TOWARDS THERAPEUTIC AUTOMATA AND HYPOXIA ACTIVATED SINGLET OXYGEN GENERATORS

Seylan AYAN
Ph.D. in Chemistry
Advisor: Engin Umut AKKAYA
August 2019

Photodynamic therapy (PDT) is a treatment modality depends on the efficient generation of singlet oxygen ($^1O_2$) through excitation of a particular chromophore (sensitizer) followed by an energy transfer to the dissolved oxygen in tumor tissues. Cytotoxic singlet oxygen and other secondary products (reactive oxygen species, ROS) are responsible for the apoptotic and necrotic deaths of the tumor cells. We present a molecular 1:2 demultiplexer (DEMUX) which acts as a "terminator" automaton: once powered up by photoexcitation, the agent releases singlet oxygen to kill cancer cells. Once the cancer cells start apoptosis, the agent interacts with the exposed phosphatidylserines on the external leaflet, and autonomously switches to the signaling mode, turning on a bright emission signal, and turning off singlet oxygen generation. So, the output can switch between singlet oxygen and a confirmatory fluorescence emission for apoptosis, which are mutually exclusive in this design.

The automaton that we present here, is based on logic gate considerations and a sound photophysical understanding of the system, and should be a very convincing case of molecular logic with a clear path of progress towards practicality.

In another project, we are very much interested in transforming PDT into a more manageable and broadly applicable therapeutic protocol. Our approach to achieve that is to separate photosensitization event from the delivery of singlet oxygen, which is the primary cytotoxic agent of PDT. Thus, a storage compound (endoperoxide) for singlet oxygen has to be designed, which can react with molecular oxygen under typical photosensitization conditions, and then the metastable compound has to be transferred to the tumor site which would release its cargo in response to a chemical or enzymatic cue. This approach assumes that singlet oxygen produced stoichiometrically (as opposed to catalytically through photosensitization) by the chemical transformation of the carrier molecule, would be enough to trigger apoptotic response in cancer cells.

Keywords: Photodynamic therapy, photosensitizer, singlet oxygen, hypoxia, endoperoxide

ÖZET

TERAPÖTİK OTOMATLARA GİDİŞ VE HİPOKSİ İLE AKTİVE OLAN SİNGLET OKSİJEN ÜRETİCİLERİ

Seylan AYAN
Kimya, Doktora
Tez Danışmanı: Engin Umut AKKAYA
August 2019

Fotodinamik terapi (PDT), belirli bir kromoforun (sensitizer) uyarılması ve ardından tümör dokularında çözünmüş oksijene bir enerji aktarımı yoluyla singlet oksijenin verimli bir şekilde üretilmesine ($^1O_2$) bağlıdır. Sitotoksik singlet oksijen ve diğer ikincil ürünler (reaktif oksijen türleri, ROS), tümör hücrelerinin apoptotik ve nekrotik ölümlerinden sorumludur. Bu bağlamda "terminatör" otomatiği olarak hareket eden moleküler 1: 2 demultiplexer (DEMUX) ajanı tasarlanmıştır: bir zamanlar foto eksitasyon ile çalıştırılan ajan kanser hücrelerini öldürmek için singlet oksijen üretir. Kanser hücreleri apoptoz başlattığında, ajan hücre duvarının dış kısmındaki fosfatidilserinler ile etkileşime girer ve özerk bir şekilde işaretleme moduna geçer, parlak bir emisyon sinyalini açar ve singlet oksijen üretimini kapatır. Bu nedenle, çıkış singlet oksijen ile apoptosis için onaylayıcı bir floresan emisyonu arasında geçiş yapabilir.

Burada sunduğumuz otomat, mantık kapısı düşüncelerine ve sistemin sağlam bir fotofiziksel anlayışına dayanmaktadır ve pratiklik konusunda açık bir ilerleme yolu olan çok inandırıcı bir moleküler mantık olgusu olmalıdır.

Bir diğer projede, PDT'yi daha kontrol edilebilir ve geniş çapta uygulanabilir bir terapötik protokole dönüştürmek hedeflenmiştir. Bunu başarma yaklaşımımız, fotosensitizasyon olayını PDT'nin primer sitotoksik ajanı olan singlet oksijen dağıtımından ayırmaktır. Bu nedenle, tekli oksijen için tipik bir ışığa duyarlılaştırma koşulları altında moleküler oksijen ile reaksiyona girebilen bir depolama bileşiği (endoperoksit) tasarlanmak zorundadır ve daha sonra bu yarı kararlı bileşik, kimyasal veya enzimatik bir ipucuna karşılık olarak yükünü serbest bırakacak olan tümör bölgesine aktarılmalıdır. Bu yaklaşımın, taşıyıcı molekülün kimyasal transformasyonu ile stokiyometrik olarak (katalitik olan fotoduyarlaştırmanın aksine) üretilen singlet oksijenin, kanser hücrelerinde apoptotik yanıtı tetiklemek için yeterli olacağını amaçlıyoruz.

Anahtar sözcükler: Fotodinamik terapi, aktifleşebilir fotoduyarlaştırıcı, singlet oksijen, hipoksi, endoperoksit

Acknowledgement

I would like to express my sincere thanks to my PhD supervisor Prof. Engin U. Akkaya, whom I will definitely miss after finishing my studies at Bilkent University. He is the genius, confidential, foreseeing, enthusiastic, kind, problem-solving and the funniest person that I have ever met. I feel proud and lucky for being a member of his research group. In the most troubled and desperate moments of my PhD period, he always gives us scientific supports and morals that brings us hard-to-achieve success. I appreciate all his contributions, discussions and valuable thoughts to make my PhD experience productive and sensational. I will never forget him and his support throughout my life.

I am sincerely grateful to my PhD thesis committee members, Assoc. Prof. Dönüş Tuncel, Asst. Prof. Dr. Salih Özçubukçu, Asst. Prof. Dr. Sündüs Erbaş Çakmak and Asst. Prof. Dr. Safacan Kölemen for their valuable advices and fruitful discussions.

I owe a special thank to Asst. Prof. Dr. Gürcan Günaydın for his endless help and support, guidance to improve my skills in the field of biochemistry as well as his unlimited knowledge and experience that I have benefited from greatly. I would also like to express my graduate for him for his companionship.

I would like to express my special thanks to Merve Camcı, Pınar Aydoğan Göktürk, Ahmet Koç and Mustafa Emre Gedik for their friendship in my PhD studies. Their support patience and contributions are so valuable and unforgettable.

I want to thank our present and past group members Dr. Özlem Seven, Dr. İlke Şimşek Turan, Dr. Nisa Yeşilgül, Esma Uçar, Simay Aydonat, Ceren Çamur, Darika Okeava, Cansu Kaya, Özge Yılmaz, Deniz Yıldız, Abdurrahman Türksoy, Dr. Safacan Kölemen, Dr. Fazlı Sözmen, Dr. Murat Işık, Dr. Serdal Kaya, Bilge Banu Yağcı and rest of the SCL (Supramolecular Chemistry Laboratory) members for great friendships, wonderful collaborations, and perfect ambiance in the laboratory. They are very precious for me. It was wonderful to work with them.

Special thanks are extending to my beloved mother Gülcan Ayan and father Abidin Ayan, Alper Ayan, Nilgün Günaydın, Şahin Günaydın for their infinite support, huge love and understanding. It is really reassuring to known that there are always some people waiting there for you.

CONTENTS

CHAPTER 1 1

1. INTRODUCTION 1

1.1. INTRODUCTION TO SINGLET OXYGEN 1

1.2 ELECTRONIC CONFIGURATION OF THE OXYGEN MOLECULE 1

1.3 THE FORMATION OF SINGLET OXYGEN 4

1.3.1 Photosensitization Method 4

1.3.2 Chemical Methods 7

1.3.2.1 Hydrogen peroxide - hypochlorite reaction 7

1.3.2.2 Phosphite - Ozone mixture decomposition 8

1.3.2.3 Dissociation of Aromatic Endoperoxides 8

1.4 ENDOPEROXIDE AS A SOURCE OF SINGLET OXYGEN TO BE CARRIED TO TUMOUR TISSUES 13

1.5 THE MECHANISMS OF INDUCTION OF APOPTOSIS BY SINGLET OXYGEN 19

1.6 DRUG AND PRODRUG STRATEGIES FOR TUMOUR HYPOXIA 21

CHAPTER 2 25

HYPOXIA TRIGGERED INTRACELLULAR SINGLET OXYGEN RELEASE: FOUNDATIONS OF A NEW THERAPEUTIC PARADIGM 25

2.1 OBJECTIVES 26

2.2 INTRODUCTION 26

2.3 DESIGN OF THE PNZ-PROTECTED 2-PYRIDONE-ENDOPEROXIDE 29

2.4 RESULTS AND DISCUSSION 32

2.5 EXPERIMENTAL DETAILS 43

2.5.1 General Experimental Procedures 43

2.5.2 Synthesis 43

2.5.3 Hypoxia Treatment 46

2.5.4 MTT Assay 46

2.5.6 Real-time and Label-free Analyses of Cells with the iCELLigence System 50

2.5.7 Flow Cytometry 55

2.6 CONCLUSION 60

CHAPTER 3 61

3. INTRODUCTION 61

3.1 Introduction to the Fluorescence 61

3.2 Factors Affecting Fluorecence 63

3.3 Fluorescence Probes and their Design Strategies 66

3.3.1 Photoinduced Electron Transfer (PET) 71

3.4 Photodynamic Therapy 75

3.5 Photosensitizer 78

3.6 LOGIC GATE 80

3.6.1 Boolean Algebra 80

3.6.2 Molecular Logic Gates 82

3.7 Chemical Logic Gates in Biological media 84

3.8 What is a Demultiplexer (DEMUX) ? 88

3.9 Flow Cytometry and Detection of Apoptosis via Annexin V 90

CHAPTER 4 95

MOLECULAR DEMULTIPLEXER AS A TERMINATOR AUTOMATON 95

4.1 Objectives 96

4.2 Introduction 96

4.3 Design of the Molecular Demultiplexer 101

4.4 Results and Discussion 102

4.5 Experimental Details 120

4.5.1 General Experimental Procedures 120

4.5.2 Synthetic Procedures 122

4.5.3 Cell Culture and MTT Assay 129

4.5.4 Flow Cytometry 131

4.5.5 Confocal Laser Scanning Microscopy 132

4.6 Conclusion 132

REFERENCES 134

APPENDİX A 146

APPENDİX B 155

LIST OF FIGURES

FIGURE 1. MOLECULAR ORBITAL DIAGRAM OF ATOMIC AND MOLECULAR OXYGEN.....2

FIGURE 2. ELECTRONIC CONFIGURATION OF SINGLET AND TRIPLET OXYGEN AND SOME PROPERTIES OF THEM...3

FIGURE 3. SOME EXAMPLES PHOTOSENSITIZERS 4

FIGURE 4. SCHEMATIC REPRESENTATION OF SINGLET OXYGEN GENERATION BY PHOTOSENSITIZER 5

FIGURE 5. THE ELECTRON TRANSFER MECHANISM BETWEEN TRIPLET PHOTOSENSITIZER AND TRIPLET OXYGEN ..7

FIGURE 6. THE SINGLET OXYGEN GENERATION BY RUBREN ENDOPEROXIDE 8

FIGURE 7. THE SINGLET OXYGEN GENERATION BY 9,10-DIPHENYLANTHRACENE ENDOPEROXIDE 9

FIGURE 8. ALTERNATIVE DECOMPOSITION ROUTES FOR ENDOPEROXIDES (EPOS). 10

FIGURE 9.THERMOLYSIS OF ENDOPEROXIDE TO 9,10-DIPHENYLANTHRACENE. COPYRIGHT © 1981, AMERICAN CHEMICAL SOCIETY. REPRINTED WITH PERMISSION FROM REF [27]. 12

FIGURE 10.SINGLET OXYGEN GENERATION IN FRACTIONAL PDT. 17

FIGURE 11. STRUCTURE OF THE GOLD NANOROD-ENDOPEROXIDE. (AU-EPO) . COPYRIGHT © 2016 WILEY-VCH VERLAG GMBH & CO. KGAA, WEINHEIM. REPRINTED WITH PERMISSION FROM REF[34]. 18

FIGURE 12. OPERATION PRINCIPLE OF THE PRODRUG TH-302. REDUCTIVE ELIMINATION DUE TO HYPOXIC CONDITIONS LEAD TO THE GENERATION OF A CYTOTOXIC AGENT. TH-302 IS IN PHASE I/II FOR CLINICAL DEVELOPMENT. LOWER FIGURES WERE ADAPTED FROM[57]. COPYRİGHT © 2012, AMERİCAN ASSOCİATİON FOR CANCER RESEARCH. 23

FIGURE 13. TWO-STAGE, MODIFIED PDT CONCEPT, WHICH DOES NOT REQUIRE EITHER O2 OR LIGHT FOR IN SITU GENERATION OF SINGLET OXYGEN. PHOTOSENSITIZATION IS CARRIED OUT EX SITU, SO THE PROPERTIES OF THE PHOTOSENSITIZER, OR THE WAVELENGTH OF EXCITATION IS NOT RELEVANT, AS LONG AS THE ENDOPEROXIDE CAN BE OBTAINED. 28

FIGURE 14. PNZ-PROTECTED 2-PYRIDONE-ENDOPEROXIDE (1) CYCLOREVERTS TO THE PARENT COMPOUND 3 WITH HALF-LIFE OF 7.1 HOURS AT 37 ^{O}C. IN CELL CULTURES UNDER HYPOXIC CONDITIONS, PNZ GROUP IS REDUCTIVELY ELIMINATED. RESULTING PYRIDONE ENDOPEROXIDE 2, DECOMPOSES MORE THAN 5-FOLD FASTER TO RELEASE SINGLET OXYGEN. 31

FIGURE 15. EVOLUTION OF THE NMR SPECTRA OF ENDOPEROXIDE **1** WITH TIME AT 37 ^{O}C IN $CDCL_3$ AS THE SOLVENT. (SPECTRA 0 HOURS (ENDOPEROXİDE **1**), SPECTRA AFTER 3 HOURS, SPECTRA AFTER 5 HOURS, THE BOTTOM SPECTRA SHOWS COMPOUND 3). 33

FIGURE 16. DECAY OF ENDOPEROXIDE **1** OVER TIME AT 37^{O}C. THE VALUES OBTAINED FROM ^{1}H NMR IN $CDCL_3$. THE HALF-LIFE IS CALCULATED AS 7.1 H ACCORDING TO THE EQUATION 1. 34

FIGURE 17. EVOLUTION OF THE NMR SPECTRA OF ENDOPEROXIDE **1** WITH TIME AT 25 ^{O}C IN $CDCL_3$ AS THE SOLVENT. (SPECTRA 0 HOURS (ENDOPEROXİDE **1**) 35

FIGURE 18. DECAY OF ENDOPEROXIDE **1** OVER TIME AT 25^{O}C. THE VALUES OBTAINED FROM ^{1}H NMR IN $CDCL_3$. THE HALF-LIFE IS CALCULATED AS 40.7 H ACCORDING TO THE EQUATION 1. 36

FIGURE 19. DECAY OF ENDOPEROXIDE **2** OVER TIME AT 37^{O}C. THE VALUES OBTAINED FROM ^{1}H NMR IN $CDCL_3$. THE HALF-LIFE IS CALCULATED AS 1.3 H ACCORDING TO THE EQUATION 1. 36

FIGURE 20. CELL VIABILITIES OF MCF7 BREAST CANCER CELLS WERE EVALUATED WITH MTT ASSAY AFTER 24 HOURS OF TREATMENT WITH VARYING CONCENTRATIONS OF THE ENDOPEROXIDE 1 UNDER EITHER NORMOXIC OR HYPOXIC CONDITIONS; AND NORMALIZED CELL NUMBERS ARE SHOWN (MEAN ± SEM, N = 3). 38

FIGURE 21. CELL VIABILITIES OF MCF7 BREAST CANCER CELLS WERE EVALUATED WITH MTT ASSAY AFTER 24 HOURS OF TREATMENT WITH VARYING CONCENTRATIONS OF CONTROL COMPOUND 3 UNDER EITHER NORMOXIC OR HYPOXIC CONDITIONS; AND NORMALIZED CELL NUMBERS ARE SHOWN. 39

FIGURE 22. CELLULAR IMPEDANCE ANALYSIS BASED CELL VIABILITY ASSESSMENT OF MCF7 CELLS, AS A FUNCTION OF TIME.....40

FIGURE 23. THE PERCENTAGE OF FITC-ANNEXIN V STAINED CELLS ANALYZED WITH FLOW CYTOMETRY WAS HIGHER IN THE CELLS TREATED WITH 25 μM ENDOPEROXIDE **1** UNDER HYPOXIC CONDITIONS COMPARED WITH THE CELLS INCUBATED UNDER NORMOXIC CONDITIONS. 42

FIGURE 24. ENDOPEROXIDE **1** ACHIEVES POTENT CYTOTOXICITY ON CANCER CELLS UNDER CONDITIONS OF HYPOXIA.....48

CELL VIABILITIES OF MCF7 BREAST CANCER CELLS WERE EVALUATED WITH MTT ASSAY AFTER 24 HOURS OF TREATMENT WITH VARYING CONCENTRATIONS OF ENDOPEROXIDE **1** UNDER EITHER NORMOXIC (IC50: 185 μM) OR HYPOXIC (IC50:120 μM) CONDITIONS; AND NORMALIZED CELL NUMBERS ARE SHOWN (MEAN ± SEM, N = 3). 48

FIGURE 25. ENDOPEROXIDE **1** ACHIEVES POTENT CYTOTOXICITY ON CANCER CELLS UNDER CONDITIONS OF HYPOXIA.....49

CELL VIABILITIES OF K562 HUMAN CHRONIC MYELOGENOUS LEUKEMIA CELLS WERE EVALUATED WITH MTT ASSAY AFTER 24 HOURS OF TREATMENT WITH VARYING CONCENTRATIONS OF ENDOPEROXIDE **1** UNDER EITHER NORMOXIC (IC50: 40 μM) OR HYPOXIC (IC50: 28 μM) CONDITIONS; AND NORMALIZED CELL NUMBERS ARE SHOWN (MEAN ± SEM, N = 3). RED LINE CORRESPONDS TO NORMALIZED CELL NUMBER OF K562 CELLS UNDER HYPOXIC CONDITIONS. BLACK LINE CORRESPONDS TO CELLS KEPT UNDER IDENTICAL CONDITIONS OF INCUBATION WITH THE AGENT, BUT UNDER NORMOXIC CONDITIONS. POSITIVE CONTROL

corresponds to cells incubated in DMSO-growth medium mixture (50/50, v/v), negative control corresponds to cells incubated in complete growth medium, without endoperoxide 1 treatment. 50

Figure 26. The temporal profile of the effects of endoperoxide **1** on cancer cells under normoxic conditions. MCF7 cells were seeded in ACEA E-Plates. After 48 h of incubation under normoxic conditions, the cells were treated with varying concentrations of endoperoxide **1**. 51

Figure 27. The temporal profile of the effects of endoperoxide **1** on cancer cells demonstrated potent cytotoxicity under hypoxic conditions, underlining the acute efficiency in hypoxia. MCF7 cells were seeded in ACEA E-Plates. After a day of incubation under normoxic conditions, hypoxic group of the cells were incubated 24 h further under conditions of hypoxia (pre-hypoxia [without drug treatment]).....52

Figure 28. The temporal profile of the effects of endoperoxide **1** on cancer cells demonstrated potent cytotoxicity under hypoxic conditions. HeLa cells were seeded in ACEA E-Plates. After a day of incubation under normoxic conditions, both groups of the cells were treated with varying concentrations of endoperoxide **1**. 54

Figure 29. Endoperoxide **1** potently induces apoptosis in cancer cells under conditions of hypoxia.....56

The percentage of FITC-Annexin V stained cells analyzed with flow cytometry was 25.3 % in the cells treated with 25 μM endoperoxide **1** under hypoxic conditions. Red shaded area represents the cells incubated under hypoxic conditions in the histogram. 56

Figure 30. The effect of endoperoxide **1** on apoptosis in cancer cells under conditions of normoxia. 56

The percentage of FITC-Annexin V stained cells analyzed with flow cytometry was 16.0 % in the cells treated with 25 μM endoperoxide **1** under normoxic conditions. Blue shaded area represents the cells incubated under normoxic conditions in the histogram. 57

Figure 31. Endoperoxide **1** potently induces apoptosis in cancer cells under conditions of hypoxia.....57

The percentage of FITC-Annexin V stained cells analyzed with flow cytometry was higher in the cells treated with 12.5 μM endoperoxide **1** under hypoxic conditions compared with the ones incubated under normoxic conditions (18.3% vs. 6.75% at 12.5 μM). Blue shaded area

REPRESENTS THE CELLS INCUBATED UNDER NORMOXIC CONDITIONS, RED SHADED AREA REPRESENTS THE CELLS INCUBATED UNDER HYPOXIC CONDITIONS) IN THE OVERLAY GRAPH. 57

FIGURE 32. ENDOPEROXIDE 1 POTENTLY INDUCES APOPTOSIS IN CANCER CELLS UNDER CONDITIONS OF HYPOXIA. THE PERCENTAGE OF FITC-ANNEXIN V STAINED CELLS ANALYZED WITH FLOW CYTOMETRY WAS 18.3 % IN THE CELLS TREATED WITH 12.5 μM ENDOPEROXIDE **1** UNDER HYPOXIC CONDITIONS. RED SHADED AREA REPRESENTS THE CELLS INCUBATED UNDER HYPOXIC CONDITIONS IN THE HISTOGRAM. 58

FIGURE 33. THE EFFECT OF ENDOPEROXIDE 1 ON APOPTOSIS IN CANCER CELLS UNDER CONDITIONS OF NORMOXIA. THE PERCENTAGE OF FITC-ANNEXIN V STAINED CELLS ANALYZED WITH FLOW CYTOMETRY WAS 6.75 % IN THE CELLS TREATED WITH 12.5 μM ENDOPEROXIDE **1** UNDER NORMOXIC CONDITIONS. BLUE SHADED AREA REPRESENTS THE CELLS INCUBATED UNDER NORMOXIC CONDITIONS IN THE HISTOGRAM. 58

FIGURE 34. ANALYSIS OF K562 CELL VIABILITY BY TRYPAN BLUE STAIN DEMONSTRATED THAT ENDOPEROXIDE **1** ACHIEVES POTENT CYTOTOXICITY ON CANCER CELLS UNDER CONDITIONS OF HYPOXIA. 59

FIGURE 35. THE DIFFERENCE OBSERVED IN QUANTUM YIELDS FOR FLUORENE AND BIPHENYL COMPOUNDS 64

FIGURE 36. THE RESONANCE FORMS OF ANILINE AND ANILINIUM, RESPECTIVELY. 64

FIGURE 37. MOLECULAR STRUCTURES OF SOME COMMON FLUORESCENCE PROBES 67

FIGURE 38. SOME EXAMPLES OF PH SENSITIVE FLUOREGENIC PROBES 69

FIGURE 39. CARBON-CARBON BOND FORMATION OF FLUOREGENIC PROBE 70

FIGURE 40. FLUOROGENIC PROBE WORK ON COMPLEXATION WITH METAL IONS 71

FIGURE 41. SIMPLE MOLECULAR ORBITAL DIAGRAM OF PET MECHANISM 73

FIGURE 42. EXAMPLE COMPOUND FOR PET BASED CHEMOSENSOR. 73

FIGURE 43. SIMPLE MOLECULAR ORBITAL DIAGRAM OF REVERSE PET MECHANISM 74

FIGURE 44. AN EXAMPLE MOLECULAR SENSOR FOR REVERSE PET 75

FIGURE 45. SINGLET OXYGEN GENERATION BY SENSITIZATION. RELEVANT PROCESSES ARE IDENTIFIED BY NUMBERS: 1-ABSORPTION, 2-EMISSION, 3-NON-RADIATIVE TRANSITION, 4- INTERSYSTEM CROSSING, 5-PHOSPHORESCENCE, 6-ENERGY TRANSFER. 77

FIGURE 46. THE COMMON PSS USE IN PDT 79

FIGURE 47. COMMON LOGIC GATES SCHEMATIC DRAWINGS AND TRUTH TABLES 81

FIGURE 48. LITERATURE EXAMPLE OF AND LOGIC GATE BY DE SILVA ET AL. 82

FIGURE 49. AND LOGIC GATE BY DE SILVA ET AL. 83

FIGURE 50. THE CONCATENATION OF TWO LOGIC GATE BY AKKAYA ET AL. 84

FIGURE 51. AND LOGIC GATE FOR SMART DRUG DESIGN BY AKKAYA ET AL. 86

FIGURE 52. AND LOGIC GATE FOR SMART DRUG DESIGN BY AKKAYA ET AL. 87

FIGURE 54. DEMULTIPLEXER BLOCK DIAGRAM 88

FIGURE 55. TYPICAL APPLICATION OF A DEMUX 89

FIGURE 56. MODULAR ASSEMBLY OF THE MOLECULAR DEMUX DEVİCE WİTH TWO DİFFERENT OUTPUTS DEPENDİNG ON THE ACİDİTY OF THE MEDİUM. 90

FIGURE 57. TWO DIFFERENT REPRESENTATIONS AND THE TRUTH TABLE FOR THE 1:2 DEMUX COMBINATORIAL CIRCUIT; AND THE STRUCTURES OF THE PARENT BODIPY COMPOUND AS WELL AS ITS DERIVATIVES. 98

FIGURE 58. THE STRUCTURES OF THE ZINC(II) COMPLEXES OF THE TERPYRIDYL-FUNCTIONALIZED BODIPY COMPOUNDS T-1 AND T-2, AND THE MODIFIED JABLONSKI DIAGRAM DEPICTING PHOTOPHYSICAL PROCESSES INVOLVED LEADING TO DEMUX ACTION. 100

FIGURE 59. **T-1** INDUCES APOPTOSIS, THEN SWITCHES TO DIAGNOSTIC MODE AND FLUORESCENTLY TAGS APOPTOTIC CELLS. BLUE POLAR HEADS REPRESENT PHOSPHATIDYLCHOLINE AND SPHINGOMYELINS, WHEREAS YELLOW, PINK AND PURPLE HEADS REPRESENT PHOSPHATIDYLSERINE, PHOSPHATIDYLINOSITOL AND OTHER NEGATIVELY CHARGED LIPIDS. APOPTOSIS IS ACCOMPANIED BY A LOSS OF MEMBRANE ASYMMETRY 102

FIGURE 60. FLUORESCENCE EMISSION SPECTRA OF BODIPY **T-2** (2 μM) UPON INCREASED **ZN** CONCENTRATIONS (0-20 EQUIV.) IN CH3CN (ΛEX= 475 NM AT 25 ^{o}C). 103

FIGURE 61. FLUORESCENCE EMISSION SPECTRA OF BODIPY **T-2** (2 μM)- ***ZN*** (5 EQUIV.) CONJUGATE UPON INCREASING CONCENTRATIONS OF ***P*** (0 -30 EQUIV.) IN CH_3CN (Λ_{EX}= 475 NM AT 25 ^{o}C). 103

FIGURE 62. NORMALIZED FLUORESCENCE EMISSION SPECTRA OF (**T-2**), (**T-2-ZN**), (**T-2-ZN-P**) IN CH_3CN WHEREIN CONCENTRATIONS ARE 2μM FOR **T-2**, 10 μM FOR ***ZN*** AND 30 μM FOR ***P***. 104

FIGURE 63. NORMALIZED ELECTRONIC ABSORPTION SPECTRA OF T, (**T-2 -*ZN***), (**T-2 -*ZN-P***) IN CH_3CN WHEREIN CONCENTRATIONS ARE 2μM FOR **T-2**, 10 μM FOR ***ZN*** AND 30 μM FOR ***P***. 105

FIGURE 64. ELECTRONIC ABSORPTION SPECTRA OF BODIPY **T-2** (2μM) UPON INCREASED ZN CONCENTRATIONS (0-10EQUIV.) IN CH_3CN. 105

FIGURE 65. ELECTRONIC ABSORPTION SPECTRA OF BODIPY **T-2** (2μM) –**ZN** (5EQUIV.) CONJUGATE UPON INCREASED CONCENTRATIONS OF **P** (0-30EQUIV.) IN CH3CN. 106

FIGURE 66. FLUORESCENCE EMISSION SPECTRA OF BODIPY **T-1** (1 μM) UPON INCREASED ***ZN*** CONCENTRATIONS (0-2 EQUIV.) IN CH_3CN (Λ_{EX}= 480 NM AT 25 ^{o}C). 107

FIGURE 67. FLUORESCENCE EMISSION SPECTRA OF BODIPY **T-1** (1 μM)- ***ZN*** (2 EQUIV.) CONJUGATE UPON INCREASING CONCENTRATIONS OF ***P*** (0 -7 EQUIV.) IN CH_3CN (Λ_{EX}= 480 NM AT 25 ^{o}C) 107

FIGURE 68. NORMALIZED FLUORESCENCE EMISSION SPECTRA OF (**T-1**), (**T-1-ZN**), (**T-1-ZN-P**) IN CH_3CN WHEREIN CONCENTRATIONS ARE 1 μM FOR **T-1**, 2 μM FOR ***ZN*** AND 7 μM FOR ***P***. 108

FIGURE 69. NORMALIZED ELECTRONIC ABSORPTION SPECTRA OF (**T-1**), (**T-1 -ZN**), (**T-1 -ZN-P**) IN CH_3CN WHEREIN CONCENTRATIONS ARE 1 μM FOR **T-1**, 2 μM FOR ***ZN*** AND 7 μM FOR ***P***. 109

FIGURE 70. ELECTRONIC ABSORPTION SPECTRA OF BODIPY **T-1** (1 μM) UPON INCREASED ***ZN*** CONCENTRATIONS (0-2 EQUIV.) IN CH_3CN. 109

FIGURE 71. ELECTRONIC ABSORPTION SPECTRA OF BODIPY **T-2** (1 μM) –***ZN*** (2 EQUIV.) CONJUGATE UPON INCREASED CONCENTRATIONS OF ***P*** (0 -7 EQUIV.) IN CH_3CN. 110

FIGURE 72.REACTION OF SINGLET OXYGEN WITH 1,3-DIPHENYLISOBENZOFURAN. 110

FIGURE 73. THE DECREASE IN THE ABSORBANCE AT 411 NM, IN AN OXYGEN SATURATED ETHANOL SOLUTION OF SELECTIVE SINGLET OXYGEN TRAP DPBF (50 μM) IN THE PRESENCE OF 2.0 μM **T-2** AND UNDER IRRADIATION WITH 522 NM GREEN LED LIGHT SOURCE (SOLID BLUE SQUARES). THE SINGLET OXYGEN QUANTUM YIELD (Φ_Δ) OF **T-2** IS 0.11. THE ADDITION OF PHOSPHATE (RED OPEN CIRCLES) DESTABILIZES THE CTS STATE, BLOCKING ACCESS TO THE TRIPLET MANIFOLD. THE ABSORBANCE DATA PRESENTED IS THE NET ABSORBANCE VALUES OBTAINED BY SUBTRACTING ANY BACKGROUND DECREASE IN THE PROBE ABSORBANCE DUE TO LIGHT ALONE. 112

FIGURE 74. (A) THE TRUTH TABLE WITH THE DATA AND SWITCH INPUTS, AND THE CORRESPONDING OUTPUTS CLEARLY IDENTIFIED, AND THE PARTICULAR SET OF CONDITIONS VALID UNDER THE LIGHT IRRADIATION CONDITIONS ON POWER-UP WERE HIGHLIGHTED. **(B)** SWITCH INPUT (NO ADDED PHOSPHATE IN THE MODEL SYSTEM OR LACK OF PHOSPHATIDYLSERINE(PS) IN THE EXTERNAL LEAFLET OF THE CELL MEMBRANE IN THE CELL CULTURES) SELECTS SINGLET OXYGEN AS THE PRIMARY OUTPUT. **(C)** THE MODEL COMPOUND **T-2**, WHICH IS THE Zn^{2+} COMPLEX OF THE *MESO*-TERPYRIDYLBODIPY COMPOUND, HAS A VERY LOW FLUORESCENCE EMISSION INTENSITY IN ACETONITRILE. **(D)** THE ADDITION OF PHOSPHATE IONS RESULTS IN A VERY SHARP INCREASE IN EMISSION INTENSITY. THE LOW EMISSION INTENSITY IS DUE TO THE AVAILABILITY OF A CHARGE TRANSFER STATE (CTS) RESULTING IN ENHANCED INTERSYSTEM CROSSING, WHICH IN TURN LEADS TO EFFICIENT GENERATION OF SINGLET OXYGEN.....113

FIGURE 75. POWERING UP THE AUTOMATON: PERCENT CELL DEATH AS A FUNCTION OF INCREASING CONCENTRATIONS OF THE MOLECULAR TERMINATOR AUTOMATON **T-1**, QUANTIFIED BY MTT ASSAYS AND PHOSPHATE, AS THE "SWITCH" INPUT, CHANGING OUTPUT FROM SINGLET OXYGEN TO EMISSION. GREEN OPEN CIRCLES CORRESPOND TO PERCENT DEATH OF K562 CELLS UNDER IRRADIATION AT 522 NM FOR 12 HOURS FOLLOWED BY CONTINUED INCUBATION IN DARK FOR ANOTHER 12 HOURS. SOLID BLACK CIRCLES CORRESPOND TO CELLS KEPT UNDER IDENTICAL CONDITIONS OF INCUBATION WITH THE AGENT, BUT IN

dark. Positive control (dashes at 100 % line) corresponds to cells incubated in DMSO-growth medium mixture (50/50, v/v). 115

Figure 76. Kill confirmed: **T-1** signals apoptosis by switching to diagnostic mode. Flow cytometry data and confocal microscopy images for PE-Annexin V and molecular automaton **T-1**. **(A)** PE-Annexin labels most of the cells incubated with **T-1** under light irradiation (Annexin V (+) region of the green area). **(B)** Green channel: Cells incubated with **T-1** under irradiation. **(C)** Green channel: Cells incubated with **T-1** in the dark. **(D)** 2D plot for both green and red channels: **T-1** and PE-Annexin V (a specific apoptosis marker) stain the same kind of cells with a large (86%) agreement: 70% of the irradiated cells were co-stained with both **T-1** and PE-Annexin V, indicating only apoptotic cells are fluorescently labeled with **T-1. (E)** The truth table with input, the switch and the outputs clearly identified, and the particular set of conditions were highlighted. **(F)** Switch input (appearance of phosphatidylserine in the external leaflet of the cell membrane) selects fluorescence emission as the primary output. 117

Figure 77. **(A)** Cells treated with PE-Annexin V and the **T-1,** and kept in dark, show no signs of morphological change, and the cellular membranes are not stained with either one of the agents (scale bar, 10 mm). **(B)** and **(C)** cells were incubated with **T-1**, irradiated with the LED light source, then treated with PE-Annexin V. The two agents (**T-1** and PE-Annexin V, green and red, respectively) label the same regions in the cells undergoing apoptosis (scale bar, 10 mm). 119

Figure 78. Total synthesis of **T-1** (**7**). 122

Figure 79. Raw data for the decrease in absorbance of DPBF in ethanol in the presence of **T2+Zn** and **phosphate** in medium. Singlet oxygen quantum yields were calculated as previously described using initial rate of decrease in the DPBF absorbance once any changes in absorbance of the DPBF without any agent added were subtracted[152]. In this particular case, the changes in absorbance is the same as the decrease in absorbance of DPBF alone, under irradiation. 129

LIST OF TABLES

TABLE 1. CYCLOREVERSION HALF-LIFE VALUES RATES OF SELECTED NAPHTHALENE ENDOPEROXIDES IN WATER AT 37 ^{0}C AND PERCENT SINGLET OXYGEN RELEASE[25, 26]. 11

TABLE 2. TISSUE PENETRATION DEPTHS OF LIGHT AT DIFFERENT WAVELENGTHS. PENETRATION DEPTH IS DEFINED AS THE DISTANCE, WHICH REDUCES THE INTENSITY AT THE SURFACE TO 1/E OF THE ORIGINAL VALUE (APPROXIMATELY 37 % OF THE ORIGINAL INTENSITY AT THE SURFACE[28]) 13

TABLE 3. CYCLOREVERSION RATES OF SELECTED 2-PYRIDONE ENDOPEROXIDES AT 37 ^{O}C IN H_2O[30]. 15

TABLE 4. CYCLOREVERSION RATES OF SELECTED ENDOPEROXIDES AT 25 ^{O}C 30

TABLE 5. PHOTOPHYSICAL DATA FOR (**T-2**), (**T-2-*ZN***), (**T-2-*ZN-P***), (**T-1**), (**T-1-*ZN***), (**T-1-*ZN-P***) 111

List of Abbreviations

PDT: Photodynamic Theraphy

PS: Photosensitizer

BODIPY: Boradiazadacene

LED: Light Emitting Diode

ROS: Reactive Oxygen Species

PEG: Poly (ethylene glycol)

DMF: Dimethylformamide

THF: Tetrahydrofuran

TFA: Trifluoroacetic Acid

EtOAc: Ethyl Acetate

DCM: Dicholoromethane

DMSO: Dimethylsulfoxide

TLC: Thin Layer Chromatography

HRMS-TOF: High Resolution Mass Spectroscopy- Time of Flight

NMR: Nuclear Magnetic Resonance

TBAF: Tetra-n-butylammonium Fluoride

ISC: Intersystem Crossing

TPP: Tetraphenylporphyrin

$^1O_2$: Singlet oxygen

λ: Wavelength

Φ_f: Fluorescence quantum yield

Φ_Δ: Singlet oxygen quantum yield

CHAPTER 1

1. INTRODUCTION

1.1. Introduction to Singlet Oxygen

Although the presence of singlet oxygen was first determined in 1924, chemistry began to focus on singlet oxygen only after the 1960s [1]. Singlet oxygen ($a^1\Delta_g$) is a highly reactive species with a short lifetime and belongs to the class of reactive intermediates and it is extremely important for both chemical reactions and biochemical transformations[2-7]. In order to understand the concept of reactivity and reactions of singlet oxygen, it is necessary to figure out the basic structure of triplet oxygen and electronic structures of singlet oxygen.

1.2 Electronic Configuration of the Oxygen Molecule

The electronic configuration of oxygen in the ground state is a triplet state. Singlet oxygen, compared to the ground state triplet oxygen; is an oxygen molecule in two different unstable configurations with higher energy levels.

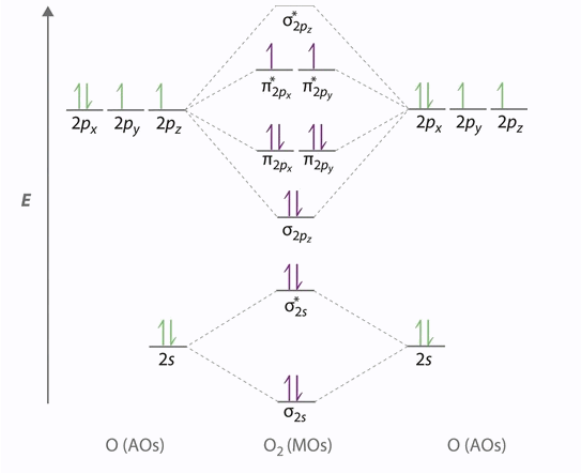

Figure 1. Molecular orbital diagram of atomic and molecular oxygen

Since the energy levels of the two orbitals (π^*_{2px}, π^*_{2py}) shown in figure 1 are same, these orbitals are called as degenerate orbitals. According to Hund's law [8], electrons must first occupy the empty orbitals then double occupying them. The magnetic quantum number is determined according to the M=2I+1 (I = Spin quantum number) formula. When the spins of these two electrons are in the same direction, the total spin I = 1/2 + 1/2 = 1 and the magnetic quantum number is M = 2.1 + 1 = 3 and this configuration of the oxygen molecule is called a *triplet*. Since HOMO (Highest occupied molecular orbital) orbitals of oxygen are found by parallel spin, the oxygen has a triplet configuration and shows paramagnetic properties. The oxygen molecule is very reactive because it acts as a diradical. Because of this property, oxygen easily reacts with many compounds. Therefore, oxygen sensitive reactions are carried out under inert gas.

To understand the other electronic configurations of oxygen [9], we can examine the orbitals shown in figure 2. If two electrons are directed antiparallel position, the total

spin will be I =1/2 + - 1/2 = 0, M = 2. 0 + 1 = 1, and the corresponding oxygen molecule

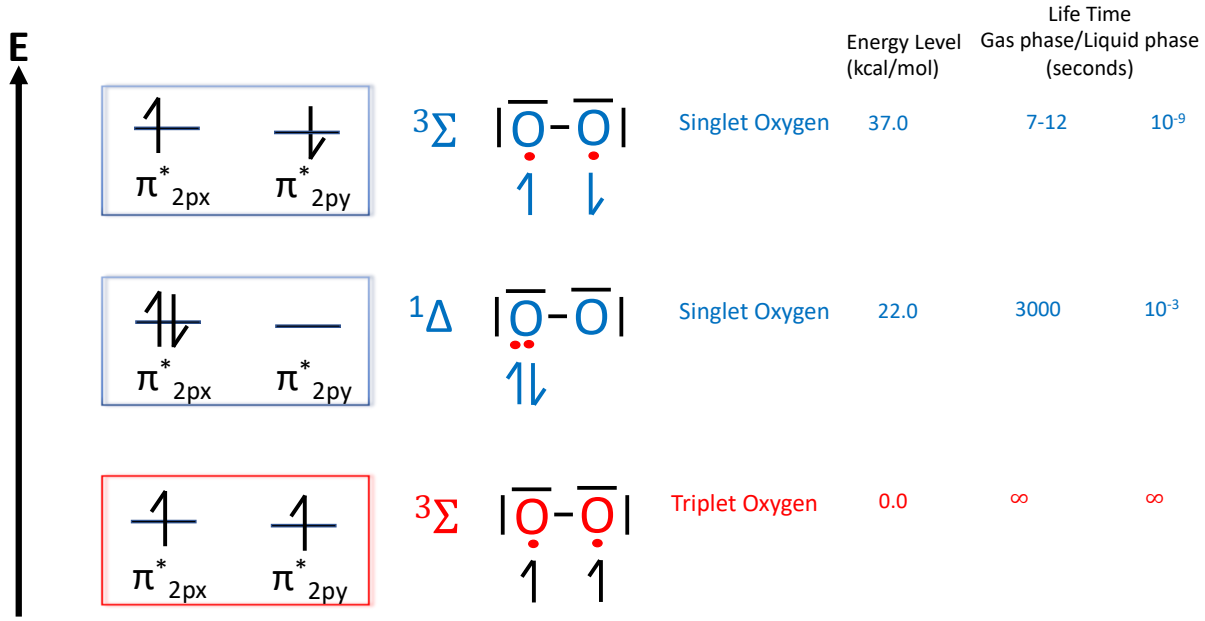

Figure 2. Electronic configuration of singlet and triplet oxygen and some properties of them

is called *singlet oxygen*. It is shown in figure 2, there are two different electronic configurations for singlet oxygen. Two electrons can exist in a single orbital with parallel spins or they can locate in different orbitals. The singlet oxygen ($^1\Delta$) is the state where electrons are paired in a single orbital. The energy required to stimulate singlet oxygen to this configuration is 22.0 kcal / mol [10]. A gas phase at low pressure, $^1\Delta$ the lifetime of the singlet oxygen is about 45-50 minutes [11]. In the liquid phase, as a result of the collision of molecules in liquid media, energy transfer occurs faster and the lifetime of singlet oxygen is reduced to 10^{-3} seconds [12]. This time period is sufficient for a chemical reaction to take place. Therefore, the singlet oxygen that undergoes chemical reactions is the singlet oxygen in the ($^1\Delta$) configuration. $^1\sum$ is singlet oxygen which has

a higher energy level and contains electrons in different orbitals with antiparallel spins. The excitation energy is around 37.0 kcal / mol, the lifetime in the gas phase is 7-12 seconds [13], and in the liquid and solid phases it immediately converts to $^1\Delta$ singlet oxygen. Since the lifetime of the $^1\sum$ singlet oxygen is very short (10^{-9} seconds), this time period is not sufficient for chemical reactions.

1.3 The Formation of Singlet Oxygen

Singlet oxygen will be produced by using chemical and photosensitization methods. If singlet oxygen is to be used as a reactant in a chemical reaction, the singlet oxygen must be formed in the reaction medium because the lifetime of this molecule is very short.

1.3.1 Photosensitization Method

Direct excitation of singlet oxygen by irradiation is a difficult process. Therefore, there is a need for some sensitizers for stimulation. These sensitizers are generally compounds with triplet energies between 30 and 70 kcal / mol. Tetraphenylporphyrin, benzophenone, eosin, methylene blue, rose bengal are some of these sensitizers (Figure 3).

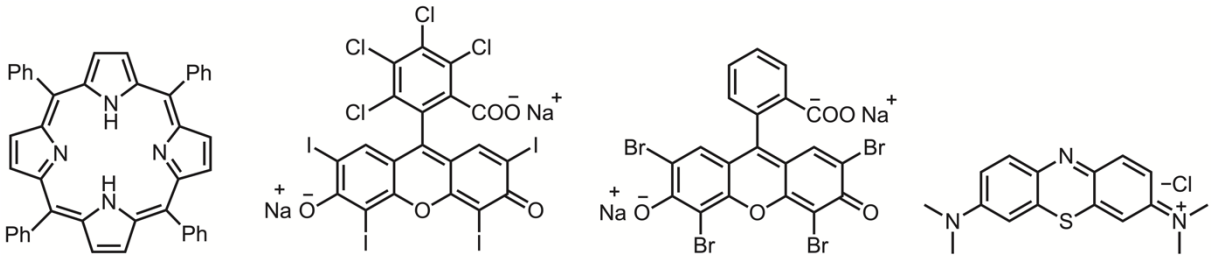

Figure 3. Some examples photosensitizers

As the oxygen gas is passed through the reaction media at where a sensitizer is also added, the irradiation is applied from the inside or the outside of the reaction by a light source. The energy from the light source must be sufficient to activate the sensitizer[14].

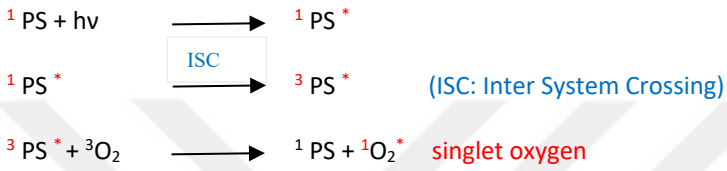

Figure 4. Schematic representation of singlet oxygen generation by photosensitizer

The photosensitizer is excited by absorbing the beam, one of the electrons in the outer is excited to an upper orbital preserving spin direction and singlet configuration. In other words, one of the electrons ($^1S_0$) in the ground state excited to an upper orbital ($^1S_1$). It is also possible for the electron to transfer to the higher orbitals ($^1S_2$, $^1S_3$, ext). In these cases, the electronic configuration (singlet) of the molecule is retained. However, if the electron has excited to higher orbitals such as $^1S_2$, $^1S_3$, the electron can return to the $^1S_1$ position from these levels. These processes are permissible transitions since there is no electron spin multiplicity. The excitation of the electron in the $^1S_1$ position is called the *fluorescence* state. At this level, the lifetime of the electron is about 10^{-8} – 10^{-9} seconds. Electron which is excited to the $^1S_1$ position can be returned to the ground state by various mechanisms. This event is called r*elaxation* or *vibrational relaxation*. *Fluorescence* is a term that the relaxation of the electron to the ground state by emitting photons by radiation. The fluorescence emission spectrum shifts to the long

wavelength according to the absorption spectrum. Because if the electron first shifted from $^1S_2$ or $^1S_3$ to $^1S_1$, it gave some of its energy to the environment as heat. Another way to move from the fluorescence ($^1S_1$) position to the ground state is the transfer of excess energy to the underlying similar or another molecule. According to the dipole-dipole interaction mechanism, the donor emission band and the acceptor band must be intersected (FRET) for energy transfer to occur.

Another valid mechanism for relaxation is the *Inter System Crossing* (ISC) mechanism. According to this mechanism, the electron must transfer from the $^1S_1$ position to the lowest triplet energy level ($^3T_1$). This transition will occur when the electron spin multiplicity occurs. It is a forbidden transition process. Such a transition is possible if there are heavy atoms in the molecule, environment or solvent molecules. At the $^3T_1$ level, an excited molecule can return to its ground state ($^1S_0$). This phenomenon is called *phosphorescence*. Photosensitizers which are excited to the $^3T_1$ position are chemically highly reactive due to their unpaired electrons and long relaxation periods.

Singlet oxygen generates when the excited sensitizer ($^3T_1$) transfers energy to molecular oxygen ($^3O_2$). The transffered energy should be at least about 22.0 kcal / mol. The triplet energy level of many organic compounds can generate singlet oxygen. At this stage, the sensitizer changes from a triplet position to a singlet, while the oxygen, which is essentially a triplet, changes to a singlet position. Both molecules also have spin multiplicity at the same time. It assumed that spin rotations occur according to the electron exchange mechanism as shown in figure 5.

Figure 5. The electron transfer mechanism between triplet photosensitizer and triplet oxygen

Singlet oxygen is generated according to this mechanism. In addition to this mechanism, the photosensitizer itself is oxidized by transferring an electron to the oxygen molecule, while the oxygen molecule is reduced to the radical anion.

1.3.2 Chemical Methods

Singlet oxygen generation is generally effective in photosensitization method, but there are some chemical methods.

1.3.2.1 Hydrogen peroxide - hypochlorite reaction

In 1927, Malet determined that *chemiluminescance* occurred in the reaction of hydrogen peroxide with hypochlorite [15]. First, Khan and Kasha [16, 17] later Arnold [18] found that the emission bands seen in chemical irradiation came from the excited oxygen molecule. Foote and Wexler [19] found that when the dienes and oxygen (generated from the reaction between hydrogen peroxide and hypochlorite) gave reaction, the products was same as the products produced by the photosensitization method, revealed that the oxygen produced by chemical method as singlet oxygen form.

1.3.2.2 Phosphite - Ozone mixture decomposition

Triphenylphosphite reacts with ozone at low temperatures to form a phosphite-ozone complex. These complexes are not stable and decompose over -20°C to release singlet oxygen [20].

1.3.2.3 Dissociation of Aromatic Endoperoxides

The first example of endoperoxides discovered was the case of rubrene, and 9,10-diphenylanthracene is another example. In 1926, when Moreau heated the rubren endoperoxide (Figure 6) [21], he determined that rubren and active oxygen molecules were formed.

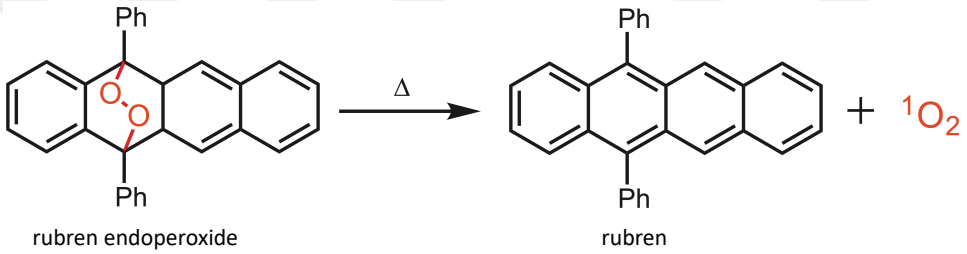

Figure 6. The singlet oxygen generation by rubren endoperoxide

Subsequently, Wassermann determined that 9,10-diphenylanthracene endoperoxide is [22] also converted to singlet oxygen when heated in the same manner, and this method was used as the source of singlet oxygen in many reactions (Figure 7).

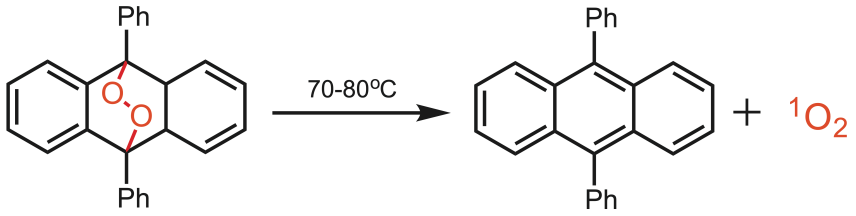

9,10-Diphenylanthracene endoperoxide

Figure 7. The singlet oxygen generation by 9,10-Diphenylanthracene endoperoxide

These compounds can also be viewed as compounds that store singlet oxygen at some point. The advantages of the method are; It is able to produce singlet oxygen at high concentration and without using light source. As can be seen in detail in the reactions of singlet oxygen, the oxygen-oxygen bond is one of the weakest bonds in organic chemistry. When we apply heat, it is expected that the oxygen-oxygen bond is broken homolytically at first, but the more stable carbon-oxygen bond is preferably broken in these reactions. This behavior of endoperoxides only applies to systems in which stable aromatic compounds are formed by decomposition.

As reversible carriers for singlet oxygen, certain aromatic compounds are very suitable. Many polycyclic aromatic compounds can trap singlet oxygen, and some of these resulting endoperoxides exhibit an interesting feature, which is the release of oxygen - in the excited state- (i.e., singlet oxygen, $^1O_2$) on warming.

There are alternative decomposition routes for endoperoxides as seen in figure 8 [23]. They can dissociate in two ways that are photolysis and thermolysis. In thermolysis

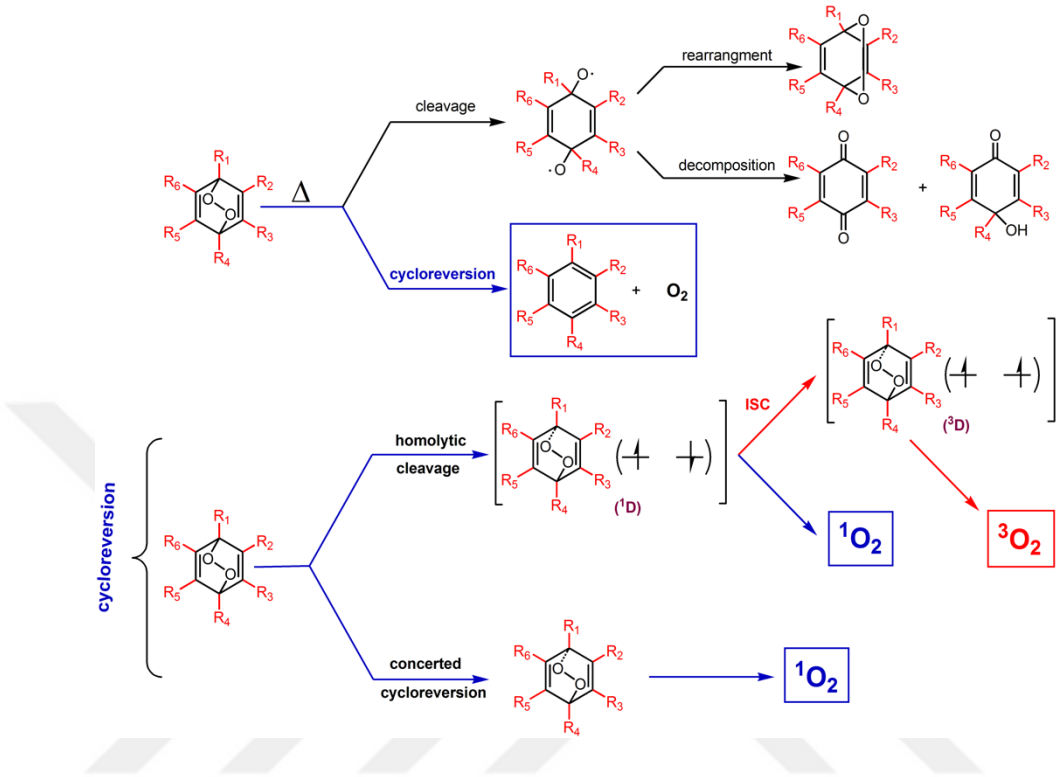

Figure 8. Alternative decomposition routes for endoperoxides (EPOs).

process, there are two different mechanisms. The homolytic cleavage of the endoperoxide bond gives two products according to rearrangement and decomposition (It is the opening of the peroxide ring in the basic medium to obtain the quinone and unsaturated hydroxyketones derivatives) processes. In cycloreversion process, singlet oxygen generation will be obtained by homolytic cleavage and concerted cycloreversion pathways. In homolytic cleavage, some of singlet state diradicals can convert into triplet oxygen by intersystem crossing [24]. A mechanism involving the concerted cleavage of both C-O bonds give directly singlet oxygen.

Further investigations showed that in some instances (naphthalene endoperoxides), the dissociation to produce singlet oxygen can take place at room temperature. It is

now clear that by different substitution patterns, it is possible to control the rate of cycloreversion process[25, 26].

Most of these endoperoxides (EPOs) themselves are prepared by photosensitized oxygenation which involves [4+2] cycloaddition of $^1O_2$. Due to the electrophilic nature of $^1O_2$, the reactivity of aromatic hydrocarbons with $^1O_2$ increases with electron density of the hydrocarbons involved. In addition to electronic effects, steric effects also play an important part in determining the reaction rate.

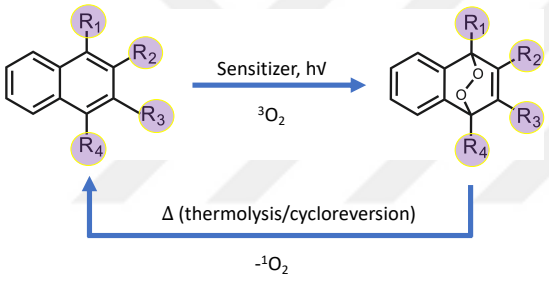

compound	half-life/hr	% $^1O_2$ release
$R_1 = CH_3$; $R_2 = -CH_2COOH$; $R_3 = H$	0.38	45
$R_1 = -CH_2COOH$; $R_2 = -CH_2COOH$; $R_3 = H$	0.38	50
$R_1 = -CH_2CH_2N(CH_3)_3^+$; $R_2 = CH_3$; $R_3 = H$	0.37	65
$R_1 = R_4 = CH_2OH$; $R^2 = R^3 = CH_3$	indefinite[a]	-
$R_1 = R_2 = CH_3$; $R_3 = CH_2OH$	4.37[a]	n.d.[b]
$R_1 = R_2 = CH_2OH$; $R_3 = H$	1.17	51

[a] in $CDCl_3$. [b] n.d. = not determined

Table 1. Cycloreversion half-life values rates of selected naphthalene endoperoxides in water at 37 ^{0}C and percent singlet oxygen release[25, 26].

On brief inspection of above data for the naphthalene-endoperoxides, it appears that substitution on positions 2 and 3 inhibits cycloreversion. The steric repulsions between methyl groups on positions 1<->2 and 3<->4 are somewhat relieved in the cycloadduct, but the reverse reaction would be unfavorable due to increased steric repulsions. The effect of additional steric bulk however, was not investigated for most positions on the ring, the available data is only for methyl substitutions. Additionally, other results show that incorporation of endoperoxides to polymers reduce the free volume, thus inhibit

the cycloreversion process. Work on anthracene derivatives on the other hand, show electronic factors playing roles in changing the rates of cycloaddition. Not surprisingly, electron donating substituents on 9,10-positions facilitate the reactions in both directions, since singlet oxygen is an electrophilic agent.

Moreover, the temperature changes strongly affect the cycloreversion process efficiency besides structure of the substrate or attached substituents. In a previous study by Turro, the appearance of phenylanthracene (PA) measured by UV absorptivity. The graph was drawn as a function of time at various temperatures[27]. As it can seen from figure 9, in each case excellent first-order kinetics were seen and as the temperature increases singlet oxygen generation increases.

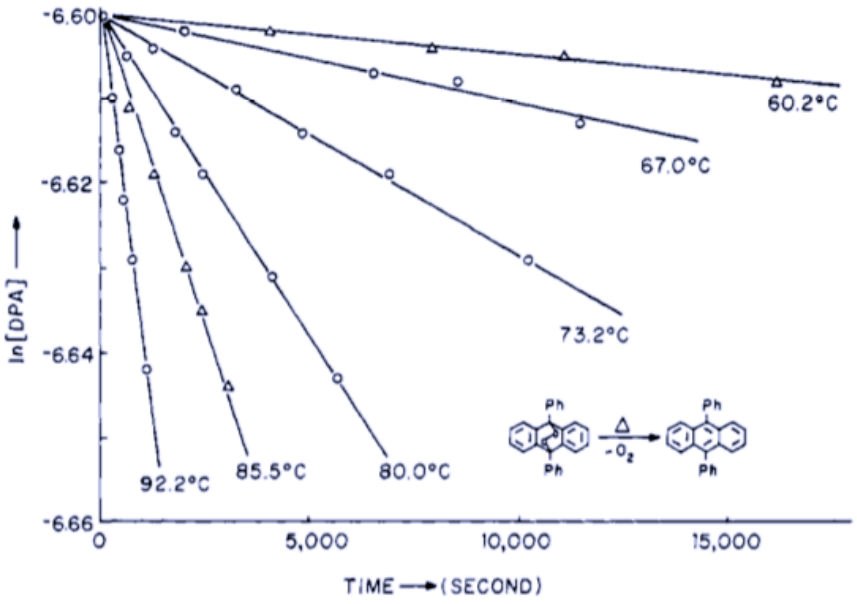

Figure 9. Thermolysis of endoperoxide to 9,10-diphenylanthracene. Copyright © 1981, American Chemical Society. Reprinted with permission from ref [27].

1.4 Endoperoxide as a source of singlet oxygen to be carried to tumour tissues

Photodynamic thearpy (PDT) depends on the efficient generation of singlet oxygen ($^1O_2$) through excitation of a particular chromophore (sensitizer) followed by an energy transfer to the dissolved oxygen in tumor tissues. Cytotoxic singlet oxygen and other secondary products (reactive oxygen species, ROS) are responsible for the apoptotic and necrotic deaths of the tumor cells. There are some advantages and disadvantages of this technique. One of the disadvantage is the requirement for light excitation. Actually, It is both an advantage and a disadvantage. The photosensitizer will not be active and generate cytotoxic singlet oxygen, unless it is excited.

Tissue	$\lambda_{632.8\ nm}$ (mm)	$\lambda_{675\ nm}$ (mm)	$\lambda_{780\ nm}$ (mm)	$\lambda_{835\ nm}$ (mm)
Blood	0.19±0.01	0.28±0.01	0.42±0.02	0.51±0.02
Lung	0.81±0.06	1.09±0.11	1.86±0.12	2.47±0.03
Thyroid gland	1.23±0.08	1.42±0.15	1.70±0.16	3.04±0.05
Pelvic ganglion	1.39±0.11	1.42±0.01	1.83±0.02	2.32±0.03
Hepatic metastasis	1.53±0.15	1.81±0.21	2.48±0.30	3.27±0.03
Lung carcinoma	1.68±0.15	2.01±0.27	2.82±0.31	3.89±0.03
Mammary tissue	2.59±0.18	2.87±0.30	3.12±0.32	3.54±0.40
Mammary displasia	2.21±0.20	2.68±0.29	3.03±0.33	-
Mammary carcinoma	2.87±0.22	3.14±0.36	3.62±0.41	4.23±0.04
Uterus	2.14±0.18	2.40±0.22	2.61±0.25	3.31±0.02
Axillar epidermoid carcinoma	2.12±0.18	2.51±0.22	2.64±0.23	3.24±0.03

Table 2. Tissue penetration depths of light at different wavelengths. Penetration depth is defined as the distance, which reduces the intensity at the surface to 1/e of the original value (approximately 37 % of the original intensity at the surface[28])

This brings an inherent selectivity to the procedure, since one can choose the direction and the area of irradiation; but at the same time, light cannot penetrate[28] beyond a few millimeters (Table 2), limiting the therapeutic potential to superficial tumors. Large numbers of potential PDT photosensitizers are being synthesized every year, but this fundamental problem remains as intractable as ever. Even using intense laser light sources at the most penetrating wavelengths (650-850 nm), or by employing two photon approach or using upconversion nanoparticles, any tumors buried more than a few millimeters inside, will likely be outside the reach of PDT modality.

The other potentially unsurpassable problem is hypoxia. Tumor tissues are lack of oxygen as a result of their rapid growth related insufficient vasculature. But PDT requires oxygen, too. In fact, in both tumor models and in clinical application of PDT, it was observed that photosensitization itself depletes cellular oxygen very fast, so that the light dose has to be carefully adjusted and preferably, the light has to be introduced in pulses (fractionated) [29]. For this reason, PDT is considered a self-limiting modality, as it causes its own inhibition.

As a result of these limitations, transforming PDT into a more manageable and broadly applicable therapeutic protocol is extremely important. If we can separate photosensitization event from the delivery of singlet oxygen, the light and penetration problem of PDT can be mistaken for history. Thus, a storage compounds for singlet oxygen are studied by many groups recently. A storage compound can react with molecular oxygen under typical photosensitization conditions, and then the metastable

compound has to be transferred to the tumor site which would release its cargo in response to a chemical or enzymatic cue. This approach assumes that singlet oxygen produced stoichiometrically (as opposed to catalytically through photosensitization) by the chemical transformation of the carrier molecule, would be enough to trigger apoptotic response in cancer cells.

As for the strorage compound for singlet oxygen various arenes, 2-pyridone and furan derivatives were considered. They all form endoperoxides of varying thermal stabilities when reacted with singlet oxygen generated by photosensitization. Most of these endoperoxides release singlet oxygen when they undergo cycloreversion.

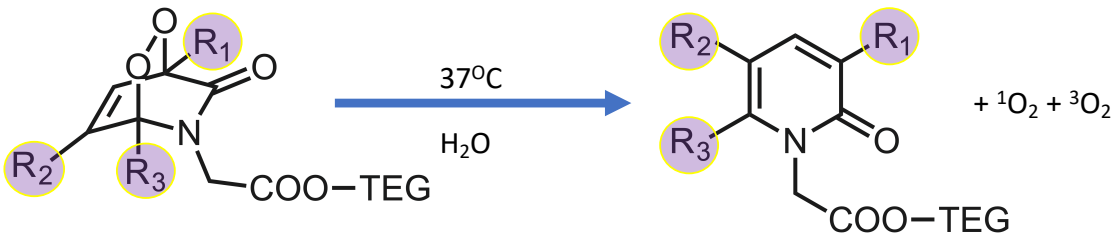

compound	half-life/hrs	Percent cycloreversion
$R^1 = R^2 = R^3 = H$	0.5	18
$R^1 = CH_3$; $R^2 = R^3 = H$	8.5	78
$R^1 = H$; $R^2 = H$; $R^3 = CH_3$	4	ca. 50
$R^1 = R^2 = CH_3$; $R^3 = H$	13	47
$R^1 = CH_3$; $R^2 = H$; $R^3 = CH_3$	4	ca. 50
$R^1 = R^2 = R^3 = CH_3$	15	ca. 10

Table 3. Cycloreversion rates of selected 2-pyridone endoperoxides at 37 °C in H_2O[30].

2-Pyridone endoperoxides studied and shown to be clean sources of singlet oxygen. Substitutions on the bridgehead positions of the endoperoxides are expected to alter

the reaction rate. A recent study provides convincing evidence of this. In a recent study by Jessen[30], 2-pyridone endoperoxides were studied in cell cultures as a source of oxygen, keeping anoxic cells alive. Singlet oxygen damage was inhibited by the addition of Vitamin C (Table 3). The results are encouraging, suggesting a biocompatibility for the 2-pyridone endoperoxides, since the cell culture was kept alive in the presence of these endoperoxides. Again just to emphasize one more, singlet oxygen produced in this work was quenched and/or trapped.

Another study by Ilke [31], a photosensitizer with an additional 2-pyridone module for trapping singlet oxygen was used in fractional PDT. In the study, 2-pyridone endoperoxide is generated along with singlet oxygen in the light cycle. The endoperoxide undergoes thermal cycloreversion to produce singlet oxygen in the dark cycle and regenerating the 2-pyridone module (Figure 10). As a result, the photodynamic process can continue in the dark as well as in the light cycles. The compound was studied in vitro in HeLa cell culture with cell viability/cytotoxicity assays (MTT). The results showed that, the generation of cytotoxic singlet oxygen continued caused cell death both light and dark cycle.

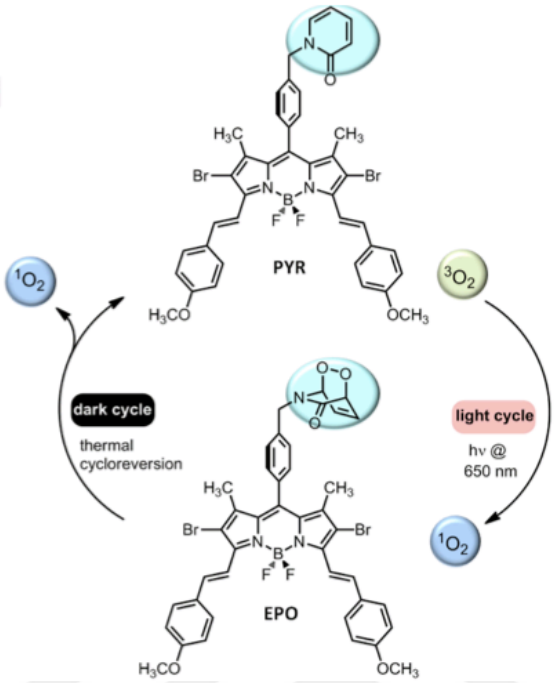

Figure 10. Singlet oxygen generation in fractional PDT.

To conclude, all of the above classes of endoperoxides offer ample opportunities for controlled generation of singlet oxygen. While electronic factors play a role, our primary handle will be steric. Cycloreversion reaction has a transition state, which is very sensitive to the bulk at the middle carbons of the "diene". It should be possible to increase the bulk following the endoperoxide formation and inhibit cycloreversion, just like using a stopper.

There are cell culture studies showing the effects of naphthalene-endoperoxide derivatives which spontaneously produce singlet oxygen [32, 33] at 37 ^{o}C in an attempt to elucidate PDT induced processes at cellular level. In the more recent study[32], it was shown that the apoptosis resulting from endoperoxide generated singlet oxygen, is different and could have additional therapeutic advantages as caspase activation is

suppressed. These studies are very important in that, they demonstrate if one can find a way of turning the cycloreversion rate of these endoperoxides rate up and down as needed, a very unique therapeutic agent may be at hand.

Safacan et. al. made important contributions[34] in assessing cytotoxicity of singlet oxygen delivered by controlled decomposition of endoperoxides (Figure 11). Anthracene endoperoxide derivative with water solubilizing side chain was attached to gold nanorods (40 nm, with an aspect ratio of 4) through thiol end groups. Irradiation at 808 nm led to plasmonic heating of the gold nanorods. Cell culture studies unequivocally showed that the cell death for the HeLa cancer cells was due to singlet oxygen generated by the thermal decomposition of the endoperoxide, and not due to warming of the culture medium. This was a proof of principle for the effectiveness of controlled singlet generation in a biological media. The work was also important to show that very small concentration endoperoxide would trigger apoptotic cell death response in cell cultures.

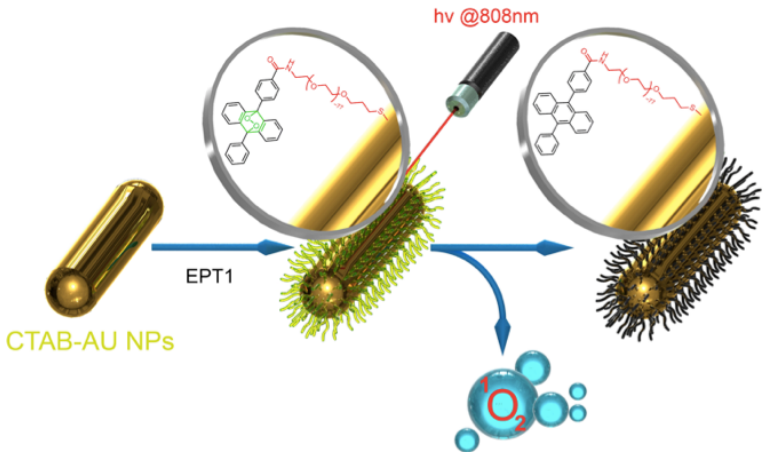

Figure 11. Structure of the gold nanorod-endoperoxide. (Au-EPO) . Copyright © 2016 WILEY-VCH Verlag GmbH & Co. KGaA, Weinheim. Reprinted with permission from ref[34].

1.5 The Mechanisms of Induction of Apoptosis by Singlet Oxygen

Photodynamic therapy demonstrates it effects through three important components: photosensitizer, visible light and oxygen. These three components act together to generate Reactive Oxygen Species (ROS). ROS then results in cytotoxicity as well as cell death. Photodynamic therapy causes tumor destruction by several mechanisms including direct cancer cell killing, damaging vascular structures as well as recruiting immune cells which are implicated in antitumor immune responses [35, 36]. When the photosensitizer is excited with a specific light, it transfers its energy to ground state triplet oxygen and causes production of singlet oxygen. In turn, singlet oxygen is highly reactive and can destroy tumor cells via apoptosis, autophagy, necrosis, vascular damage, hypoxia induction.

Several photodynamic therapy agents cross through the cellular plasma membrane and localize in the cytoplasm. When these agents are excited with a specific wavelength light, they produce reactive oxygen species. This, in turn, results in induction of cell death in cancer cells in a time-dependent manner. The induction of apoptosis by such agents is achieved through several mechanisms. Photodynamic therapy induced apoptosis and the mechanisms underlying it have been thoroughly studied in the literature [37].

One of these mechanisms is the mitochondrial (intrinsic) apoptosis pathway [38]. Singlet oxygen first activates caspase 9. Bax molecules in the cytoplasm pass to the outer mitochondrial membrane, causing a change in the mitochondrial transmembrane

potential. Then, cytochrome *C* is released into the cytosol through the pores generated by several mechanisms due to Bax molecules. Another mechanism of induction of apoptosis by singlet oxygen is the extrinsic apoptosis pathway [39, 40]. Reactive oxygen species cause trimerization of death receptors (e.g. TNF-α). This in turn activates caspase 8 and results in apoptosis. On the other hand, Endoplasmic Reticulum stress-mediated apoptosis pathway may also be utilized. This is marked by the upregulation of glucose-regulated protein 78 and the phosphorylation of eukaryotic Initiation Factor 2 alpha. This pathway involves caspase 12 cleavage [41]. In addition, caspase-independent pathway is also implicated in photodynamic therapy induced apoptosis. This pathway involves the release of apoptogenic molecules from mitochondria after the change of mitochondrial transmembrane potential [42, 43]. This causes chromatin fragmentation without caspase 3. Last but not least, autophagy has also been proposed as a mechanism related with photodynamic therapy [44]. Autophagy (eating of self) is a self-degradative process which is crucial for the turnover of damaged organelles and balancing sources of energy through the endosomal-lysosomal system [45]. Since reactive oxygen species produced as a result of thermal decomposition of endoperoxide are very reactive, they oxidatively damage cellular organelles. This, in turn, triggers autophagy to remove and recycle those organelles [46]. Singlet oxygen has been reported to induce cell death via autophagy [47]. Finally, very limited and negligible level of necrotic cell death may also be induced due to singlet oxygen generation in the medium [48].

The generated singlet oxygen induces cell death both in malignant and non-malignant cells, without discrimination. On the other hand, release of singlet oxygen in the extracellular compartment results in apoptosis especially in malignant cells via singlet oxygen-mediated deactivation of catalase, which protects malignant cells [49]. It is known that malignant cells are protected from intercellular apoptosis-inducing signaling by the expression of membrane-associated catalase and superoxide dismutase [50]. Exogenous singlet oxygen results in inactivation of this protective catalase. Such a process seems to be specific for tumor cells [50].

1.6 Drug and Prodrug Strategies for Tumour Hypoxia

Hypoxia means that the reduction of oxygen level in body tissues. It is a characteristic of most solid tumors. Such tumors develop regions of severe hypoxia (oxygen concentrations typically less than 1 %) as result of structurally and/or functionally abnormal microvascular systems. Hypoxic zones of tumors are highly resistant to therapy; the required dose of radiation is typically 2.5 to 3 times greater for hypoxic cells[51]. Hypoxia induced resistance to chemotherapy is also well documented for drugs such as, cyclophosphamide, carboplatin and doxorubicin [52]. To make matters worse, hypoxic tumor cells are much more invasive and metastatic [53], to improve patient prognosis, they are considered to be the most important tumor fraction.

Even though there exist several different therapeutic approaches, most prove to be ineffective because of tumor hypoxia. Tumor hypoxia causes such unsuccesful results

due to several factors. One reason for this is the fact that most cells under conditions of hypoxia are dormant and not hyperproliferative. Most of the therapeutic approaches usually target the hyperprolifeartive capability of tumor cells. Since hypoxic cells are not hyperproliferative, such approaches have limited efficiacy against those cells. In addition, regions of hypoxia in the tumor tissue are relatively inaccessible. Furthermore, radiotherapy requires oxygen in order to be able to induce cytotoxicity. Last but not least, specific proteins related with drug resistance are induced as a result of hypoxia. Therefore, hypoxia presents itself as a crucial issue in cancer therapy as well as an important therapeutic target.

Inconsequentiality, there are some methabolic differences between normal cells and cancer cells. By using these differences, various drug development programs identified the biomolecular targets (such as Hypoxia Induced factor-HIF family of proteins; or carbonic anhydrase-IX) involved in hypoxia.

There is also some evidence that some of the clinically important anti-cancer drugs (such as bevacizumab [54]) may induce additional hypoxia, as they inhibit blood flow. Thus, hypoxia targeting drugs can be very useful in combination therapies as well.
The extent and magnitude of tumor hypoxia is very important in assessing the progression of the disease [55].

Another class of drugs, which received attention in recent years are Hypoxia Activated Prodrugs (HAPs). These compounds, instead of targeting a particular biomolecule, they are activated in a relatively non-specific manner, by the bioreductive

microenvironment of the hypoxic tumors. This approach is considered highly promising, as there are more than a few of such prodrugs under various stages clinical evaluation [56].

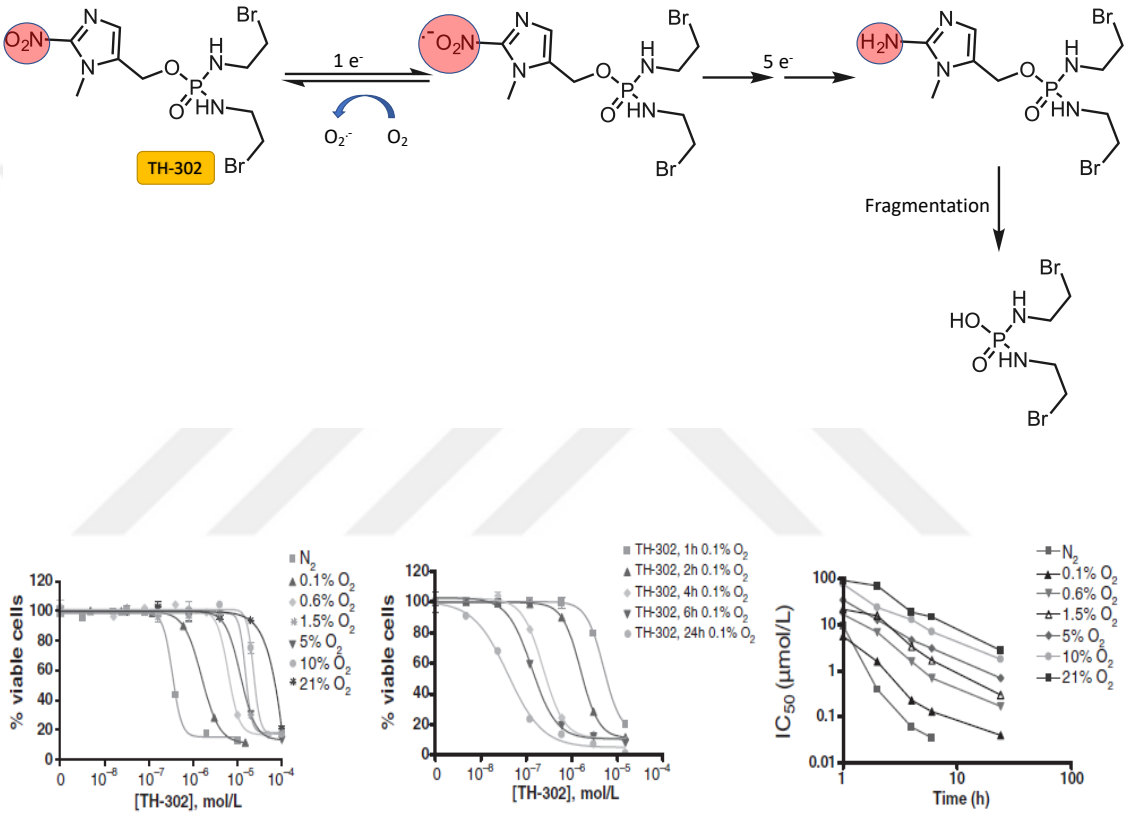

Figure 12. Operation principle of the prodrug TH-302. Reductive elimination due to hypoxic conditions lead to the generation of a cytotoxic agent. TH-302 is in Phase I/II for clinical development. Lower figures were adapted from[57]. Copyright © 2012, American Association for Cancer Research.

One particularly promising compound and its principle operation (a prodrug) is shown in Figure 12. Reduction of the prodrug leads to the release of a cytotoxic nitrogen-mustard gas. Nitrophenyl groups are reduced only at highly hypoxic states. This is good,

in this way, the toxic agent is not produced accidentally in relatively hypoxic but normal tissues cells. On the other hand, in addition to the most hypoxic core, the tumor has cells of moderate hypoxia. Stable (relatively) cytotoxic agent, which is produced by the reductive activation of the prodrug, can diffuse to neighboring, less hypoxic tumor cells and kill them, too (bystander effect). Alternatively, the drug can be designed in such a way that it can be reductively activated at lower levels of hypoxia (Tripazamine is an example of such a prodrug). Considering the fact that one of the urgent clinical needs in cancer therapy is the development of therapeutic agents which can target the hypoxic fraction of cells, the current excitement around HAPs is understandable: following the success of phase 2 trials, in 2012, Merck KGaA signed a deal with Threshold Pharmaceuticals for a joint development of TH-302.

To conclude this section, targeting hypoxia for cancer therapeutics is clearly a very smart choice.

HYPOXIA TRIGGERED INTRACELLULAR SINGLET OXYGEN RELEASE: FOUNDATIONS OF A NEW THERAPEUTIC PARADIGM

Ozlem Seven,[†] Seylan Ayan,[†] Gurcan Gunaydin, Nisa Yesilgul Mehmetcik, M. Emre Gedik and Engin U. Akkaya

2.1 Objectives

Considering the rate determining factors in endoperoxide decomposition leading to singlet oxygen release, and the structural features of hypoxia activated probes and prodrugs, a 2-pyridone-derived endoperoxide was designed and synthesized. The target compound shows significantly faster release of singlet oxygen under hypoxic conditions in cell cultures compared to normoxic conditions. The potential of this approach, especially regarding deep seated tumors with hypoxic regions, is exciting.

2.2 Introduction

Photodynamic Therapy (PDT) has been considered a cancer treatment methodology of great potential [58, 59]. This optimism stems from the fact,

i) EPR (enhanced permeation and retention) concentrates photosensitizers in the tumors,

ii) light can be directed to the tumor region (regioselectivity),

iii) the side effects are minimal,

iv) unlike the standard chemotherapy regimens, the immune response is enhanced [35].

However, more than 100 years after its initial discovery [60], clinical applications of PDT are still severely limited. The primary reason for this surprising state of affairs is the fact that two critical components of PDT, namely oxygen and light, are very scarce inside a tumor, regardless of the wavelength of the irradiation.

While recent years witnessed an impressive rise in the interest for photodynamic action and its control[61-67], until now there has been no convincing approach to successfully address these two pesky issues of light penetration and tumor hypoxia.

We are very much interested in transforming PDT into a more manageable and broadly applicable therapeutic protocol [31, 34, 68]. Our approach to achieve that is to separate photosensitization event from the delivery of singlet oxygen, which is the primary cytotoxic agent of PDT [30, 69]. Thus, a storage compound for singlet oxygen has to be designed, which can react with molecular oxygen under typical photosensitization conditions (Figure 13), and then the metastable compound has to be transferred to the tumor site which would release its cargo in response to a chemical or enzymatic cue. This approach assumes that singlet oxygen produced stoichiometrically (as opposed to catalytically through photosensitization) by the chemical transformation of the carrier molecule, would be enough to trigger apoptotic response in cancer cells.

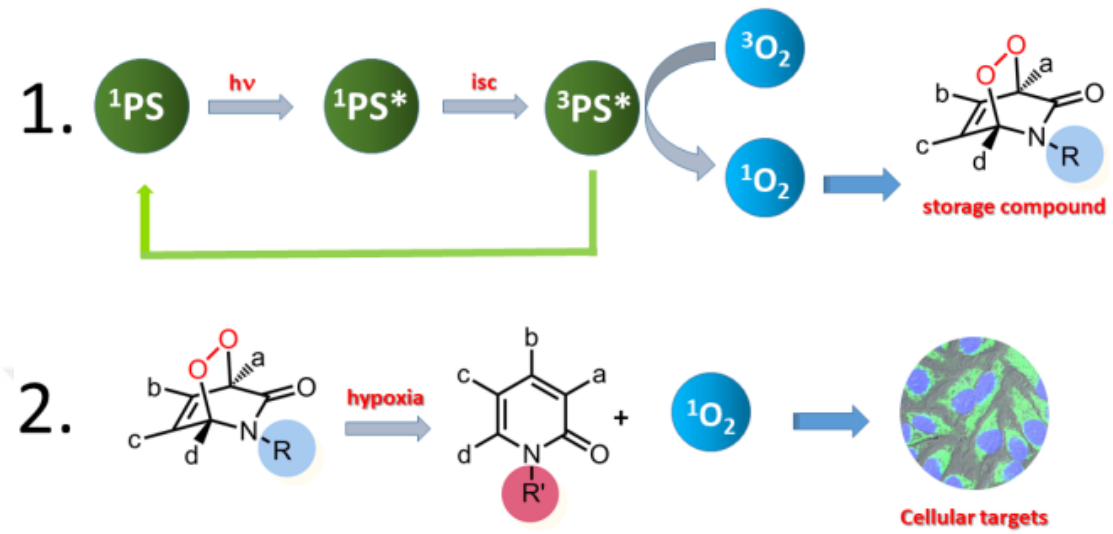

Figure 13. Two-stage, modified PDT concept, which does not require either O2 or light for in situ generation of singlet oxygen. Photosensitization is carried out ex situ, so the properties of the photosensitizer, or the wavelength of excitation is not relevant, as long as the endoperoxide can be obtained.

As for the storage compound for singlet oxygen, various arenes, 2-pyridone and furan derivatives were considered. They all form endoperoxides of varying thermal stabilities when reacted with singlet oxygen generated by photosensitization. Most of these endoperoxides release singlet oxygen when they undergo cycloreversion.

Kölemen et. al.[34] demonstrated that photothermally generated singlet oxygen from endoperoxides attached to gold nanorods clearly led to apoptosis in cancer cell cultures. Since endoperoxide decomposition rates generating singlet oxygen show a wide variation depending on the kind of the arene, and substituent-

related steroelectronic factors, they surmise that it should be possible to control singlet oxygen generation rates by structural changes which can be induced in vivo. This could generate singlet oxygen in principle, where it is needed without any need for oxygen or light.

2.3 Design of the pNZ-protected 2-pyridone-endoperoxide

Our goal in this project is to be able to develop a novel modality of cancer therapeutics. In a way, in can be interpreted as a fusion of Hypoxia Activated Prodrug (HAP) concept[56], with Photodynamic therapy ideas.

The initial objective of the proposed work is to synthesize a set of stable endoperoxides, which can be reduced under hypoxic conditions to form more labile endoperoxides.

The initial objective of the proposed work is to synthesize a set of stable endoperoxides, which can be reduced under hypoxic conditions to form more labile endoperoxides.

Both 2-pyridone endoperoxides and naphthalene endoperoxides, even with the limited amount of data vailable in the literature, show clear indications of highly variable cycloreversion rates depending on the steric and electronic nature of the substituents. Our assertion is that, it is possible to change the nature of the substituents drastically by bioreduction in a hypoxic tumor, so that singlet oxygen producing cycloreversion becomes much faster.

Synthesis of a library of endoperoxides with different substitution patterns are performed and characterized. After that, we studied the rate of cycloreversion of

endoperoxide compounds with different solvents and the rate constant and half-life calculations were done in accordance to the first-order reaction rate equations. The calculated values are summarized in the table Table 4.

Compounds	Half-life (Hour)
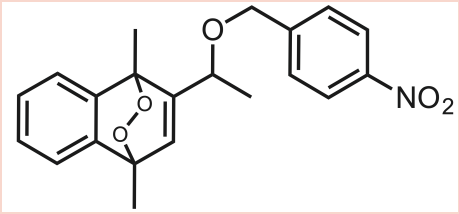	$t_{1/2}$ = 22.5 ($CDCl_3$)
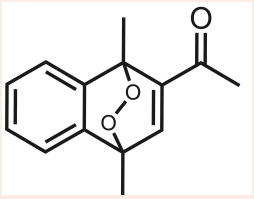	$t_{1/2}$ = 770 ($CDCl_3$)
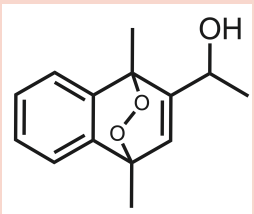	$t_{1/2}$ = 64.8 ($CDCl_3$) $t_{1/2}$ = 76 (DMSO-d_6) $t_{1/2}$ = 91 (DMSO-d_6/water (75/25)) $t_{1/2}$ = 106.6 (DMSO-d_6 /water (50/50))

Table 4. Cycloreversion rates of selected endoperoxides at 25 °C .

2-Pyridone endoperoxides were previously studied by us [31] and others [69] and known to be reliable sources for singlet oxygen. The cycloreversion is slower when the pyridone ring is substituted, and electron withdrawing substituents also decrease the reaction rate. On the other hand, hypoxia activated prodrugs [70] or hypoxia probes [71] make use of the reductive environment of the hypoxic tumor cells including overexpressed nitroreductase enzymes [72]. It is well known that formation of labile 4-aminobenzyloxy unit triggers a rapid bond cleavage

[73]. With these considerations, we targeted the synthesis of N-(4-nitrobenzyloxycarbonyl)-2-pyridone-endoperoxide, and we expected the cycloreversion of the pNZ-protected pyridine to be slower compared to the parent compound due to electron-withdrawing effect of the carbamate group (Figure 14). The protecting group can easily be removed under hypoxic/reductive conditions.

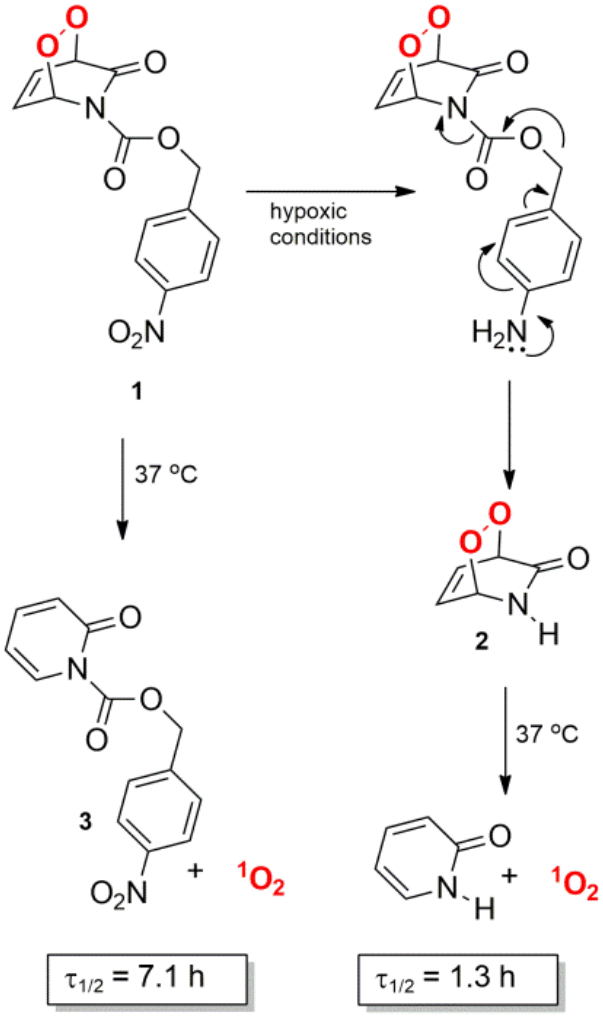

Figure 14. pNZ-protected 2-pyridone-endoperoxide (**1**) cycloreverts to the parent compound **3** with half-life of 7.1 hours at 37 °C. In cell cultures under hypoxic conditions, pNZ group is reductively eliminated. Resulting pyridone endoperoxide **2**, decomposes more than 5-fold faster.

2.4 Results and Discussion

Once we have the target compound in hand, to confirm our design expectations, we studied the rate of cycloreversion of endoperoxide compound **1** at 25 °C and 37 °C. Both reactions can be followed by 1H NMR. The half-life of the pNZ-endoperoxide (1) was 5.5 times larger. The difference in the reaction rates is large enough to have a differential impact in their effectiveness against cancer cells.

With the intention of getting more qualitative results, the NMR investigations of two systems were performed as a function of time, the solvent being $CDCl_3$. It was observed that the endoperoxide **1** had a half-life of **7.1** hours at 37 °C, while the endoperoxide **2** had a half-life of **1.3** hours according to appearance/disapearance of their normalized integral values of the selected peaks. The rate constant and half-life calculations were done in accordance to the first-order reaction rate equations. The equations are given below:

$$\ln[A] = -kt + \ln[A]_0 \quad , \quad t_{1/2} = 0.693/k \qquad \text{(Equation 1)}$$

In the following NMR spectra, it is possible to observe the evolution of peaks (7.42-7.38, 7.31, 6.67, 6.25 ppm) which belongs to Compound **3** due to endoperoxide cycloreversion. While the peaks of parent compound increases, the peaks of endoperoxide (Endoperoxide **1**) (6.85-6.81, 5.62, 5.15-5.13 ppm) decreases.

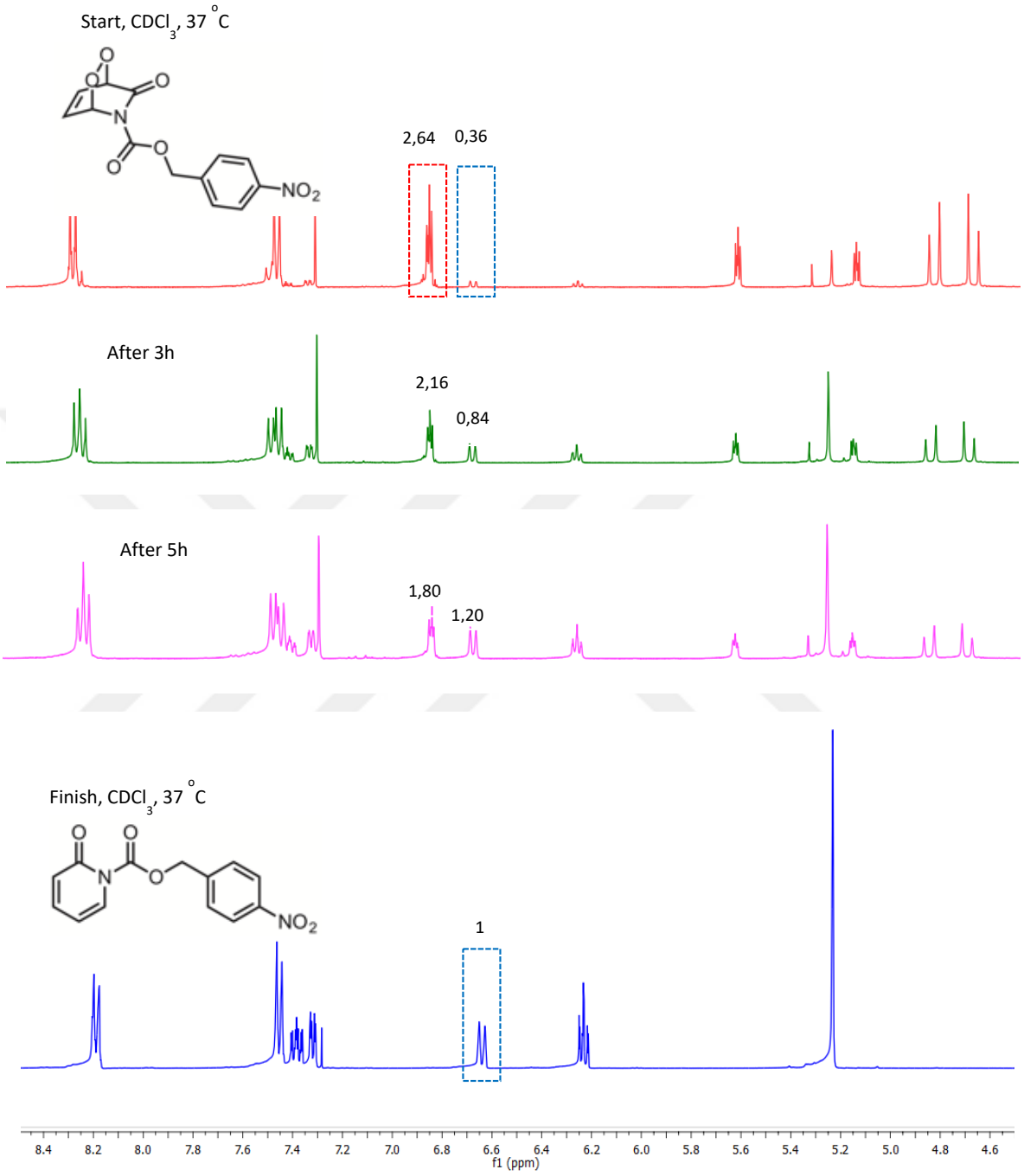

Figure 15. Evolution of the NMR spectra of Endoperoxide **1** with time at 37 °C in $CDCl_3$ as the solvent. (Spectra 0 hours (Endoperoxide **1**), Spectra after 3 hours, Spectra after 5 hours, the bottom spectra shows Compound 3).

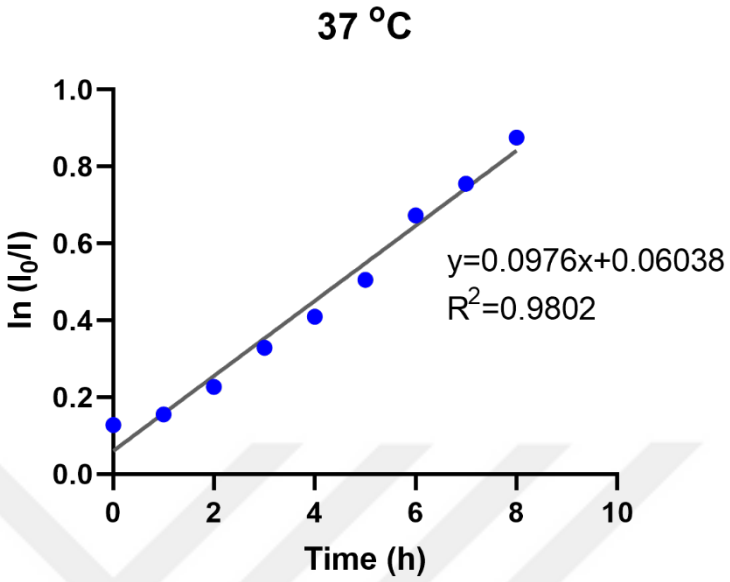

Figure 16. Decay of Endoperoxide **1** over time at 37 °C. The values obtained from ^{1}H NMR in $CDCl_3$. The half-life is calculated as 7.1 h according to the equation 1.

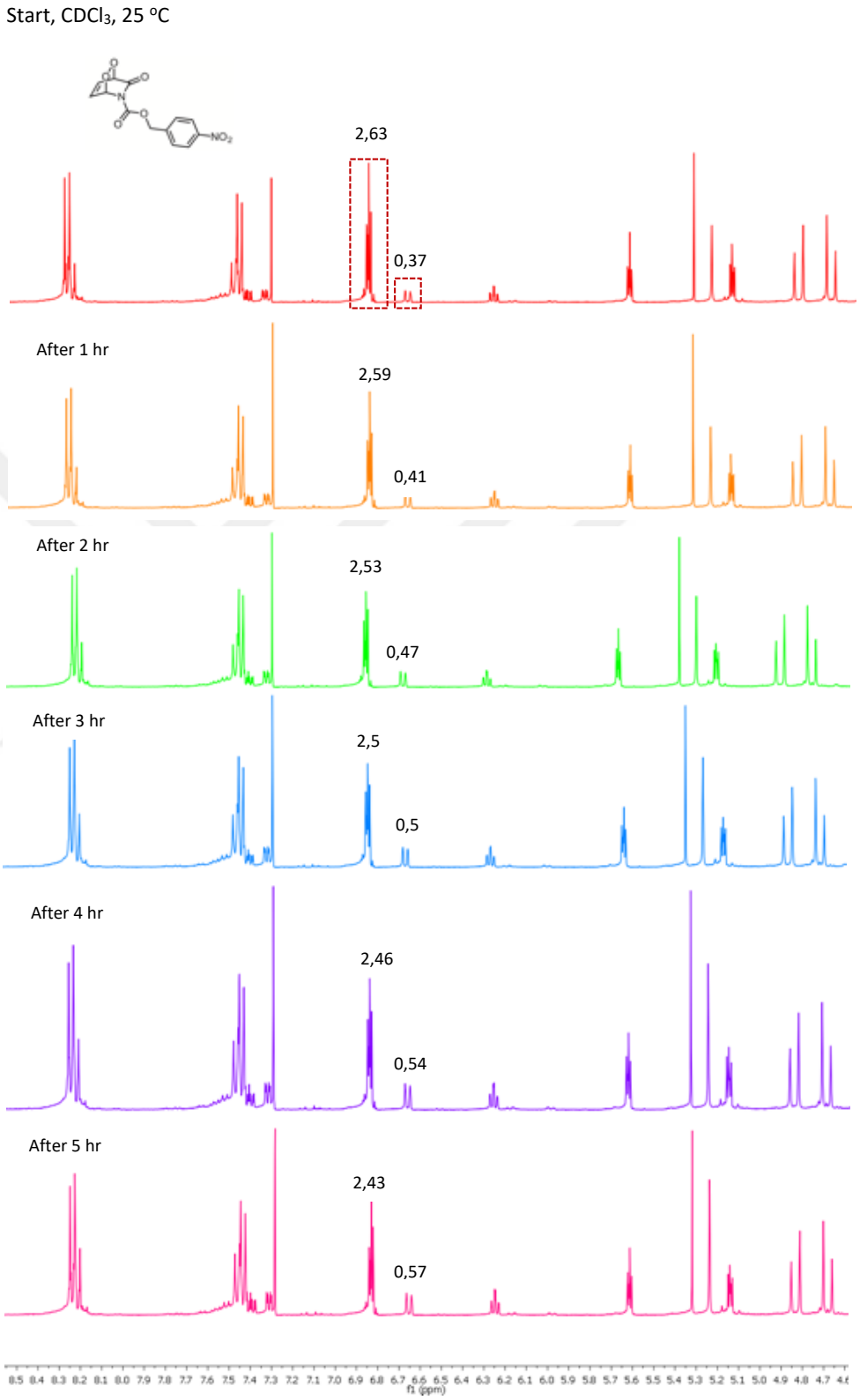

Figure 17. Evolution of the NMR spectra of Endoperoxide **1** with time at 25 ^{O}C in $CDCl_3$ as the solvent.

(Spectra 0 hours (Endoperoxide **1**)

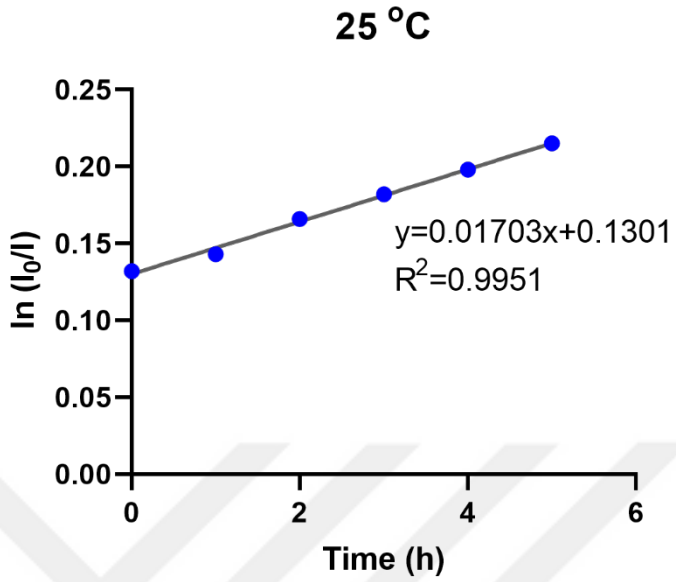

Figure 18. Decay of Endoperoxide **1** over time at 25 °C. The values obtained from ^{1}H NMR in $CDCl_3$. The half-life is calculated as 40.7 h according to the equation 1.

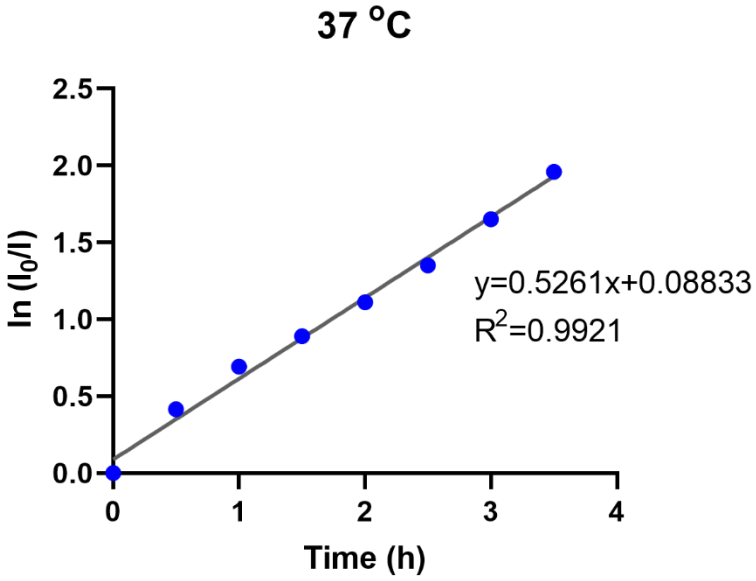

Figure 19. Decay of Endoperoxide **2** over time at 37 °C. The values obtained from ^{1}H NMR in $CDCl_3$. The half-life is calculated as 1.3 h according to the equation 1.

In order to investigate the cellular effects of the endoperoxide **1**, cell culture assays were performed with a human cancer suspension cell line-chronic myelogenous leukemia (K562) and a human breast adenocarcinoma cell line (MCF7).

In order to assess cytotoxicity of the target endoperoxide under normoxic and hypoxic conditions, cells were placed in a humidified modular incubator chamber containing 0.5% O_2, 5% CO_2 and 94.5% N_2 (v/v). Control cells were incubated in identical conditions for the same duration under normoxic conditions, 21% O_2, 5% CO_2 and 74% N_2 (v/v). When the cells reached to a confluency of larger than 70% in the culture conditions, they were seeded in 96-well plates for the MTT analyses. Cells were cultured for 24 h at normoxic conditions in order to achieve proper adhesion of the cells to the plates. Subsequently, hypoxic group of the cells were incubated 24 h further under conditions of hypoxia (pre-hypoxia [without endoperoxide treatment]); whereas, normoxic group of the cells were kept under normoxic conditions for the same period of time. While there is some toxicity of endoperoxide **1** even in normoxic conditions, the toxicity is more pronounced under hypoxic conditions.

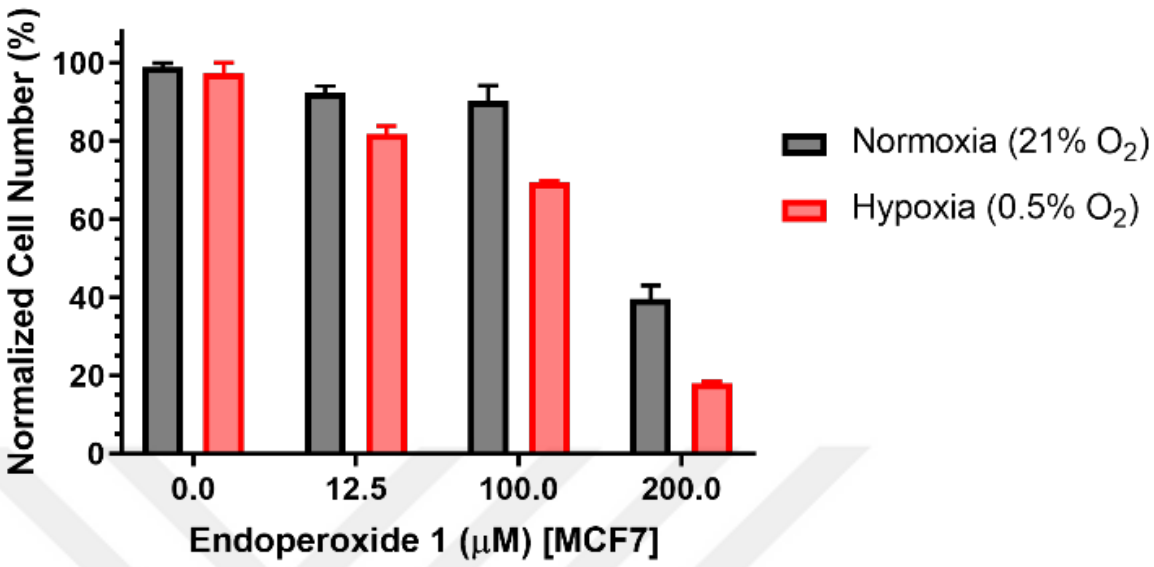

Figure 20. Cell viabilities of MCF7 breast cancer cells were evaluated with MTT assay after 24 hours of treatment with varying concentrations of the endoperoxide 1 under either normoxic or hypoxic conditions; and normalized cell numbers are shown (mean ± SEM, n = 3).

Red bars correspond to normalized cell number of MCF7 cells under hypoxic conditions. Grey bars correspond to cells kept under identical conditions of incubation with the agent, but under normoxic conditions. Positive control corresponds to cells incubated in DMSO-growth medium mixture (50/50, v/v), negative control corresponds to cells incubated in complete growth medium, without endoperoxide 1 treatment.

At 100 µM endoperoxide concentration cell death percentage is **10 %** under normoxia, whereas under hypoxia the cell death jumps to **31 %** as shown in figure 20. IC_{50} values were determined to be **185 µM** for normoxic and **120 µM** for hypoxic conditions. We also had to eliminate any complications that may arise from a possible cyto- toxicity of the compound **3** and any other reduction by-product.

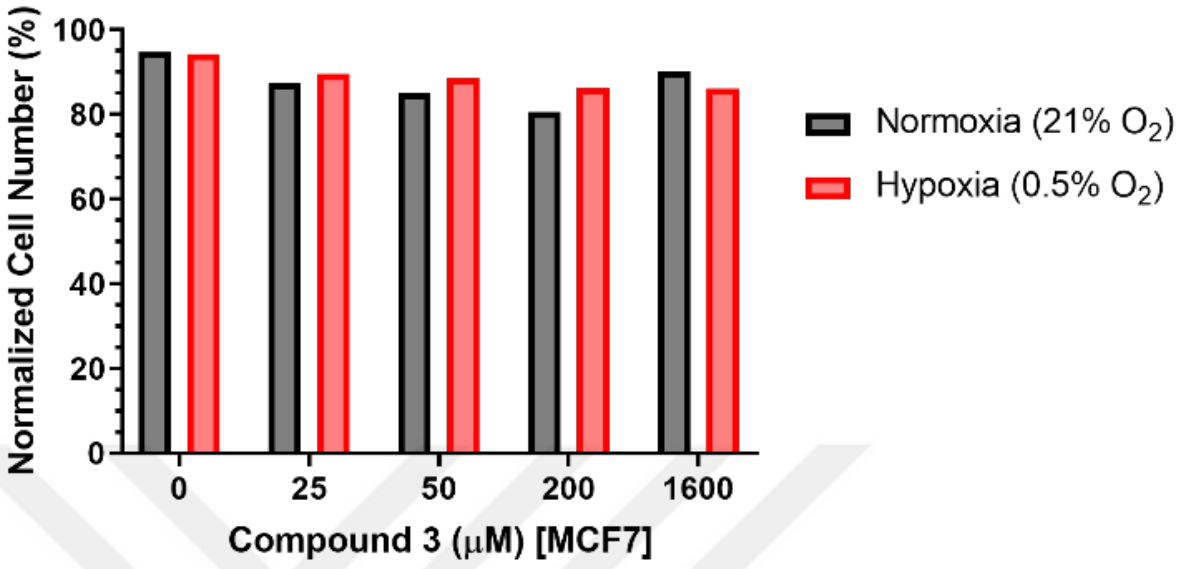

Figure 21. Cell viabilities of MCF7 breast cancer cells were evaluated with MTT assay after 24 hours of treatment with varying concentrations of control compound 3 under either normoxic or hypoxic conditions; and normalized cell numbers are shown.

Red bars correspond to normalized cell number of MCF7 cells under hypoxic conditions. Grey bars correspond to cells kept under identical conditions of incubation with the agent, but under normoxic conditions. Positive control corresponds to cells incubated in DMSO-growth medium mixture (50/50, v/v), negative control corresponds to cells incubated in complete growth medium, without control compound 3 treatment.

We demonstrated that (Figure 21) the control compound (compound 3) had no significant toxicity either under hypoxic or normoxic conditions, even at very large concentrations of 1.6 mM. Another interesting study we carried out was to follow the time course of cell viabilities. This is important because processes like the establishment of the hypoxic conditions, reductive elimination of pNZ group, release of singlet oxygen, they have to take place within a certain timeline, and it may be possible to observe some of those changes by recording cellular impedence. The temporal

profile of the effects of endoperoxide **1** on cancer cells (Figure 22) demonstrated potent cytotoxicity under hypoxic conditions, underlining the acute efficiency in hypoxia.

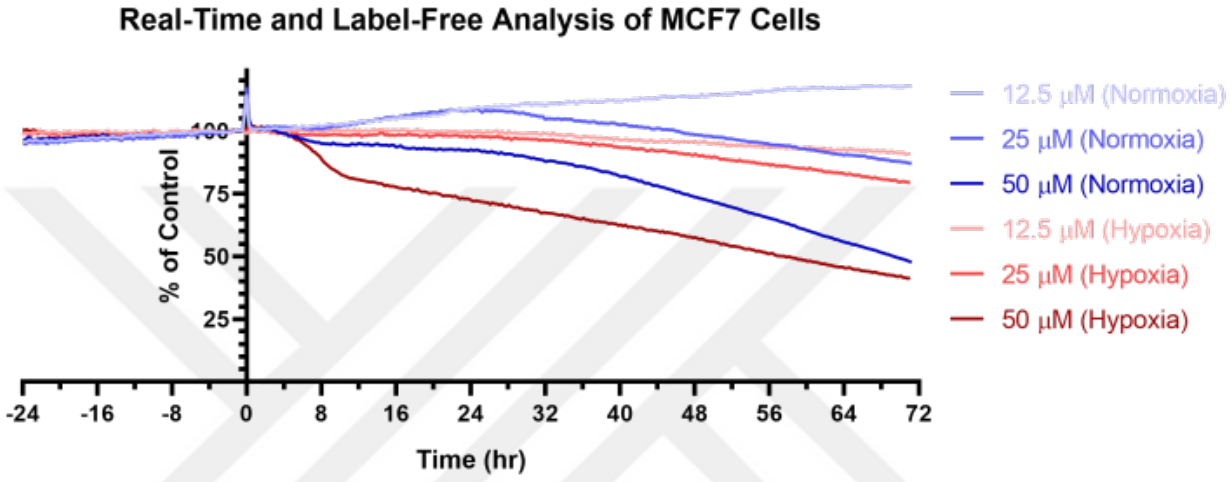

Figure 22. Cellular impedance analysis based cell viability assessment of MCF7 cells, as a function of time.

Red lines correspond to normalized cell number of MCF7 cells under hypoxic conditions (dark red: 50 µM, red: 25 µM, light red: 12.5 µM). Blue lines correspond to cells kept under identical conditions of incubation with the agent, but under normoxic conditions (dark blue: 50 µM, blue: 25 µM, light blue: 12.5 µM). Control corresponds to cells incubated in complete growth medium, without endoperoxide **1** treatment, under either normoxic or hypoxic conditions.

After a day of incubation under normoxic conditions, hypoxic group of the cells were incubated 24 h further under conditions of hypoxia (without endoperoxide **1** treatment); whereas, normoxic group of the cells were kept under normoxic conditions for the same period of time. At the end of this period, both groups of the cells were treated with varying concentrations of endoperoxide **1**. The hypoxia group of the cells

were incubated further under conditions of hypoxia with endoperoxide **1**; while normoxia group of the cells were incubated further under conditions of normoxia with endoperoxide **1**. The cell indices were measured by electrical impedance over an additional period of 72 hours. The results of each of the groups (hypoxia and normoxia) were normalized to relevant untreated control samples in either hypoxic or normoxic conditions, and the results were shown as a "percent of control" (t= 0 h corresponds to time of addition of endoperoxide, thus, 0 h values were used for the time point for temporal normalization). It is very significant that at 50 µM concentration of the endoperoxide **1**, there is significant dip in cell viability between 4-12 h region under hypoxia. Corresponding change under normoxic conditions is minimal. The KT50 (the amount of time it takes to kill 50% of the cancer cells) values for the 50 µM compound in the hypoxic and normoxic conditions were approximately **58.5 h** and **71.5 h**, respectively.

Flow cytometry is also useful in assessing differential cytotoxicity of the endoperoxide **1** under hypoxic and normoxic conditions. As singlet oxygen induces apoptosis, cells were incubated with FITC-Annexin V and then the change in the percentage of apoptotic fractions following endoperoxide **1** treatment were analysed.

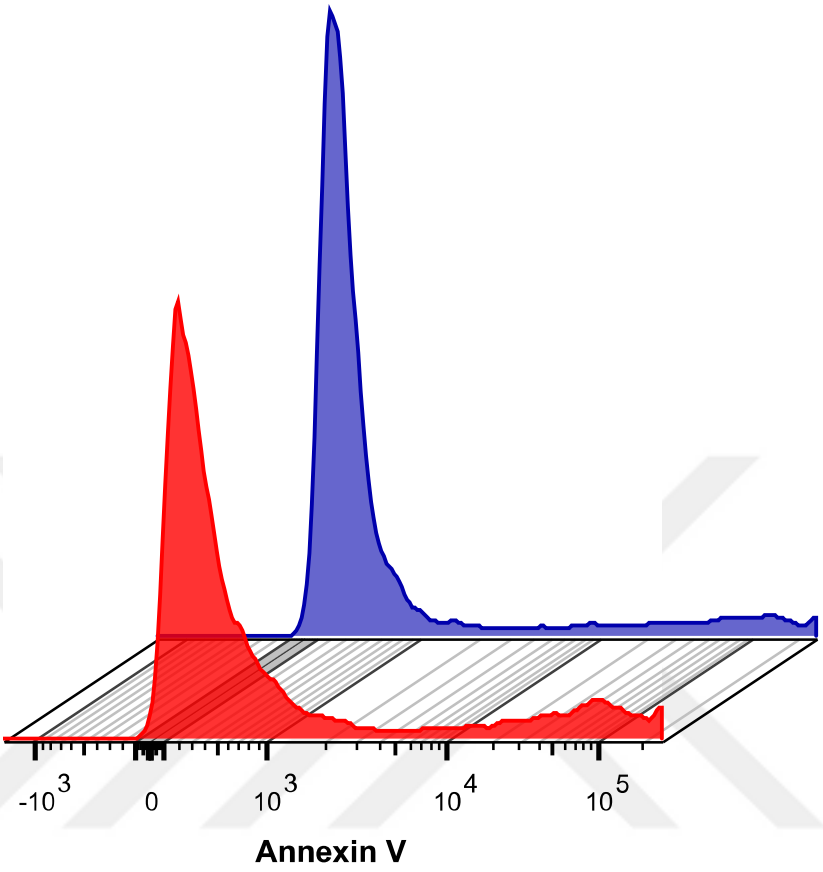

Figure 23. The percentage of FITC-Annexin V stained cells analyzed with flow cytometry was higher in the cells treated with 25 µM endoperoxide **1** under hypoxic conditions compared with the cells incubated under normoxic conditions.

Blue shaded area represents the cells incubated under normoxic conditions, red shaded area represents the cells incubated under hypoxic conditions) in the overlay graph.

The number of cells labelled with Annexin V is larger under hypoxia, compared to normoxia (**25.3**% vs. **16.0**% at 25 µM) (Figure 23). This is yet another demonstration of higher cytotoxicity of the endoperoxide **1** under hypoxic conditions.

2.5 Experimental Details

2.5.1 General Experimental Procedures

All reagents and solvents were purchased from commercial suppliers and used without further purification. Reactions were monitored by thin layer chromatography using Merck TLC Silica gel 60 F254. Column chromatography was performed by using Merck Silica Gel 60 (particle size: 0.040-0.063 mm, 230-400 mesh ASTM).

The ^{1}H and ^{13}C NMR spectra were recorded using Bruker DPX-400 (operating at 400 MHz for ^{1}H NMR and 100 MHz for ^{13}C NMR) at 298 K using deuterated solvents with tetramethylsilane (TMS) as internal standard. Chemical shifts were reported in parts per million (ppm) and coupling constants (*J* values) are given in Hz. Splitting patterns are indicated as follow s, singlet; d, doublet; t, triplet; m, multiplet. Mass spectra were recorded with Agilent Technologies 6224 TOF LC/MS.

2.5.2 Synthesis

Synthesis of Compound 3

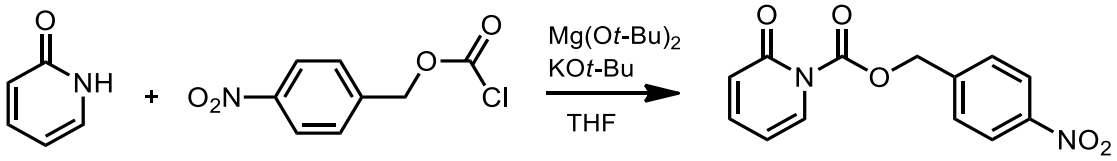

$Mg(O\textit{t}\text{-}Bu)_2$ (896 mg, 5.26 mmol, 1.05 eq), KO*t*-Bu (309.7 mg, 2.76 mmol, 1.05 eq) and 2-pyridone (250 mg, 2.63 mmol, 1 eq) were added to schelenk tube. After purged with argon, dry THF (3 mL) was added and stirred for 10 min. To the resulting mixture was

charged 4-nitrobenzyl chloroformate (850 mg, 3.94 mmol, 1.5 eq). The resulting mixture was stirred at room temperature for 2.5 h and then heated at 35 °C for 48h. The reaction mixture was cooled to room temperature and quenched with HCl (3M, 6 mL). The mixture was extracted with EtOAc. The combined organic layers were dried over Na_2SO_4 and concentrated in vacuo. The crude product was purified by column chromatography and then preparative thin layer chromatography using DCM:MeOH (98:2, v/v). Compound 1 was obtained as yellowish solid (64 mg, 9%).

^{1}H NMR (400 MHz, $CDCl_3$): δ 8.22 (d, *J* = 8.8 Hz, 2H), 7.47 (d, *J* = 8.4 Hz, 2H), 7.42-7.38 (m, 1H) 7.31 (dd, J_1 = 2.0 Hz, J_2=4.8 Hz, 1H), 6.67 (d, *J* = 10.0 Hz, 1H), 6.25 (dt, J_1 = 1.2 Hz, J_2 = 6.8 Hz, 1H), 5.25 (s, 2H).

^{13}C NMR (100 MHz, $CDCl_3$): δ 139.9, 137.1, 128.6, 124.1, 121.7, 106.7, 51.8.

MS (TOF-ESI) m/z calcd for $C_{13}H_{10}N_2O_5$: 275.06625 $[M+H]^+$, found 275.06354 $[M+H]^+$, Δ= 9.84 ppm

Synthesis of Endoperoxide 1

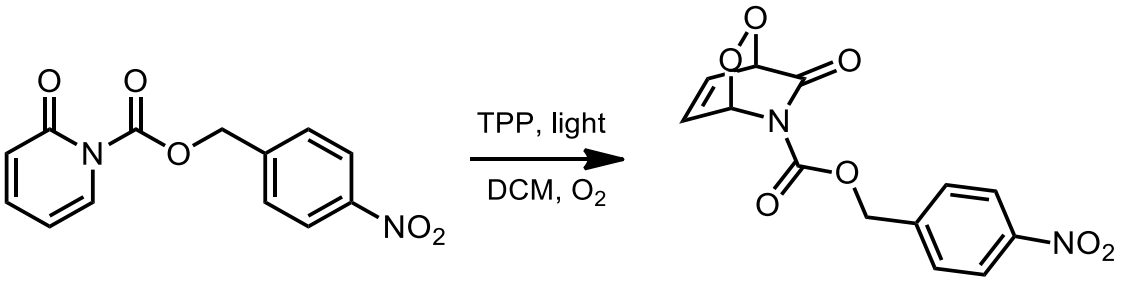

Compound **3** (33.4 mg, 0.122 mmol) was dissolved in DCM. TPP (~5.0 mg) was added to the reaction mixture at -78 °C which was irradiated while oxygen gas was passing through it. The progress of the reaction was monitored by TLC. When TLC showed no

starting material, the mixture was concentrated in vacuo at 25 °C and the residue was purified by silica gel flash column chromatography with DCM:MeOH (99:1, v/v) as the eluent. Compound **2** was obtained as pale yellowish solid (30 mg, 81%).

^{1}H NMR (400 MHz, $CDCl_3$): δ 8.23 (d, *J* = 8.8 Hz, 2H), 7.43 (d, *J* = 8.8 Hz, 2H), 6.85-6.81 (m, 2H), 5.62 (t, *J* = 4.0 Hz, 1H), 5.15-5.13 (m, 1H), 4.83 (d, *J* = 16 Hz, 1H), 4.68 (d, *J* = 16.0 Hz, 1H).

MS (TOF-ESI) m/z calcd for $C_{13}H_{10}N_2O_7$: 305.04152 $[M-H]^-$, found 305.04066 $[M-H]^-$, Δ= 2.83 ppm

Cell Studies

Cell Culture:

In order to investigate the cellular effects of the endoperoxide **1**, cell culture assays were performed with a human cancer suspension cell line-chronic myelogenous leukemia (K562) and a human breast adenocarcinoma cell line (MCF7). K562 cells were incubated in 25 cm^3 culture flasks with Dulbecco's Modified Eagle Medium (DMEM) supplemented with 20 % FBS at the environmental conditions of 37 ^oC, 5% CO_2 and 60 % humidity. MCF7 cells were incubated in 25 cm^2 culture flasks with Dulbecco's Modified Eagle Medium (DMEM) supplemented with 10% FBS at the environmental conditions of 37 ^oC, 5% CO_2 and 60% humidity. Cells were exposed to varying concentrations of the endoperoxide **1** and incubated under conditions of either normoxia (21% O_2, 5% CO_2, 74% N_2) or hypoxia (0.5% O_2, 5% CO_2, 94.5% N_2). Untreated

samples were used as negative controls for both of the drug treatments under hypoxia or normoxia.

2.5.3 Hypoxia Treatment

In order to simulate hypoxic conditions, cells were placed in a humidified modular incubator chamber (Billups-Rothenberg, Inc., USA) [74] containing 0.5% O_2, 5% CO_2 and 94.5% N_2 (v/v), by flushing the gas mixture for at least 6 min at a flow rate of 30 L min^{-1}. The modular incubator chamber was then sealed and placed in a conventional cell incubator at 37 ^oC. The chamber was re-flushed after 1 hour of incubating to remove any residual trapped gasses. Control cells were incubated in identical conditions for the same duration under normoxic conditions, 21% O_2, 5% CO_2 and 74% N_2 (v/v). When the cells reached to a confluency of >70% in the culture conditions, they were seeded in 96-well plates for the MTT analyses and in E-Plates for the real-time and label-free analyses with the iCELLigence system. Cells were cultured for 24 h at normoxic conditions in order to achieve proper adhesion of the cells to the plates. Subsequently, hypoxic group of the cells were incubated 24 h further under conditions of hypoxia (pre-hypoxia [without drug treatment]); whereas, normoxic group of the cells were kept under normoxic conditions for the same period of time.

2.5.4 MTT Assay

The main *in vitro* functional goal of the current study is to study the difference of cytotoxicity of endoperoxide **1** under hypoxic and normoxic conditions. Both normoxia

group and the hypoxia group (at the end of the pre-hypoxia period) of the cells were treated with varying concentrations of endoperoxide **1**. The compound was diluted in cell culture medium and assay concentrations were freshly prepared. The hypoxia group of the cells were incubated further under conditions of hypoxia with endoperoxide **1**; while normoxia group of the cells were incubated further under conditions of normoxia with endoperoxide **1**. Untreated samples were used as negative controls for both of the drug treatments under hypoxia or normoxia. Cell viability / death was evaluated by MTT (3-(4, 5-dimethylthiazolyl-2)-2,5-diphenyltetrazolium bromide) assay. Briefly, 50 µL cell suspensions in culture medium containing MCF7 or K562 cells were plated in 96-well flat-bottom culture plates (Corning, MA, USA) and incubated for 24 hours to recover from handling. Varying concentrations of the chemical compound in cell culture medium was added into each well in triplicate. The experimental group of the cells were incubated under hypoxic conditions, as explained in the "4.2. Hypoxia Treatment" section. The normoxia group of the cells were incubated in normoxic conditons, for the exact duration under identical environmental conditions except O_2 tension. According to the assay protocol, 25 µl of the MTT reagent (Sigma-Aldrich, MO, USA) was added to each well in order to assess cell viability (final concentration: 1 mg/ml) at the end of the 24-h drug treatment period. Following a 4-h incubation of the cells with the MTT reagent, the generated formazan precipitates were solubilized by the addition of the lysing buffer (80 µL, pH: 4.7), which is composed of 23% SDS (Sodium dodecyl sulfate) dissolved in a solution of 45% DMF (N,N-Dimethylformamide). After an overnight incubation at 37 ^{o}C, the absorbance values (of

each well) were measured at 570 nm in a microtiter plate reader (Spectramax Plus, Molecular Devices, CA, USA) at 25 °C. Cells incubated in culture medium only (without the compound) served as the control for cell viability for the plates incubated in either hypoxia or normoxia; whereas DMSO (50%, v/v) was used to observe maximum cell death (positive control).

The results of each of the groups (hypoxia and normoxia) were normalized to untreated negative control samples in either hypoxic or normoxic conditions. Therefore, the sole effect of hypoxic conditions (without drug treatment) on the cells could be eliminated and the observed effects in MTT results were made sure to be due to the effects of endoperoxide **1**, solely.

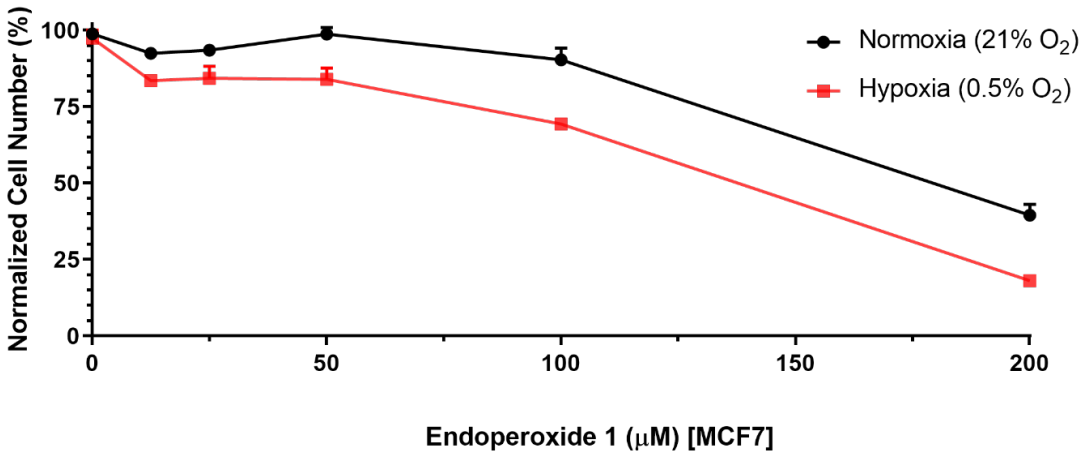

Figure 24. Endoperoxide **1** achieves potent cytotoxicity on cancer cells under conditions of hypoxia. Cell viabilities of MCF7 breast cancer cells were evaluated with MTT assay after 24 hours of treatment with varying concentrations of endoperoxide **1** under either normoxic (IC50: 185 μM) or hypoxic (IC50:120 μM) conditions; and normalized cell numbers are shown (mean ± SEM, n = 3). Red line corresponds to normalized cell number of MCF7 cells under hypoxic conditions. Black line corresponds

to cells kept under identical conditions of incubation with the agent, but under normoxic conditions. Positive control corresponds to cells incubated in DMSO-growth medium mixture (50/50, v/v), negative control corresponds to cells incubated in complete growth medium, without endoperoxide **1** treatment.

Lower doses of endoperoxide **1** seem to have resulted in a significant decrease of the cell viability under hypoxic conditions (Figure 24, points and error bars designate means and SEM, respectively), in contrast to normoxic conditions. The IC_{50} values of the compound in the hypoxic and normoxic conditions were estimated by fitting a model with non-linear regression (approximately 120 µM under hypoxia and 185 µM under normoxia for MCF cells [Figure 24]; 28 µM under hypoxia and 40 µM under normoxia for K562 cells [Figure 25]). On the contrary, control compound **3** does not cause any cytotoxicity on cancer cells under conditions of hypoxia or normoxia (Figure 21).

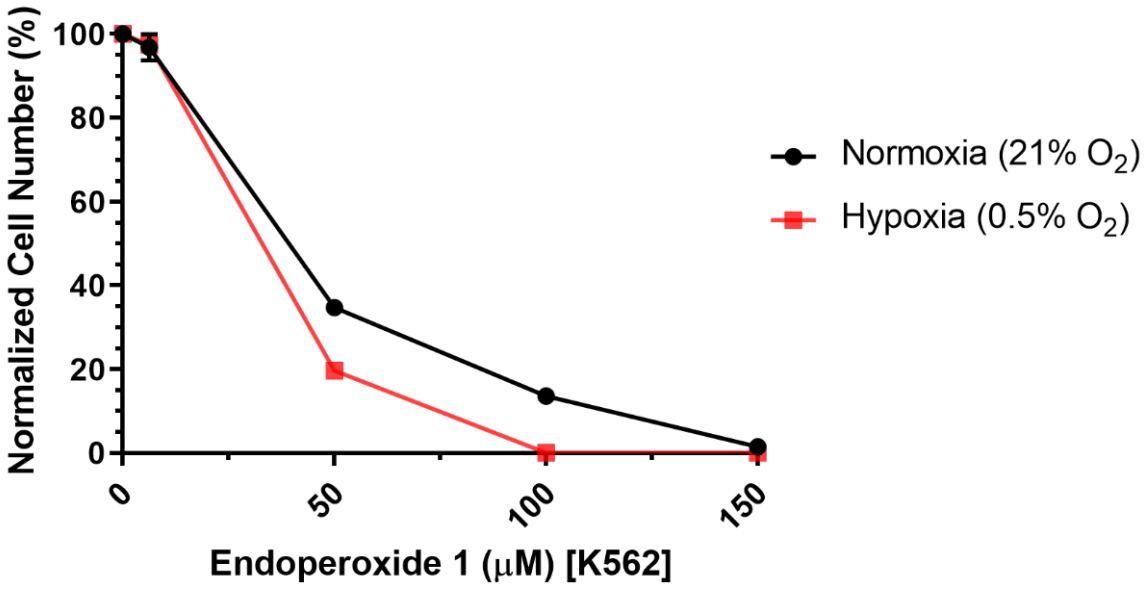

Figure 25. Endoperoxide **1** achieves potent cytotoxicity on cancer cells under conditions of hypoxia.

Cell viabilities of K562 human chronic myelogenous leukemia cells were evaluated with MTT assay after 24 hours of treatment with varying concentrations of endoperoxide **1** under either normoxic (IC50: 40 µM) or hypoxic (IC50: 28 µM) conditions; and normalized cell numbers are shown (mean ± SEM, n = 3). Red line corresponds to normalized cell number of K562 cells under hypoxic conditions. Black line corresponds to cells kept under identical conditions of incubation with the agent, but under normoxic conditions. Positive control corresponds to cells incubated in DMSO-growth medium mixture (50/50, v/v), negative control corresponds to cells incubated in complete growth medium, without endoperoxide 1 treatment.

2.5.6 Real-time and Label-free Analyses of Cells with the iCELLigence System

In order to reveal the temporal profile of the endoperoxide **1** responses in real time, allowing for the observation of both acute responses and longer-term responses within the same assay; we performed functional analyses with the RTCA iCELLigence System (ACEA, San Diego, CA, USA) [75]. This approach provides a method for spatial and temporal dynamic view of the cell populations with the effect of endoperoxide **1** under hypoxic or normoxic conditions. As a result, both the short- and long-term effects of endoperoxide **1** under hypoxia and normoxia could be visualized, at an unprecedented level of detail. The system utilizes gold biosensor microelectrodes to measure electrical impedance. The background impedances of the microelectrodes were first measured with cell culture medium. Then, MCF7 cancer cells were added to each well of the E-Plate and cultured for 24 h at normoxic conditions in order to achieve proper adhesion of the cells to the E-Plates. Subsequently, hypoxic group of the cells were incubated 24 h further under conditions of hypoxia (pre-hypoxia [without drug treatment]); whereas, normoxic group of the cells were kept under normoxic conditions for the same period

of time (as explained in the "Hypoxia Treatment" section). At the end of this period, both groups of the cells were treated with varying concentrations of endoperoxide **1**. The hypoxia group of the cells were incubated further under conditions of hypoxia with endoperoxide **1**; while normoxia group of the cells were incubated further under conditions of normoxia with endoperoxide **1**. The cell indices were measured by electrical impedance over an additional period of 72 hours. Untreated samples were used as negative controls for both of the drug treatments under hypoxia or normoxia. The results of each of the groups (hypoxia and normoxia) were normalized to relevant untreated negative control samples in either hypoxic or normoxic conditions, and the results were shown as a "% of Control". Therefore, the sole effect of hypoxic conditions (without drug treatment) on the cells could be eliminated and the observed effects in iCELLigence results were made sure to be due to the effects of endoperoxide **1**, exclusively.

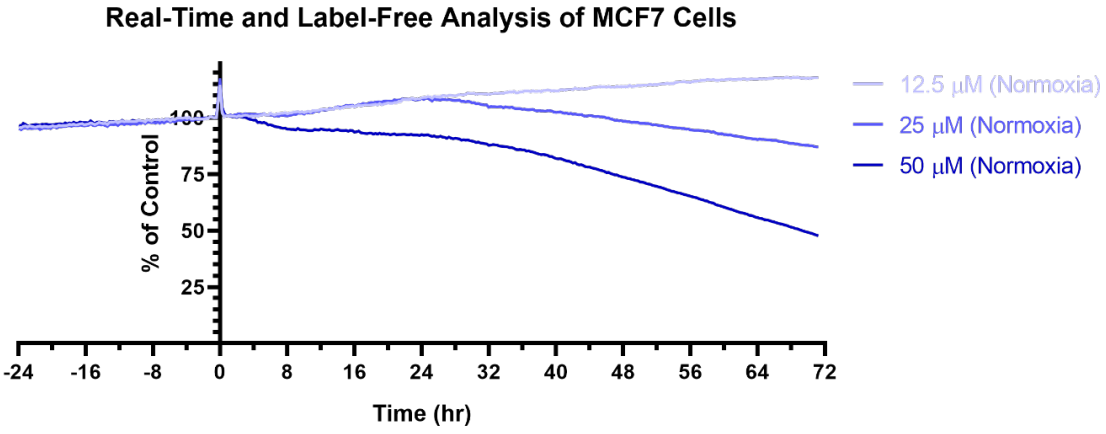

Figure 26. The temporal profile of the effects of endoperoxide **1** on cancer cells under normoxic conditions. MCF7 cells were seeded in ACEA E-Plates. After 48 h of incubation under normoxic conditions, the cells were treated with varying concentrations of endoperoxide **1**.

The cells were then incubated further under conditions of normoxia with endoperoxide **1**. The cell indices were measured by electrical impedance over an additional period of 72 hours. Blue lines correspond to normalized cell number of MCF7 cells under normoxic conditions (dark blue: 50 µM, blue: 25 µM, light blue: 12.5 µM). Control corresponds to cells incubated in complete growth medium, without endoperoxide **1** treatment, under normoxic conditions. The results of the groups were normalized to untreated control samples in normoxic conditions, and the results were shown as a "% of Control" (drug treatments were initiated at 0 h; thus, 0 h was used as the time for temporal normalization). The KT_{50} (the amount of time it takes to kill 50% of the cancer cells) value of the 50 µM compound in normoxic condition was approximately 71.5 h. The KT_{50} for 25 µM compound in normoxia was approximately 149.5 h. The KT_{50} value of 12.5 µM compound in the normoxic condition cannot be estimated since its projection is way out of the scale of the model fit.

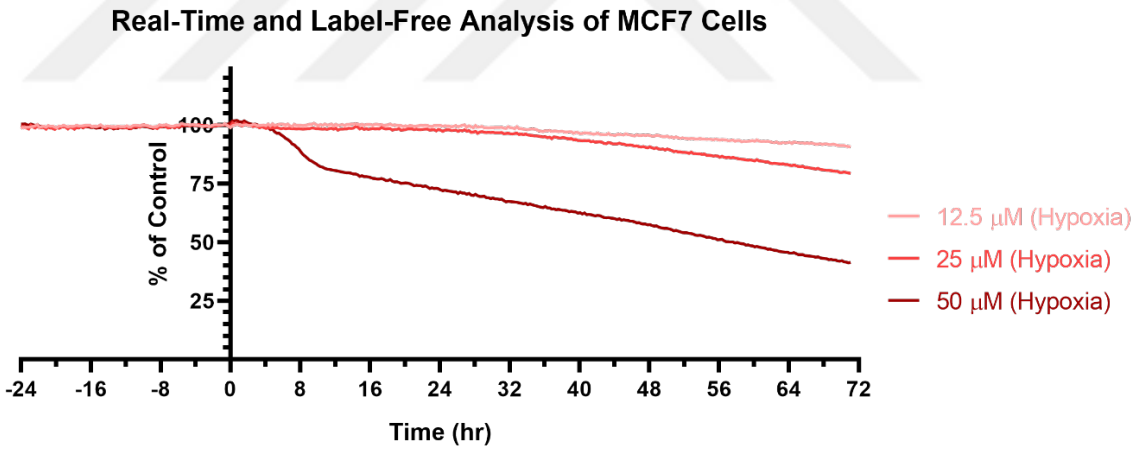

Figure 27. The temporal profile of the effects of endoperoxide **1** on cancer cells demonstrated potent cytotoxicity under hypoxic conditions, underlining the acute efficiency in hypoxia. MCF7 cells were seeded in ACEA E-Plates. After a day of incubation under normoxic conditions, hypoxic group of the cells were incubated 24 h further under conditions of hypoxia (pre-hypoxia [without drug treatment]).

At the end of this period, the cells were treated with varying concentrations of endoperoxide **1**; and they were incubated further under conditions of hypoxia with endoperoxide **1**. The cell indices were measured by electrical impedance over an additional period of 72 hours. Red lines correspond to

normalized cell number of MCF7 cells under hypoxic conditions (dark red: 50 µM, red: 25 µM, light red: 12.5 µM). Control corresponds to cells incubated in complete growth medium, without endoperoxide **1** treatment, under hypoxic conditions. The results of the groups were normalized to untreated control samples in hypoxic conditions, and the results were shown as a "% of Control" (drug treatments were initiated at 0 h; thus, 0 h was used as the time for temporal normalization). The KT_{50} (the amount of time it takes to kill 50% of the cancer cells) value of the 50 µM compound in hypoxic conditions was approximately 58.5 h. The KT_{50} for 25 µM compound in hypoxia was approximately 138.5 h and the KT_{50} for 12.5 µM compound in hypoxia was approximately 200 h.

Lower doses of endoperoxide **1** seem to have resulted in a significant decrease of the cell viability under hypoxic conditions at a much earlier time (Figure 26, Figure 27), in contrast to normoxic conditions (Figure 28 demonstrates iCELLigence results for HeLa cells). The KT_{50} (the amount of time it takes to kill 50% of the cancer cells) values of the 50 µM compound in the hypoxic and normoxic conditions were approximately 58.5 h and 71.5 h, respectively. The KT_{50} for 25 µM compound in hypoxia and normoxia were approximately 138.5 h and 149.5 h, respectively. The KT_{50} for 12.5 µM compound in hypoxia was approximately 200 h; whereas, the KT_{50} value of 12.5 µM compound in the normoxic condition cannot be estimated since its projection is way out of the scale of the model fit. It is important to note the acute effect of the compound seen under hypoxia at 50 µM (initial ~10 h) in contrast to late-onset effects under normoxia. In summary, our results show the value of such a real-time approach in measuring the cytotoxic response across the temporal scale, clearly demonstrating the value of endoperoxide **1** at a temporal dimension.

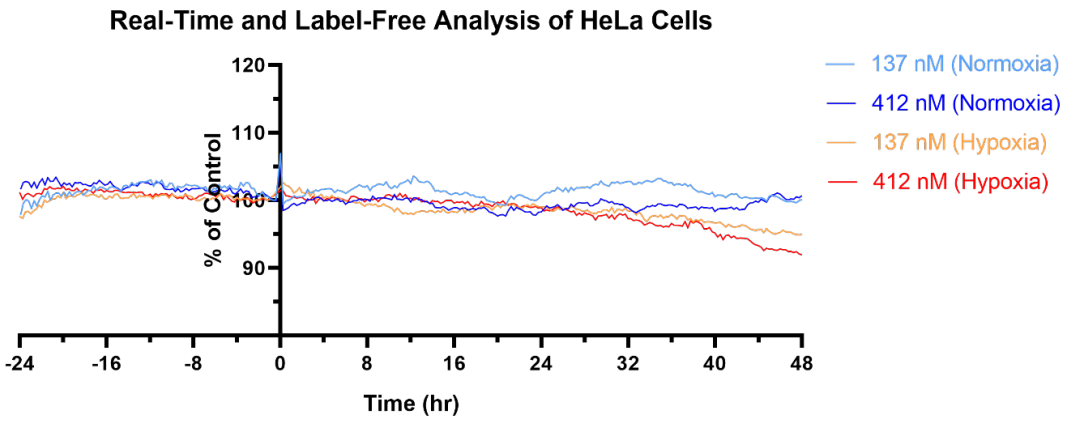

Figure 28. The temporal profile of the effects of endoperoxide **1** on cancer cells demonstrated potent cytotoxicity under hypoxic conditions. HeLa cells were seeded in ACEA E-Plates. After a day of incubation under normoxic conditions, both groups of the cells were treated with varying concentrations of endoperoxide **1**.

HeLa human cervix adenocarcinoma cells were cultured in 25 cm^2 culture flasks containing Dulbecco's Modified Eagle Medium (DMEM, Gibco, 11971-025) supplemented with 10 % fetal bovine serum in a cell culture incubator at 37°C, 5 % CO_2 and 60 % humidity. The hypoxia group of the cells were incubated further under conditions of hypoxia with endoperoxide **1**; while normoxia group of the cells were incubated further under conditions of normoxia with endoperoxide **1**. The cell indices were measured by electrical impedance over an additional period of 48 hours. Lines correspond to normalized cell number of HeLa cells under hypoxic or normoxic conditions (red: 412 nM in hypoxia, orange: 137 nM in hypoxia, blue: 412 nM in normoxia, turquoise: 137 nM in normoxia). Control corresponds to cells incubated in complete growth medium, without endoperoxide **1** treatment, under either normoxic or hypoxic conditions. The results of each of the groups (hypoxia and normoxia) were normalized to relevant untreated control samples in either hypoxic or normoxic conditions, and the results were shown as a "% of Control" (drug treatments were initiated at 0 h; thus, 0 h was used as the time for temporal normalization). The KT_{50} (the amount of time it takes to kill 50% of the cancer cells) values of the 412 nM and 137 nM compound in hypoxic conditions were estimated approximately as

108.5 h and 264.5 h, respectively. The KT_{50} values of 412 nM and 137 nM compound in the normoxic conditions cannot be estimated since their projections are way out of the scale of the model fit.

2.5.7 Flow Cytometry

In order to confirm our cytotoxicity results, Annexin V detection protocol for apoptosis using flow cytometry was performed. Annexin V flow cytometric analysis on adherent cell types (e.g MCF7, HeLa) is not routinely tested; since specific membrane damage may occur during cell detachment or harvesting. Therefore, Annexin V flow cytometric analyses were performed with a human cancer suspension cell line-chronic myelogenous leukemia (K562). K562 cells treated with endoperoxide **1** under either hypoxic or normoxic conditions were stained with Annexin V (Fluorescein isothiocyanate-FITC), as described in the technical data sheet (BD Pharmingen, USA), and were analyzed by FACS Aria II (equipped with 488 nm and 635 nm lasers) using FACS Diva software. The percentage of fluorochrome-labeled Annexin V (FITC) stained cells analyzed with flow cytometry was higher in the cells treated with endoperoxide **1** under hypoxic conditions compared with the ones incubated under normoxic conditions (25.3 % vs. 16.0 % at 25 µM and 18.3% vs. 6.75% at 12.5 µM; Figures 26-30; blue shaded areas represent the cells incubated under normoxic conditions, red shaded areas represent the cells incubated under hypoxic conditions). Our Annexin V analyses with flow cytometry confirmed both the MTT and iCELLigence results, concerning the difference of effects under hypoxia vs. normoxia. In addition, analyses of cell viability by Trypan blue stain further confirmed these results.

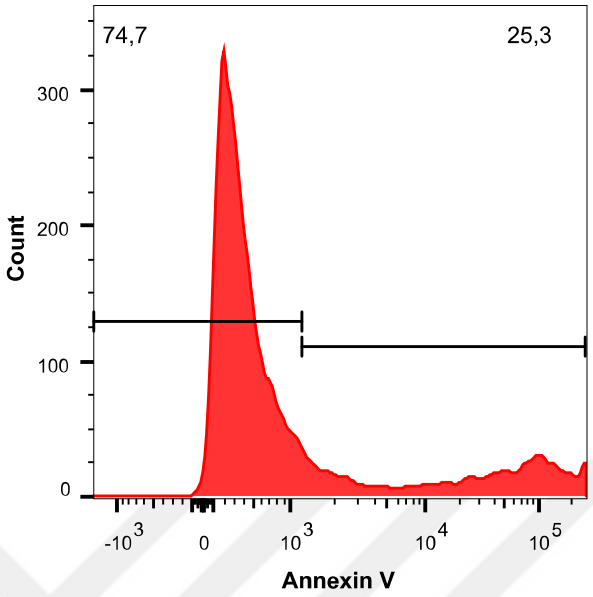

Figure 29. Endoperoxide **1** potently induces apoptosis in cancer cells under conditions of hypoxia. The percentage of FITC-Annexin V stained cells analyzed with flow cytometry was 25.3 % in the cells treated with 25 µM endoperoxide **1** under hypoxic conditions. Red shaded area represents the cells incubated under hypoxic conditions in the histogram.

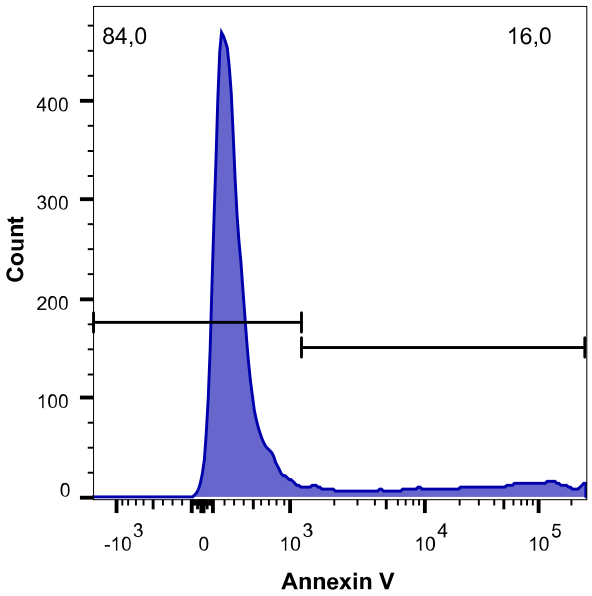

Figure 30. The effect of endoperoxide **1** on apoptosis in cancer cells under conditions of normoxia.

The percentage of FITC-Annexin V stained cells analyzed with flow cytometry was 16.0 % in the cells treated with 25 µM endoperoxide **1** under normoxic conditions. Blue shaded area represents the cells incubated under normoxic conditions in the histogram.

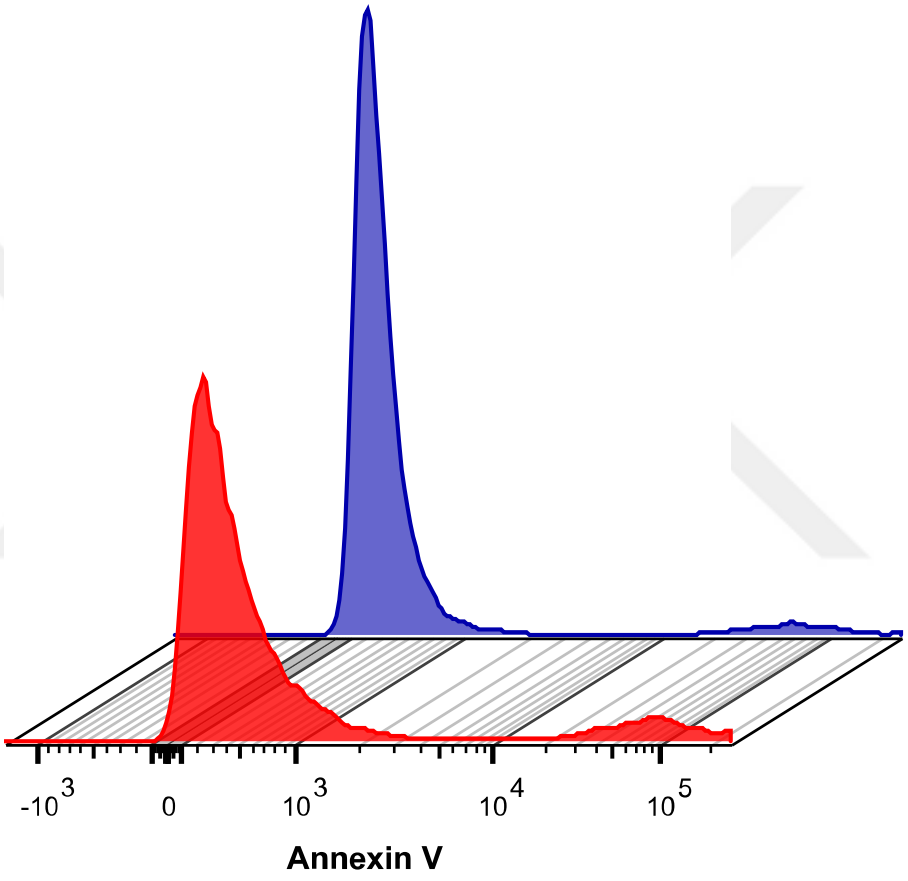

Figure 31. Endoperoxide **1** potently induces apoptosis in cancer cells under conditions of hypoxia. The percentage of FITC-Annexin V stained cells analyzed with flow cytometry was higher in the cells treated with 12.5 µM endoperoxide **1** under hypoxic conditions compared with the ones incubated under normoxic conditions (18.3% vs. 6.75% at 12.5 µM). Blue shaded area represents the cells incubated under normoxic conditions, red shaded area represents the cells incubated under hypoxic conditions) in the overlay graph.

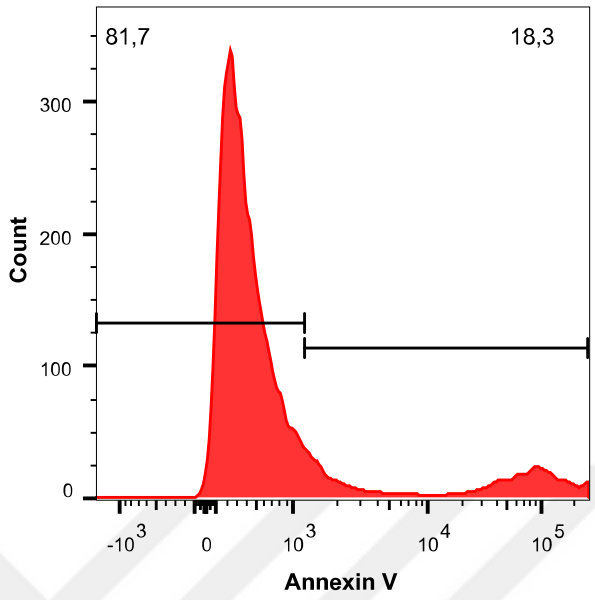

Figure 32. Endoperoxide 1 potently induces apoptosis in cancer cells under conditions of hypoxia. The percentage of FITC-Annexin V stained cells analyzed with flow cytometry was 18.3 % in the cells treated with 12.5 µM endoperoxide **1** under hypoxic conditions. Red shaded area represents the cells incubated under hypoxic conditions in the histogram.

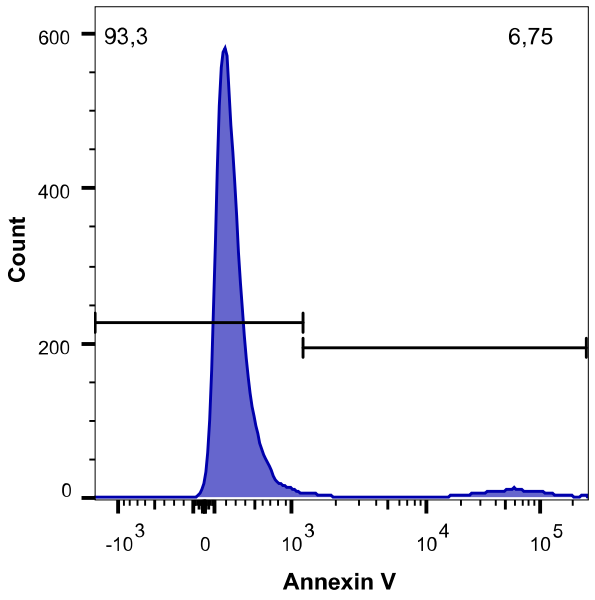

Figure 33. The effect of endoperoxide 1 on apoptosis in cancer cells under conditions of normoxia. The percentage of FITC-Annexin V stained cells analyzed with flow cytometry was 6.75 % in the cells

treated with 12.5 μM endoperoxide **1** under normoxic conditions. Blue shaded area represents the cells incubated under normoxic conditions in the histogram.

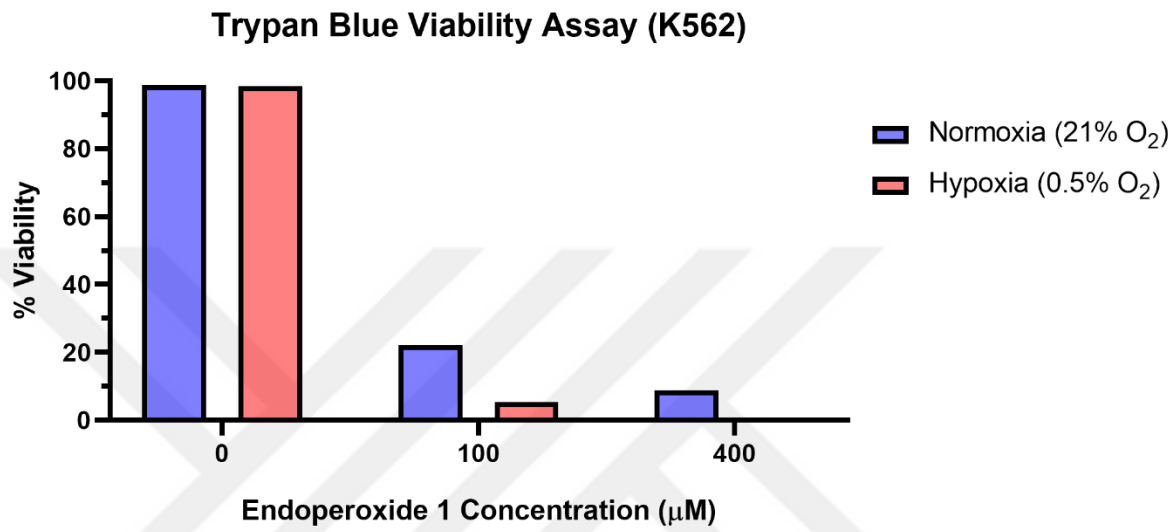

Figure 34. Analysis of K562 cell viability by Trypan blue stain demonstrated that endoperoxide **1** achieves potent cytotoxicity on cancer cells under conditions of hypoxia.

Cell viabilities of K562 cells were evaluated with Trypan blue analysis after 24 hours of treatment with varying concentrations of endoperoxide **1** under either normoxic or hypoxic conditions. Red bars correspond to the percentages of viable K562 cells under hypoxic conditions. Blue bars correspond to the percentages of viable K562 cells kept under identical conditions of incubation with the agent, but under normoxic conditions. After a day of incubation under normoxic conditions, hypoxic group of the cells were incubated 24 h further under conditions of hypoxia (pre-hypoxia [without drug treatment]); whereas, normoxic group of the cells were kept under normoxic conditions for the same period of time. At the end of this period, both groups of the cells were treated with varying concentrations of endoperoxide **1**. The hypoxia group of the cells were incubated further under conditions of hypoxia with endoperoxide **1**; while normoxia group of the cells were incubated further under conditions of normoxia with endoperoxide **1**. Cells were then harvested in PBS and stained with the Trypan Blue stain. Unstained (live) and stained/blue (dead) cells were counted on an Improved Neubauer

hemocytometer. The percentage of live cells (number of live cells divided by the total number of cells) was plotted for each condition (n = 3).

2.6 Conclusion

In conclusion, we presented a viable example for a singlet oxygen delivery agent which can be activated under hypoxic conditions. This is proof of principle for a two-stage photodynamic activity. Just like hypoxia activated drugs, an endoperoxide can be transformed to a more labile form enzymatically through reductive elimination of the protecting group, which is also electronic/steric deactivator.

The work we present here is the first demonstration of enhanced singlet oxygen generation under hypoxic conditions and at the same time, the first light on a path towards a new therapeutic paradigm, where a new kind of photodynamic therapy is possible without any need for external oxygen, or light. Our work to that end is in progress.

CHAPTER 3

3. INTRODUCTION

3.1 Introduction to the Fluorescence

Fluorescence is a term that the relaxation of the electron to the ground state by emitting photons by radiation. It emits a beam of lower energy than the excited radiation energy. The substance radiates at its specific wavelength. Fluorescence can be used to quantitatively analyze fluorescence compounds as the intensity of the emission is proportional to the compound concentration. Fluorescence technique has a variety of application fields due to the elevated sensitivity and selectivity of fluorescence. Over this, to understand and interpret the research, there are several fluorescence-related parameters that need to be learned in depth. The fluorescence emission spectrum shifts to the long wavelength according to the absorption spectrum. Because if the electron first shifted from $^1S_2$ or $^1S_3$ to $^1S_1$, it gave some of its energy to the environment as heat. Thus, as the wavelength and energy are inversely related to each other, a lower emission of energy fluorescence shifts at a longer wavelength that is spectrally red shifted. Stokes shift is defined as the wavelength or frequency difference between the maximums of the emission and absorption spectra of the same compound. There are many reasons of Stokes shift for example solvent effects, fast

decay to lowest vibrational level of S1, excited state reactions, energy transfer and complex formation.

Fluorophores (or fluorochromes) are a fluorescence chemical compounds and when they are excited by light of appropriate wavelength, they can re-emit light at higher wavelengths. The most important features of a fluorophore are quantum yield and fluorescence efficiency. The common definition of quantum yield (Φ_f) is the ratio of emitted photons (S_1) to the number of absorbed photons (S_0). The highest value of quantum yield approaches to unity in molecules relatively rigid which have large and planar conjugated systems.

Quantum yield is characteristic for every fluorescent compound. Moreover, emission and excitation wavelength do not affect quantum yield [76]. Fluorescence lifetime (τ) means that, the average value of time which is spent by molecules in the excited states before relaxing back to ground state. The decay rate of fluorescent intensity affects the fluorescence life time after a short excitation by source. The equation shows below explains this relation:

$$\Phi f = \tau / \tau n \qquad \textbf{(Equation 2)}$$

τn is the “natural” or “intrinsic” lifetime of fluorophore. It means that the lifetime in the absence of any quenching processes. It is obvious that, quenching to some degree is compulsory, as a result measured fluorescence lifetime is always lower than the intrinsic fluorescence lifetime.

The fluorescence intensity can be suppressed or decrease via different mechanism because of *fluorescence quenching*. One of the mechanisms of reduction or suppression of fluorescence intensity is that the fluorophore forms a transition complex. This complex can be formed if fluorophore molecule contacts with quencher as molecular oxygen, halogen ions or another fluorophore containing quencher. The interaction between the fluorophore and the quencher divides the quenching mechanism into static and collision mechanisms. Static quenching occurs when the fluorophore and quencher are in the ground state so that the two together form a nonfluorescence complex. In collision quenching, the excited fluorophore contacts the quencher and deactivated upon contact with it. Halogens, oxygen, amines and electron deficient molecules act as quenchers. They show different quenching mechanisms when obtain a pair with a fluorophore. If there are halogen or heavy atoms in the medium, quenching is performed via spin orbital coupling or inter system crossing[77]. Photobleaching is another quencher mechanism. It means that, unable to fluoresce. There are some reasons as cleaving of covalent bonds or non-specific reactions between the fluorophore and surrounding molecules [78].

3.2 Factors Affecting Fluorecence

Nature of molecule: Stiffness is defined as the resistance to deformation due to the load effect. It has been found empirically that fluorescence is higher in molecules with rigid structures. Stiffness reduces the rate of non-radiant relaxation, so it permits the increase of fluorescence. (Free rotations around single bonds increase the rate of non-

radiant resting, reduce fluorescence.) In the following example in figure 35, this difference observed in quantum yields (fluorene Φ_f: 1,0 and biphenyl Φ_f: 0,2) is caused by the increase in stiffness caused by bridging of methylene group in fluorene.

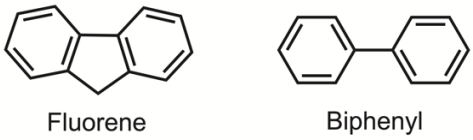

Figure 35. The difference observed in quantum yields for fluorene and biphenyl compounds

Resonance Limit Formula: The more resonance limit formula of the molecule can be written, the higher the fluorescence intensity.

pH: The fluorescence of an aromatic compound containing acidic and basic substituents generally depends on the pH. For example, anilinium has a single resonance state, while aniline has several resonance states (Figure 36).

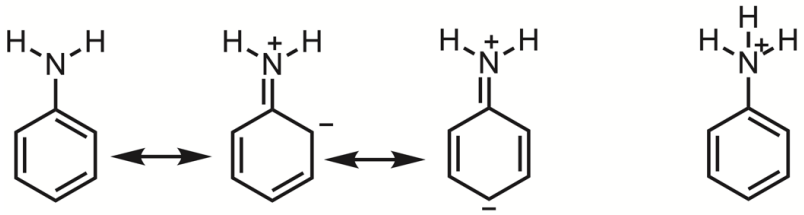

Figure 36. The resonance forms of aniline and anilinium, respectively.

Temperature and Solvent Effect: Increased collision frequency at high temperatures increases the non-radiative relaxation and decreases fluorescence.

Solvents containing heavy atoms or the molecule which is include these atoms in the structure reduce the fluorescence. For example, carbontetrabromide, ethyliodide.

(Orbital spin interactions lead to an increase in the rate of triplet formation and consequently a decrease in fluorescence).

Electronic Transitions: The more likely electronic transitions are, the higher the probability of fluorescence. The greater the transition $\pi \rightarrow \pi^*$, the greater the fluorescence. The fluorescence intensity at $n \rightarrow \pi^*$ transition is lower than $\pi \rightarrow \pi^*$ transition.

Ring Number: As the number of ringing in the molecule increases, the fluorescence property increases. (Anthracene > Naphthalene > Benzene)

Presence of Heteroatoms: Increases fluorescence property. Heteroatom-containing rings 2 and 3 combine with an aromatic ring to increase fluorescence. (The heteroatom should not disrupt the cyclization!)

Chelation Formation: Increases fluorescence property. One of the most commonly used chelators is 8-hydroxyquinoline (with a heteroatom in its structure) and has fluorescence. The fluorescence of the chelates given by Zn^{+2} and Al^{+3} with 8-hydroxyquinoline is more fluorescent than that of the chelator itself.

Viscosity: In viscous solutions, the collisions between the excited molecule and the solvent will be decrease, as a result the energy transfer will be reduced between them, so the fluorescence will be higher [79].

3.3 Fluorescence Probes and their Design Strategies

Fluorescence is the optimal signaling mechanism for optical molecular sensors with superior properties. Fluorescent probes (fluorophore) are highly sensitive molecules because the difference between the excitation and emission spectra which is called Stokes shift. As a result, a very low and near zero background signal is observed during the analyte determination. When the fluorogenic probe interacts with the analyte, a number of changes occur in the photophysical properties. These spectroscopic changes provide information about the relevant assay and can be used to determine the analyte [78-81]. Fluorescent probes have a wide range of applications due to their superior properties. These features selectivity, simplicity, sensitivity, determining dynamic changes in space and in time quickly. Chromogenic and fluorogenic probes generally consist of three parts. These parts are the recognition area, signal unit and linker. The recognition area is designed to recognize the targeted analyte. The signal unit is the part where a visible, fluorescent output is provided. The photophysical changes obtained by the reaction of the analyte and the fluorophore are responsible for this signal. The linkers are responsible for the connection of the signaling recognition section. These connections are often directly integrated. Different types of fluorescent probes have been designed for the determination of different analytes (Figure 37).

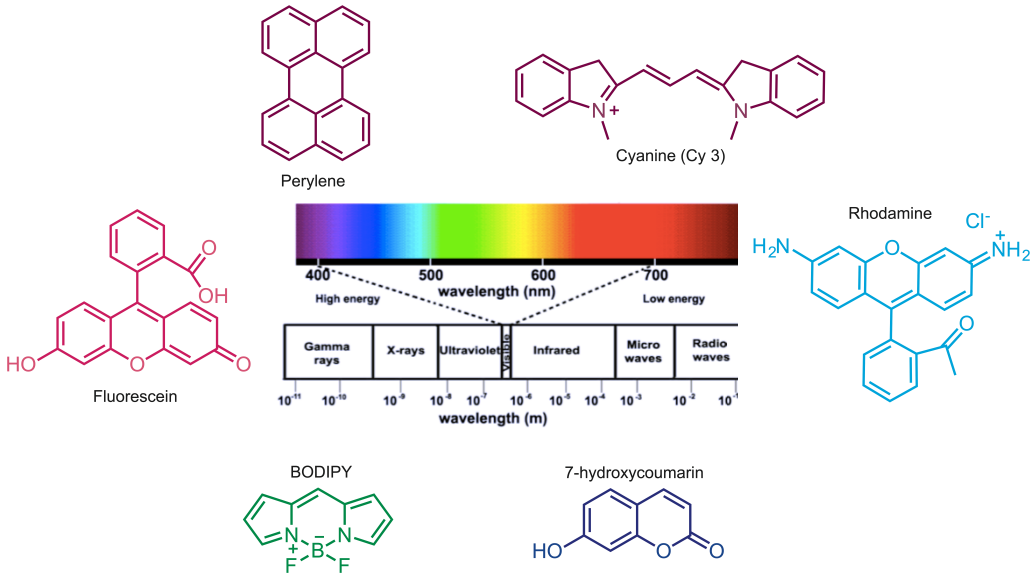

Figure 37. Molecular structures of some common fluorescence probes

Absorption and emission wavelengths of all of the probes whose molecular structures are given above can be adjusted. For example, coumarin dyes are generally used to study in the UV region. Rhodamine and fluorescein derivatives show a high emission peak in the near-IR region. Fluorophores can be classified according to their specific properties. For example, coumarin dyes exhibit a very large Stoke's shift so that they are well suited for biological studies. Heteroatom substituted coumarin dyes are widely used in the literature. Fluorescein dyes were first synthesized in 1871[82] and then they have been widely used in chemo sensor designs. These dyes show water solubility and they have very high fluorescence quantum yield, moreover it is easy to modify the sides for many different applications. On the other hand, these dyes are sensitive to pH changes and undergo very rapid photo-bleaching. Rhodamine dyes, there are adjustable absorption-emission peaks and their pH sensitivity is very low [83]. If we look

at cyanine dyes, their structure is obtained by two polymethine chains between nitrogens. They can be used as a membrane sensors or DNA stains [84]. Because of their highly flexible structure, they can do intramolecular chain twist, which leads to changes in fluorescence properties. Perylene dyes are difficult to be derivatized because of their molecular structure, so their usage area is very narrow. However, these dyes have high absorption peak in the visible region and have high fluorescence quantum yield [85]. BODIPY dyes will be explained deeply in the following section since it shows up extensively throughout this dissertation.

There is a need to develop fluorescent probes with improved selectivity and sensitivity in the biological and chemical environment with minimal degradation and minimum response time

Therefore, there are several important parameters to consider for the design of the desired fluorescent probe. These parameters can be listed as follows [86]: a) the probe must have high stability to light and other chemicals b) the probe is expected to give a bright fluorescence when it interacts with the analyte, indicating that it must achieve high quantum yield and a large extinction coefficient. c) When designing the probe, it should only respond to the targeted analyte and gives fluoresce as an output d) shifts in excitation and/or emission wavelength or fluorescence emission by turn-on is more preferencial than turn-off response.

There are many classifications in the literature to design the fluorescent probe to detect the analyte accurately. These are (a) protonation - deprotonation (b) carbon -c arbon

bond formation and rupture reactions. Nucleophilic addition/substitution type reactions are the sub title of the carbon-carbon bond forming and bond breaking reactions (c) complexation.

Protonation-deprotonation mechanism has been widely used to improve pH responsive probes. These fluorogenic probes are generally designed to operate at neutral pH. Various modifications can be made by adding different amino groups, OH and COOH groups to these molecules so that these probes can be studied in a wide pH range. In order to increase the sensitivity of the probe to H^+ ion, the responsive units which are sensitive to H^+ ion can be increased. As it is well known, amino groups, OH and COOH groups also show affinity for metal ions. Therefore, when designing the probe, electronegative groups should be avoided to form suitable cavities for metal ions. A large number of pH-sensitive probes based on xanthena [87-89], bodipy [90-93] and cyanine [94-96] have been reported in the literature (Figure 38).

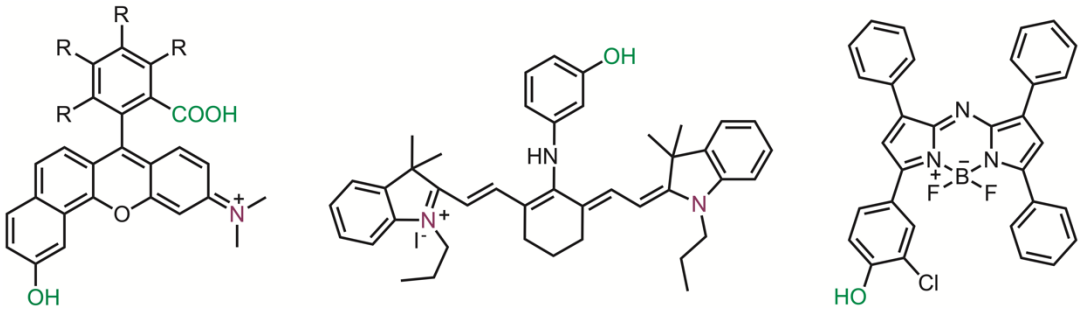

Figure 38. Some examples of pH sensitive fluoregenic probes

Carbon-carbon bond forming and breaking reactions could be classified into different groups according to the reaction types. When designing the probe, carbonyl groups can be added to the structure. Thus, nucleophilic substitutions reactions are utilized while

detecting of different anions and neutral species. Bisulfite, amines, cyanide and carboxylates may be used as the analyte for such reactions. The carbon-carbon bond forming shown in the figure 39 works according to the PeT mechanism. In the absence of cyanide (CN), fluorophore (acceptor) shows weak fluorescence because there is an electron transfer from donor (receptor) to the fluorophore, so PeT is active (on state) and there is no bright emission. In the presence of CN, CN directly attacks the carbonyl center, as a result cyanohydrin adduction is occurred, then PeT is deactivated and bright emission spectra will be obtained [97].

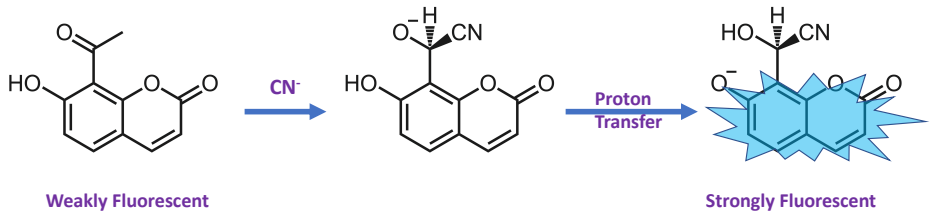

Figure 39. Carbon-carbon bond formation of fluoregenic probe

Complexation based probes could be designed according to the intramolecular interactions between receptor (recognition moiety) and reporter units. When designing such probes, the formation of receptor units show great important because covalent and non-covalent interactions between the analyte and the receptor cause the probe to exhibit different photophysical changes. The sensitivity of the probe to the metal ion to be used as the analyte is very importance because many metal ions may have similar reactivities (eg Cd^{2+} vs. Zn^{2+}, Hg^{2+} vs. Ag^{+}, Mg^{2+} vs. Ca^{2+}). The complexity shown in the figure 40 works according to the PeT mechanism. In the absence of Zn^{2+} ions, fluorophore (acceptor) shows weak fluorescence because there is an electron

transfer from donor (receptor) to the fluorophore, so PeT is active (on state) and there is no bright emission. In the presence of Zn^{2+} cation, the complexation can be occurred, as a result PeT is deactivated and bright emission spectra will be obtained [98].

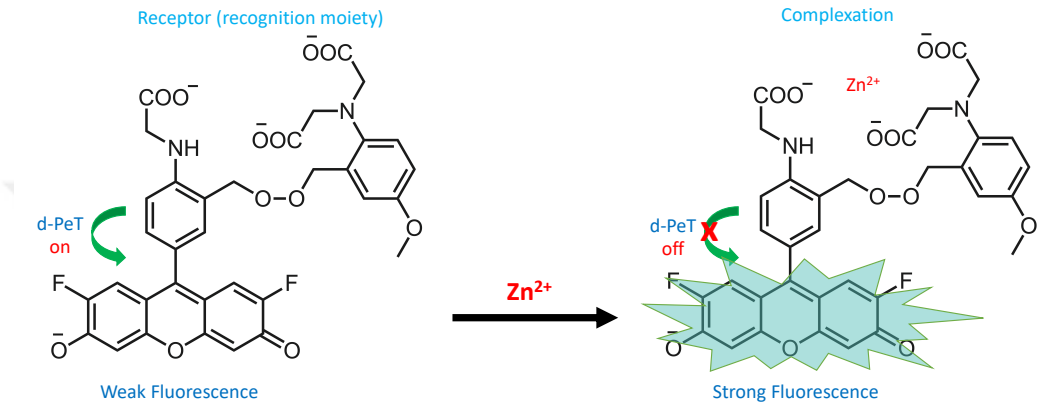

Figure 40. Fluorogenic probe work on complexation with metal ions

Although there are several photophysical processes as exciplex formation, photo induced charge transfer, quenching via collision for the changes in fluorescence, we are going to focus on how photo induced electron transfer (PeT) is working. Because, in this chapter, detection of analyze by fluorogenic probe proceed over photo induced electron transfer.

3.3.1 Photoinduced Electron Transfer (PET)

Three basic elements are required in the design of the probe to operate the system according to the PeT process. These elements are fluorophore, linker and donor (chelate constructs). The main purpose of the use of the linker group is to prevent conjugation between the receptor and the donor. We cannot talk about the PeT

process, if fluorophore and donor probes link with conjugated system. In cases where BODIPY is used as fluorophore, the donor group substituted to the meso position is often perpendicular to the BODIPY, so the connection between the donor and the binding group is disconnected. To better understand the PeT procedure, simple representative molecular orbital (MO) diagrams can be examined [99] (Figure 41). As expected, when we apply light to fluorophore, an electron is transferred from the highest occupied molecular orbital (HOMO) to the lowest molecular orbital (LUMO). At the same time, the electron from the donor's HOMO level (free acceptor) fills this gap because the donor's HOMO level is higher than the HOMO level of the fluorophore. The PeT system is now activated and the fluorescence is extinguished (i.e. Pet is active and fluorescence is off state). In order to inactivate the PeT system, analyte should be added to the medium. After adding the analyte to the medium, it binds with the chelator (bound acceptor) unit by intramolecular interactions and it gives the stability of HOMO level of acceptor unit (bound acceptor). Thus, the HOMO level of the acceptor is lower than the HOMO level of the fluorophore. From this perspective, when the fluorophore is excited by the light, the electron transfer to the excited state, then it can return to the ground state and a bright fluorescence emission can be observed (i.e. Pet is inactive and fluorescence is on state) (Figure 41).

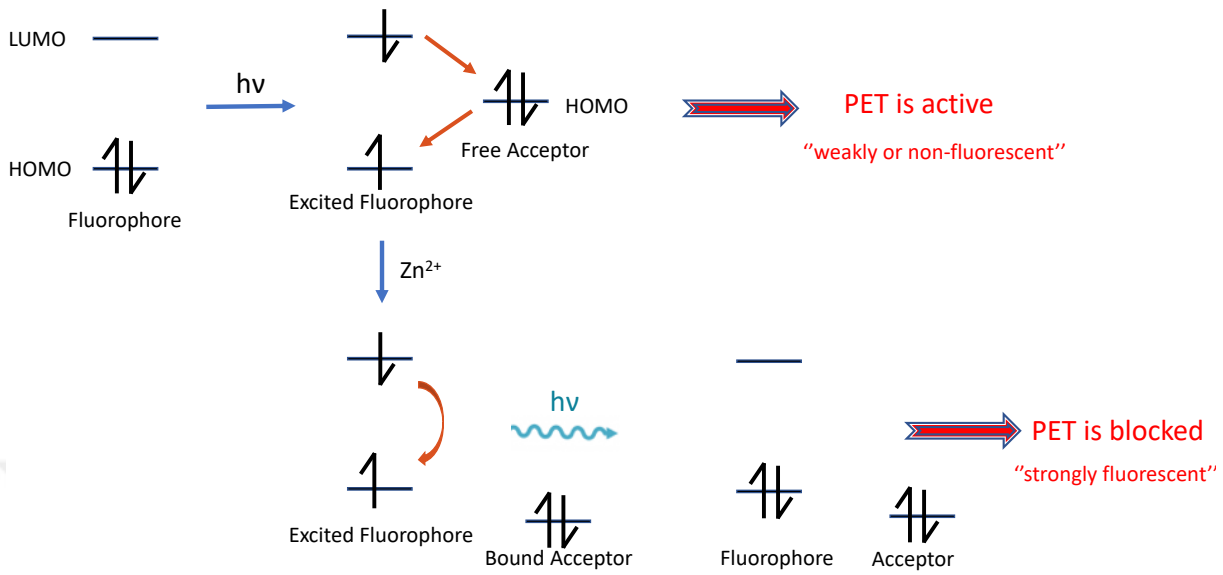

Figure 41. Simple molecular orbital diagram of PeT mechanism

If we examine the literature, we can see many chemosensor samples working according to PeT mechanism [100-102]. Figure 42 is an example selected from these. The fluorescent probe in the figure 42, whose fluorophore is anthracene, exhibits high blue emission in the presence of Zn^{2+} ion. On careful examination, it can be easily seen that there is no conjugation between fluorophore and donor.

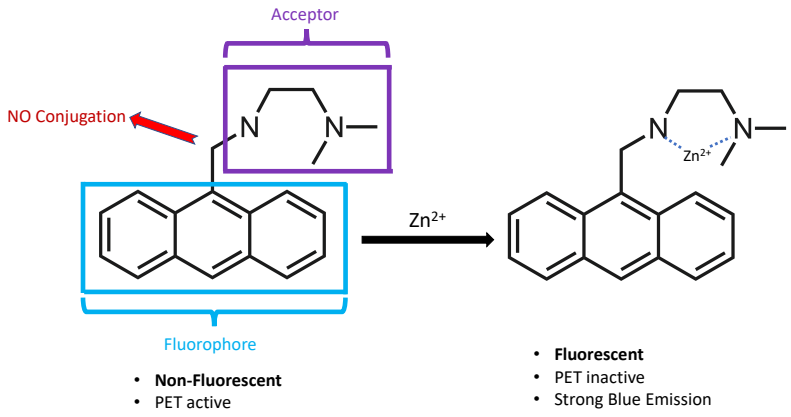

Figure 42. Example compound for PET based chemosensor.

On the contrary, some fluorescent chemosensors also work according to the reverse PeT-based (which is also called as oxidative PeT) mechanism. In such designed probes, emission quenching occurs when analyte is added to the medium. As it seen in figure 43, The LUMO level of the donor (free acceptor) atom is reduced by binding of the analyte to the acceptor (bound acceptor) unit. After that, the excited electron of the fluorophore moves over the donor's LUMO, resulting in a significant reduction in emission.

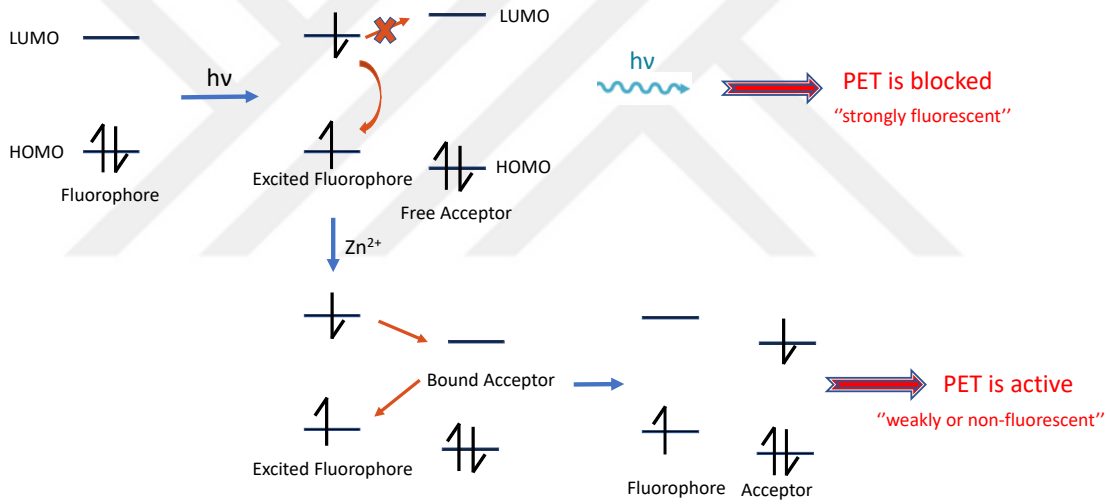

Figure 43. Simple molecular orbital diagram of reverse PeT mechanism

An example for the oxidative PET is shown in figure 44, which is designed and synthesized by Akkaya group. Fluorophore unit is BODIPY based chromophore. When the binding Zn (II) ion to bipyridine receptor is obtained, it quench the emission by oxidative PET [103].

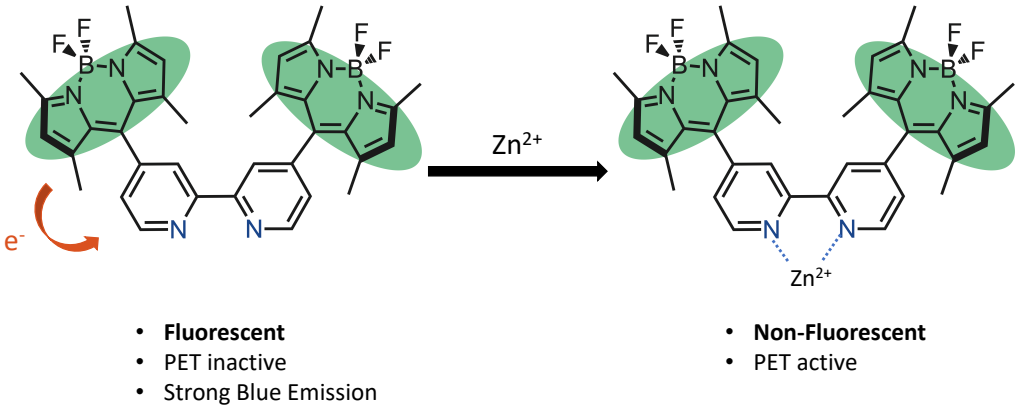

Figure 44. An example molecular sensor for reverse PET

3.4 Photodynamic Therapy

Photodynamic therapy (PDT) is a treatment modality for certain malignant (skin, head and neck, gastrointestinal, gynecological cancers), premalignant (actinic keratosis), and nonmalignant (psoriasis, AMD-age related macular degeneration) indications [35, 104]. The therapeutic action depends on the efficient generation of singlet oxygen ($^1O_2$) through excitation of a particular chromophore (sensitizer) followed by an energy transfer to the dissolved oxygen in tumor tissues. Cytotoxic singlet oxygen and other secondary products (reactive oxygen species, ROS) are responsible for the apoptotic and necrotic deaths of the tumor cells. Main cellular targets are membrane structures of the cells and organelles. Mitochondria localizing sensitizing agents induce apoptosis, while plasma membrane localizing sensitizers are more likely to cause necrosis on irradiation [105].

The earliest clinical application of photodynamic therapy was described more than a century ago (in 1903) by von Tappeiner, who applied eosin topically to basal cell carcinomas, and then subjected to visible light. Von Tappeiner later described the process which results in tissue destruction as “the dynamic interaction among a photosensitizing agent, light and oxygen” and hence the name “photodynamic” therapy [106]. However, more than 70 years had to pass before the true potential of PDT for the treatment of cancer was recognized, and that recognition was mostly due to the persistant efforts by Dougherty [107]. In 1975, he reported that hematoporphyrin “derivative” (HpD, an indefinite mixture of porphyrins) in the presence of red light, could eradicate mouse mammary tumors. Eventually, Photophyrin (commercial name for HpD) received FDA approval in 1995, and quickly clinical protocols were developed together with light applicator designs for effective light delivery to the tumor tissue. Second generation of photosensitizers were then developed in order to address some of the deficiencies of HpD. The most important among those deficiencies, in addition to the indefinite composition, was the fact that HpD had a very weak absorption in the red region of the spectrum where light penetration into tissues is better. These new sensitizers included benzoporphyrin derivatives, chlorins, phthalocyanins, texaphyrins, and natural products such as hypericin and protoporphyrin IX (PPIX). With the advent of this new generation of sensitizers, PDT applications in ophthalmological and cardiovascular diseases were also explored [108, 109]. The third-generation photosensitizers incorporated targeting and

delivery moieties, such as monoclonal antibodies, liposomes and ligands targeting overexpressed receptors[110].

Singlet oxygen ($a^1\Delta_g$) is a highly reactive species with a short lifetime in aqueous media (0.6 ms, with an approximate diffusion distance of 20-100 nm). The quenching in water is facilitated by the electronic-to-vibrational energy conversion which leads to deactivation through interactions with the vibrational states of O–H bonds. This excited state species is 94.3 kJ/mol above the ground state, however the transition between the triplet ground state ($X^3\Sigma_g^-$) and the first singlet excited state is strictly forbidden by spin, symmetry and parity selection rules.

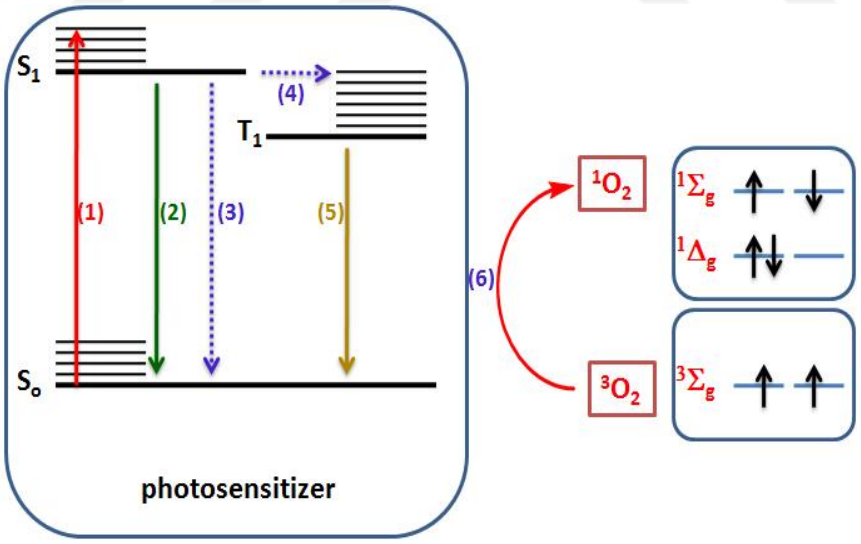

Figure 45. Singlet oxygen generation by sensitization. Relevant processes are identified by numbers: 1-absorption, 2-emission, 3-non-radiative transition, 4- intersystem crossing, 5-phosphorescence, 6-energy transfer.

Therefore, singlet oxygen cannot be produced by the direct excitation of the ground state molecular oxygen, so it is always generated by sensitization through energy transfer from dyes like Rose Bengal, Methylene Blue and Bodipy derivatives.

Photosensitization and generation of singlet oxygen in this way, with the intermediacy of these dyes also require an efficient intersystem crossing between the singlet and triplet manifolds of the sensitizer dye. In addition, for photodynamic therapy, the sensitizer dye is preferably selected to be a dye with strong absorption bands in the red- to near IR region of the visible spectrum.

3.5 Photosensitizer

There are many application fields and significant interest for photosensitizers which have strong absorption bands in the red- to near IR bands. One of the most important feature of a PS is that singlet oxygen cannot be produced by the direct excitation of the ground state molecular oxygen, so it is always generated by sensitization through energy transfer from photosensitizers. There are some characteristics of photosensitizers. At first, a photosensitizer can be suitable for the target molecule. At the same time, it should be non-toxic, removed very quickly from the body, effective in the treated area and work efficiently in-*situ* environment. In addition to these properties, short drug-light interval, solubility in aqueous media, rapid synthesis and short drug-light interval are also very important. Because of the imitation of light penetration into tissue, PS must have high extinction coefficients at longer

wavelengths, high quantum yield for singlet oxygen generation and low quantum yields of photobleaching.

In figure 46, there are PS examples which are very common and have strong absorption bands in the red- to near IR bands.

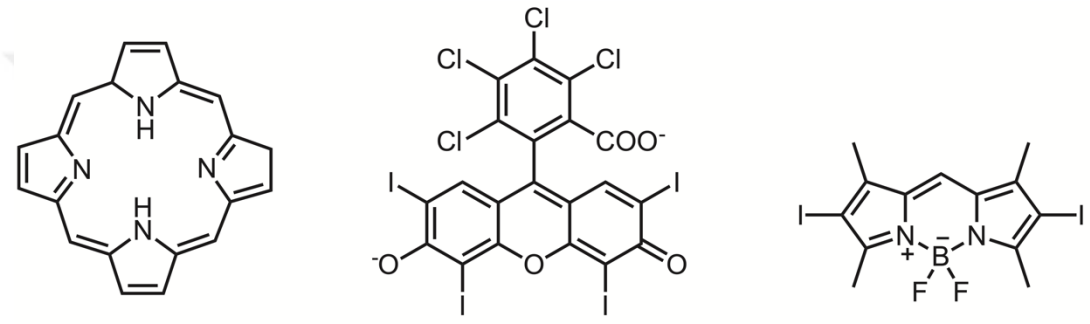

Figure 46. The common PSs use in PDT

The wavelength range between 600–800 nm is very crucial for PDT. This boundary is called ''therapeutic window'' [111]. Although, Rose Bengal and porphyrins are very common photosensitizers, they do not show strong absorption in the therapeutic window. On the other hand, the absorbance maxima of the form of Boradiazaindacene (BODIPY) shown in figure 46 is 540 nm [112].

3.6 LOGIC GATE

3.6.1 Boolean Algebra

The number ''zero'' is the neutral element of the addition and the number ''one'' is the neutral element of the multiplication. When these two simple numbers were combined, the more complicated theories were introduced into science as ''Boolean logic''. George Boole published a book which was called ‘’The Mathematical Analysis of Logic’’ in 1847 [113]. ‘’Boolean Algebra’’ or ‘’Boolean Logic’’ theory first introduced within this book. Boolean Logic is a system of algebra in which there are two possible variables expressed as true and false usually denoted by 1 and 0, respectively.

When Boolean function transforms from an algebraical representation into a circuit diagram, then it implements logic gate. A logic gate operates data and gives an output from one or more inputs. Today’s digital devices and computers are used binary logic. Binary numbers have only two possibilities 0 or 1. When dealing with circuits 0 is or it corresponds to a circuit being in the ‘’OFF’’ state. 1 corresponds to a circuit being in the ‘’ON’’ state, so if you are dealing with true and false statements an off state will be considered false and an on state will be considered true.

(0 ⟶ OFF ⟶ F) (1 ⟶ ON ⟶ T). If you are dealing with voltage an off state would have zero volts and an on state typically 5 volts but something other than zero [114].

There are 16 operations which are formed by Boolean logic functions. OR, XOR, NOR, XNOR, AND and NAND are most common functions in digital systems. Simply, XOR, XNOR and NAND are reverse functions of OR, NOR and AND, respectivelty.

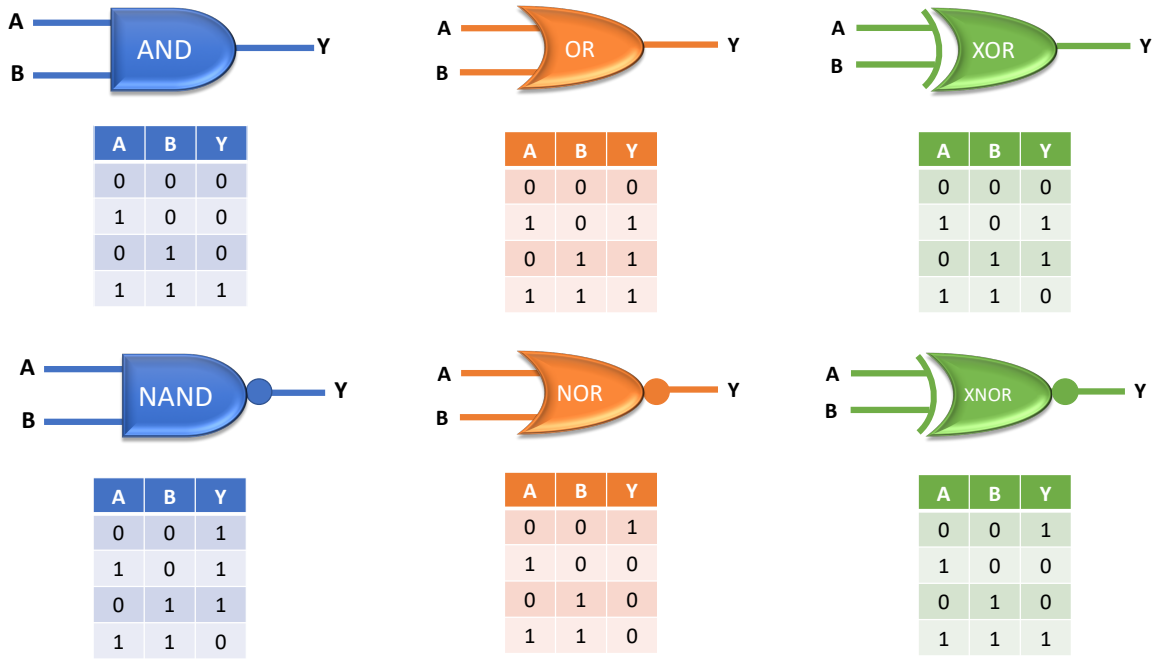

Figure 47. Common logic Gates schematic drawings and truth tables

The truth tables show that (Figure 47), there are two inputs (A&B) and one output (Y) for basic logic gates. AND logic gate states that, the output Y will be A times B. When we look at the truth table; the only way that Y can be 1 is if both inputs A and B are 1. The NAND gate is basically the complement of the AND gate. AND gate, we said it is A times B, for NAND gate it is going to be the complement of A times B. The complement of a 0 is 1 and the complement of 1 is 0, so Y column for NAND logic gate is the complement of Y column for AND logic gate. The output Y will be A plus B for the OR

logic gate. In this case, when A is on (1), but B is off (0), Y will be on (1). In an XOR gate, the Y will be 1, if one, and only one of the inputs (A&B) is 1.

3.6.2 Molecular Logic Gates

The inputs will be different from the electrical signals for logic gates. If there are optical and chemical inputs, ''Molecular logic gates'' can operate these inputs like a logic gate and produce a single output.

The birth of the title of molecular logic gates originated 26 years ago. De Silva [115] designed a molecule which has chemical inputs and spectral outputs. This molecule is the first example of molecular logic gate that works as an AND operation. The fluorescence emission of anthracene is output and ''1'' output is given only when effective PeT from crown ether and amine moieties are blocked by sodium binding and protonation respectively (Figure 48).

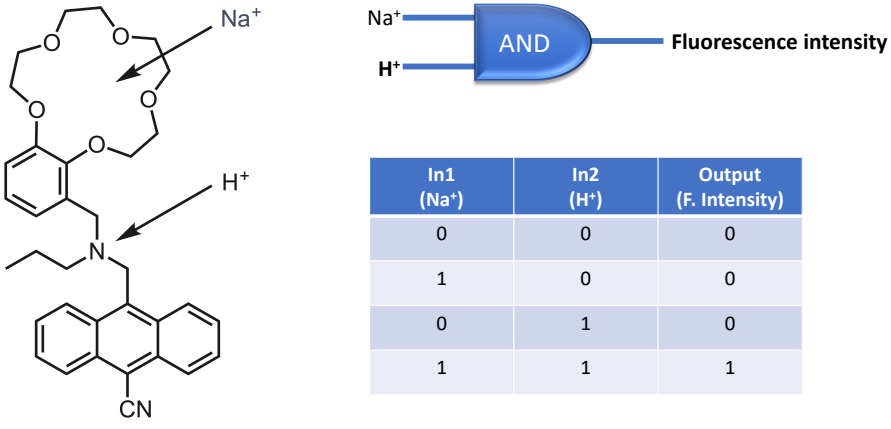

In1 (Na^+)	In2 (H^+)	Output (F. Intensity)
0	0	0
1	0	0
0	1	0
1	1	1

Figure 48. Literature example of AND logic gate by de Silva et al.

The second molecule which is working as molecular AND gate was designed by de Silva again [116]. In this study, anthracene is used as a fluorophore and two PET based receptor are directly attached to anthracene unit. In the presence of H^+ and Na^+ ions, fluorescence emission of anthracene is obtained as an output (Figure 49).

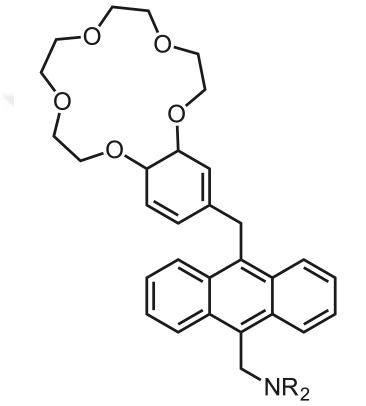

1a.; R= Et
1b; R,R= $(CH_2)_2O(CH_2)_2$

In1 (Na^+)	In2 (H^+)	Output (F. Intensity)
0	0	0
1	0	0
0	1	0
1	1	1

Figure 49. AND logic gate by de Silva et al.

In contrast to the simple molecular logic gates, it is possible to design very complex molecular logic gates by combining of two or more operations, an output of one logic gate can be an input for another molecule. Akkaya et al. designed two logic gates that can be combine to form a complex integrated logic device [117]. The styryl-bodipy derivative with a dipicolylamine (DPA) group has Hg^{2+} sensitive unit and clicked together Zn^{2+} sensitive chromophores to compose an energy transfer donor-acceptor dimer (Figure 50). If the distance is high between two chromophores, the energy transfer will be low, so by using click chemistry, we can combine them covalently and the energy transfer becomes efficient. Light at 560 nm and Zn^{2+} are used as an input for the first part of the molecule. Although, fluorescence is quenched over an efficient photo-induced electron transfer (PeT) process, in the presence of Zn^{2+} metal ions, high

emission intensity is recovered and the excitation energy is obtained as an output. Two separete units ''clicked'' together as mentioned before, so the excitation energy is transferred (FRET) to the second module as an input. In the absence of Hg^{2+} metal ions, because of intramolecular charge transfer charge-donor characteristics (ICT) of the dialkylamino group, the second module shows faded fluorescence. When the final input Hg^{2+} is added, then strong red emission is observed at 660 nm. This study gives an idea about multiple logic gates can be used for improving complex functionalities out of molecular logic cassettes like their silicon counterparts.

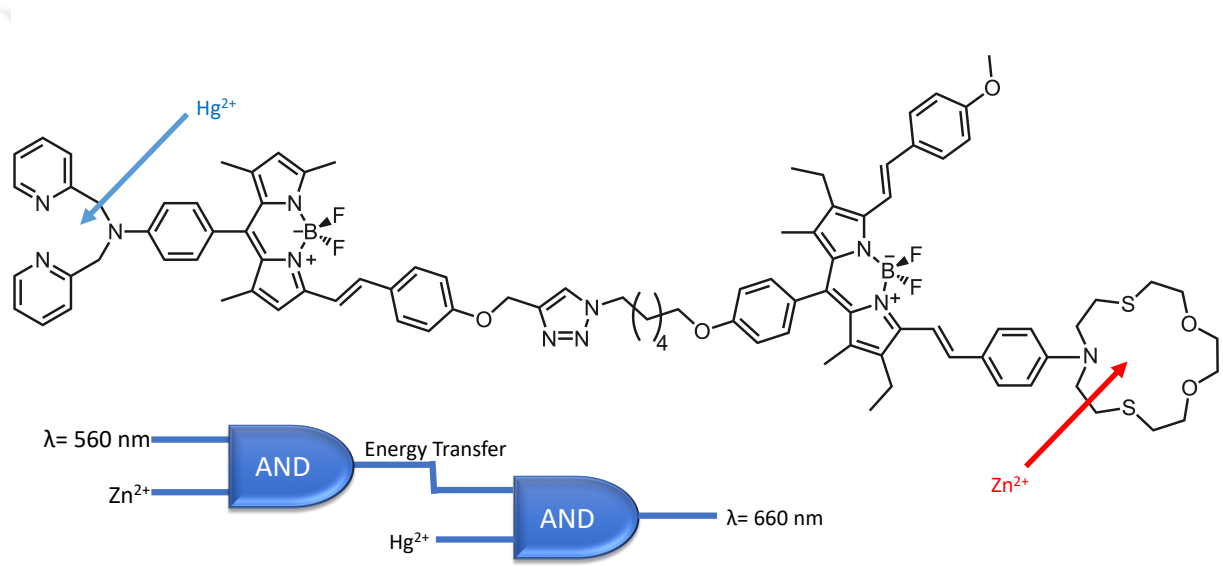

Figure 50. The concatenation of two logic gate by Akkaya et al.

3.7 Chemical Logic Gates in Biological media

Molecular logic gates initial proposal is mimic of digital logic gates and there is no significant functionality. After that, they provide greater use in biological media. The goal of the logic gate, they can be used to proceeding biochemical/chemical information, which is very important for an on-target diagnostic and personal

therapeutic applications. We can diagnose a certain stage of disease by using different important parameters as inputs for a molecular logic gate and useful outputs as drug release or fluorescence.

Biosensing is used as a first example of molecular logic gates in biological media by de Silva et. al. [118]. The de Silva group design a molecule which allows selective monitoring of Ca^{2+} and Mg^{2+} metal ions. This molecule allows construction of truth tables with OR logic, so when one or two of these metal ions are viewed in the media, then fluorescence enhancement is obtained as an output.

As previously explained, it is possible to design very complex molecular logic gates by combining of two or more operations. Katz group [119] studied multianalyte sensing by using multiple logic gate operations. This type of linked gates with biocatalytic cascades are very important because they can allow detection of different analytes at once.

A smart functional therapeutic approache which is related logic gates is demonstrated by the Akkaya group [120]. In figure 51, the molecule has BODIPY unit as a photosensitizer. It generates $^1O_2$ (output), which is extremely toxic for cell culture, only in the presence of tumor related inputs Na^+ and acidic media. AND logic gate is generated according to the protonation causes bathochromic shift and binding of Na^+ ions to the crown ether blocks PET.

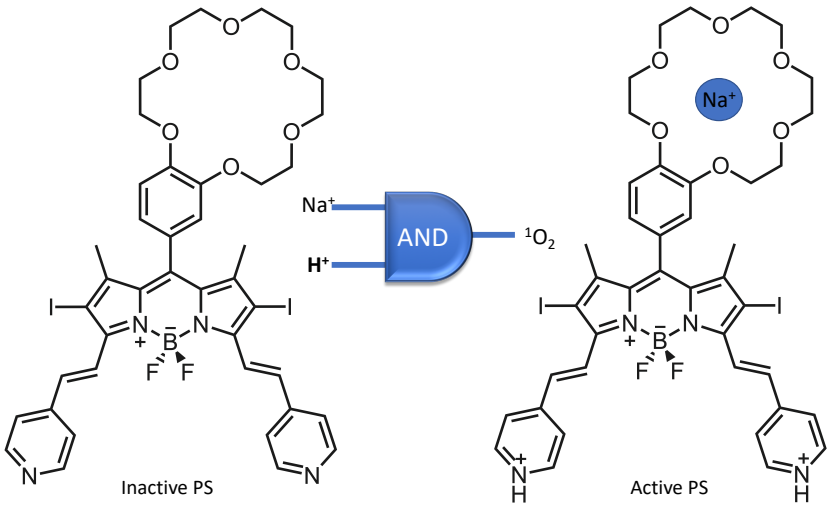

Figure 51. AND logic gate for smart drug design by Akkaya et al.

In another study from Akkaya group, they design a molecule which takes advantage of two characteristics of the tumour microenvironment, lower pH and higher glutathione (GSH) concentrations [121]. In figure 52, disulfide bond clevage is obtained in the presence of higher GSH concentration. In acidic conditions, the absorption spectral characteristics of the PS demonstrates an alteration. This change in absorption results in an augmentation of the extinction coefficient at excitation wavelength. This, in turn, facilitates activation of PS. There exists an energy acceptor, which is conjugated to the PS through a reducible disulfide bond. This energy acceptor still causes quenching of the excited state via energy transfer. Only in the state where both cancer associated inputs are present at levels which exceed the threshold values, the singlet oxygen generation by the PS was greatly increased. Logic constructs which incorporate AND based approaches that stem from cancer associated parameters as a mean of input would prove to be more targeted and selective therapeutic approaches.

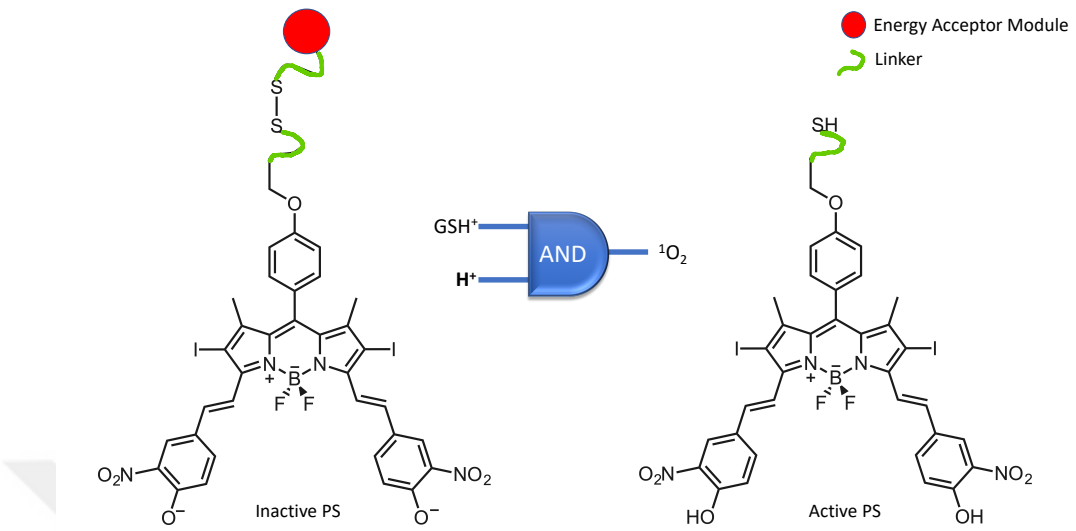

Figure 52. AND logic gate for smart drug design by Akkaya et al.

Shabat et al. study is summerized in figure 53. The molecule is designed and synthesized according to the "OR" molecular logic gate principles and it is built for smart drug release [122]. The molecule is operated by two different enzymes as an inputs. These are penicillin G amidase (PGA) or antibody 38C2. The 4-Hydroxybenzyl alcohol is used as a smart linker that is used to camouflage the doxorubicin amine functionality. In the presence of PGA or 38C2, two seperate sites forms an amine nucleophile which directly attacks the carbamate and release doxorubicin.

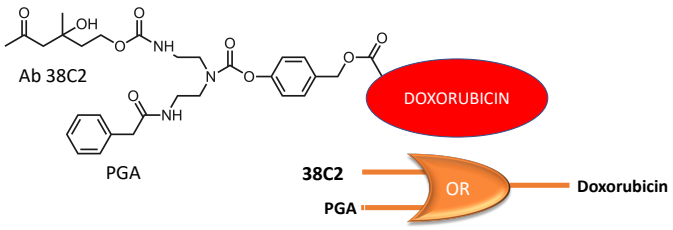

38C2	PGA	Doxorubicin
0	0	0
1	0	1
0	1	1
1	1	1

Figure 53. OR logic gate for drug release design by Shabat et al.

3.8 What is a Demultiplexer (DEMUX) ?

There are two types of electronic switches: MULTIPLEXER and DEMULTIPLEXER to check the flow of bit data according to Boolean algebra. Multiplexer is a digital switch with multiple inputs and a single output. Demultiplexer is a reverse operation of multiplexer. A DEMUX is a digital switch with a single input (source) and multiple outputs (destinations). The select lines determine which output the input is connected to.

- DEMUX Types
  - 1-to-2 (1 select line)
  - 1-to-4 (2 select line)
  - 1-to-8 (3 select line)
  - 1-to-16 (4 select line)

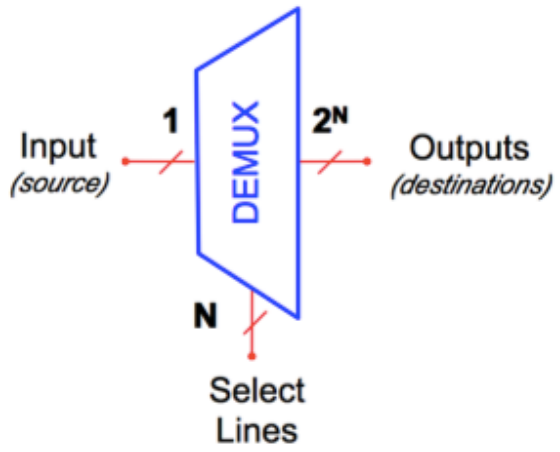

Figure 54. Demultiplexer Block Diagram

The typical of a DEMUX is shown figure 55. DEMUX is a combinational circuit having one input (single source) and many outputs depending upon the select inputs (selector) this single input is transferred to any of these outputs (multiple destinations).

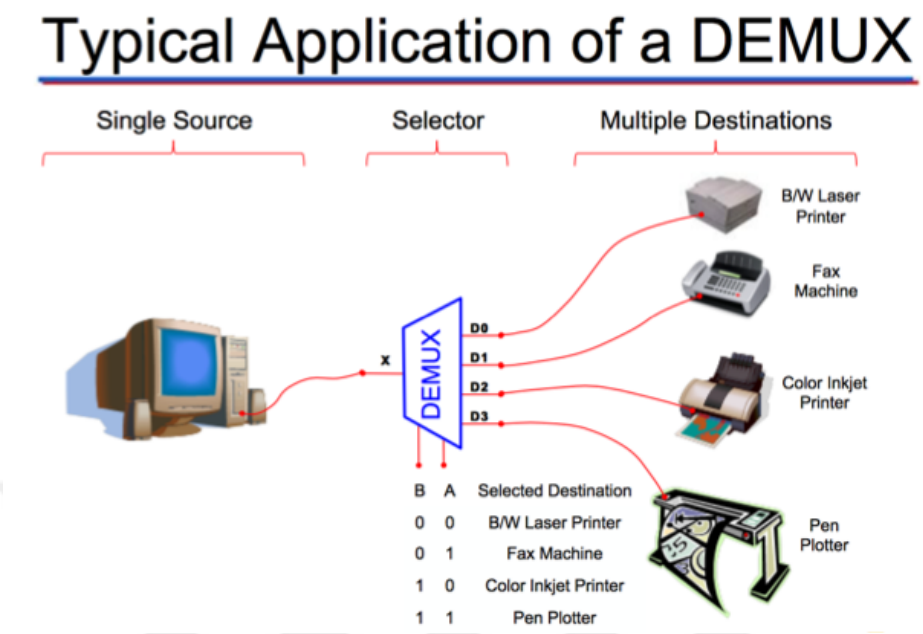

Figure 55. Typical application of a DEMUX

1 : 2 DEMUX: As the name suggests, there is a single input and two outputs. For 1-to-2 DEMUX, there is a single select input.

In a study by Sundus [123], a two-module DEMUX was synthesized. The output could be switched between emission at near IR, and cytotoxic singlet oxygen. Light at 625 nm used as the input and H^+ ion used as the control. In the absence of H^+, when the compound was excited with a light at 625 nm, the compound gave bright fluorescence. In the presence of H^+, the absorption bands of the two compounds was moved in opposite directions (Figure 56). As a result, the excitation energy transfer was reversed effectively and singlet oxygen generation would be obtained and decreased in emission intensity.

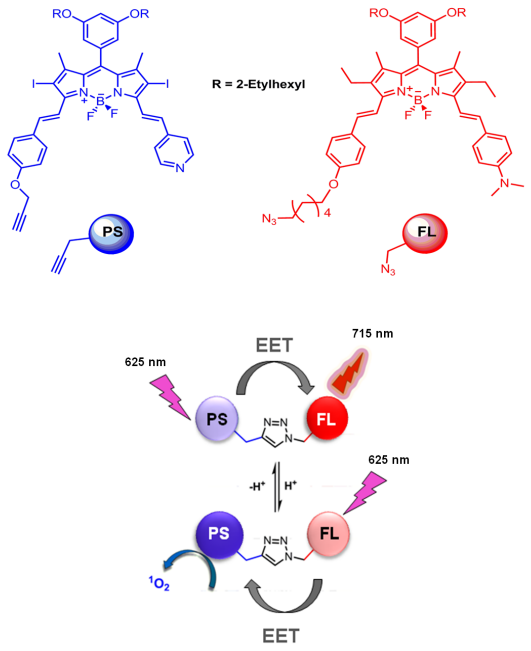

Figure 56. Modular assembly of the molecular DEMUX device with two different outputs depending on the acidity of the medium.

3.9 Flow Cytometry and Detection of Apoptosis via Annexin V

Several advances in cell biology helped researchers to investigate cellular functions, structural changes, responses to external stimuli, cellular life-cycle and death. Such findings paved the way for a better understanding of human diseases as well as determining better and well-suited therapeutic applications. Flow cytometry has proven to be one of the most valued approaches concerning such applications over the last decades. In summary, flow cytometry is a refined technological approach used for counting, examining and sorting individual cells [124]. There are several critical features of flow cytometry which demonstrate priceless advantages. First of these features is

the fact that flow cytometry analyzes each cell of a group of cells on a cell-by-cell approach. This makes it possible to investigate every cell, including those that are very scarce, among numerous cells in a sample. In addition, analyses with flow cytometry are relatively fast. The technique allows for the analysis of up to 10,000 cells in a second. It can be easily understood that this advancement is very valuable when compared with older approaches that are based on visual analysis and counting. Flow cytometry also enables the simultaneous analysis of several parameters on a single cell. By this way, it is possible to obtain more data from each and every cell of a population of cells in a sample in a brief period of time. Given such advancements, flow cytometry has proven to be a useful approach in several types of applications.

The flow cytometry system bears several important components. One of these components is the fluidics system. This component achieves the funneling of cells in the sample into a single stream. By this way, each and every cell in the sample pass through a laser beam one at a time. These cells are projected to a laser beam (one at a time), while they are inside this single stream. When a laser beam hits a single cell, the laser beam is scattered based on the characteristics of that cell in focus. In addition, the cell may also emit fluorescent light if that cell had been tagged with a fluorescent probe. These scattered light signals as well as the emitted fluorescent signal are compiled by the second component of flow cytometry, the optics system. The optics system directs the light signals to detectors. Both scattered as well as fluorescent light are collected by specially positioned lenses. A set of beam-splitters and filters routes the scattered and fluorescent light to specific detectors. The detectors transform such input into

digital numerical values by the help of the electronics component of the flow cytometry system. These numerical values can then be further analyzed via specialized software. Multiple characteristics of each cell are collected and recorded as each cell goes through the laser beam. Approximately 10,000 cells are recorded for each sample.

Each cell causes a different type and amount of laser beam scatter due to its inherent features. The light can be scattered in different ways. The amount and the direction of the scattered light give an estimate for the size and internal-complexity of each cell in focus. By utilizing XY dot plots (in which every dot demonstrates a single cell) that show such information, all data concerning a population of cells can be investigated. In addition, more information can be obtained from a sample at single cell level by using fluorescent probes that specifically mark desired targets. This approach provides additional information besides size and internal-complexity.

Monoclonal antibodies or other specific probes (e.g. Annexin V) can be attached to fluorescent dyes which emit fluorescent light when excited by a laser. This approach allows us to specifically and precisely determine the cells that are bound to specific antibodies of other markers. In general, most of the human cells do not emit fluorescent light under normal circumstances. In case a fluorescent dye-attached-antibody is bound to a cell, that cell will emit a fluorescent signal when it passes through the excitation beam. This emission signal will be recorded by the flow cytometry system.

There exist several different types of fluorescent dyes available for use with flow cytometry. These dyes are activated by different color laser beams and they are capable of emitting different colors of light when they are excited (i.e. green light emission, red light emission). By this way, it is possible to detect multiple features of a cell at the same time.

Apoptosis is an active and important process in regulation of homeostasis. The events in apoptosis are comprised of cellular morphological characteristics, plasma membrane asymmetry loss, shrinkage of cytoplasm and nucleus, etc. The loss of plasma membrane asymmetry is one of the primal changes observed during apoptosis. This loss of asymmetry results in the translocation of phospholipid phosphatidylserine from the inner side of the plasma membrane to the outer side.

Annexin V is a member of the annexin family which is capable of binding to phosphatidylserine in a calcium-dependent manner [125, 126]. Since phosphatidylserine is found in the inner portion of the plasma membrane under physiological conditions, Annexin V cannot bind to phosphatidylserine under such circumstances. On the contrary, phosphatidylserine translocates to the outer portion of the plasma membrane during the early phase of apoptosis, allowing for the binding of Annexin V [127]. Annexin V can be conjugated to fluorescent dyes so that it can be visualized by fluorescent microscopy or flow cytometry. This approach is useful as a means of specific and sensitive probe for apoptotic cells, especially to determine

apoptosis at an early stage before nuclear changes such as DNA fragmentation are evident.

MOLECULAR DEMULTIPLEXER AS A TERMINATOR AUTOMATON

Ilke S. Turan[1], Gurcan Gunaydin[2], Seylan Ayan[3], Engin U. Akkaya[1,3]

Nature Communications , 2018, 9, 805

4.1 Objectives

Molecular logic gates are expected to play an important role on the way to information processing therapeutic agents, especially considering the wide variety of physical and chemical responses that they can elicit in response to the inputs applied. Here, we show that a 1:2 demultiplexer based on a Zn(II)-terpyridine-Bodipy conjugate with a quenched fluorescent emission, is very efficient in photosensitized singlet oxygen generation, in both organic solvents and in K562 cell cultures. However, once the singlet oxygen generated by photosensitization triggers apoptotic response, the Zn(II) complex then interacts with the exposed phosphatidylserine lipids in the external leaflet of the membrane bilayer, autonomously switching off singlet oxygen generation, and simultaneously switching on a bright emission response. This is the confirmatory signal of the cancer cell death by the action of molecular automaton and the confinement of unintended damage by excessive singlet oxygen production.

4.2 Introduction

More than two decades after the seminal work by de Silva[115], molecule based logic gates have reached a level of considerable sophistication[128-130]. Many examples of basic Boolean logic gates and various implementations of both combinatorial and sequential logic were reported[131-136]. While it is clear that more advanced digital designs may require novel integration mechanisms of chemical logic gates, functional equivalents of more complex information

processing is still possible with simple molecules or molecular assemblies as a result of their unique characteristics. However, despite this impressive progress, the power of chemical and molecular logic gates beyond the exploratory phase is yet to be convincingly demonstrated,[137]with what is colloquially referred to as a “killer app”.[138]

The most likely field where molecule-based information processing agents would find a niche for true utility is therapeutic medicine. Akkaya group previously described various protocols to combine molecular logic gate notions with photosensitized generation of short-lived cytotoxic species, singlet oxygen[120, 121, 129]. Photosensitized generation of singlet oxygen in tumours, in or around cancer cells, is the essence of Photodynamic Therapy of Cancer (PDT)[104, 139-141]. The fate of the singlet excited state (S_1) of the photosensitizer is strongly related to the relative efficiencies and rates of photophysical processes involved. Among these, the most relevant are radiative transition from S_1 to S_0 (fluorescence) and intersystem crossing to T_1 triplet state (ISC). Efficiency of access to the triplet manifold is directly linked to the singlet oxygen quantum yield. Thus, considering the fact that in the photosensitization process, fluorescence and intersystem crossing (hence, singlet oxygen generation) are mutually antagonistic, and at least in principle, it should be possible to switch between these two processes. The digital equivalent is that of a demultiplexer (DEMUX) circuit[142], which takes single data input, and uses “n” select/address inputs to switch between 2^n possible outputs (Figure 57).

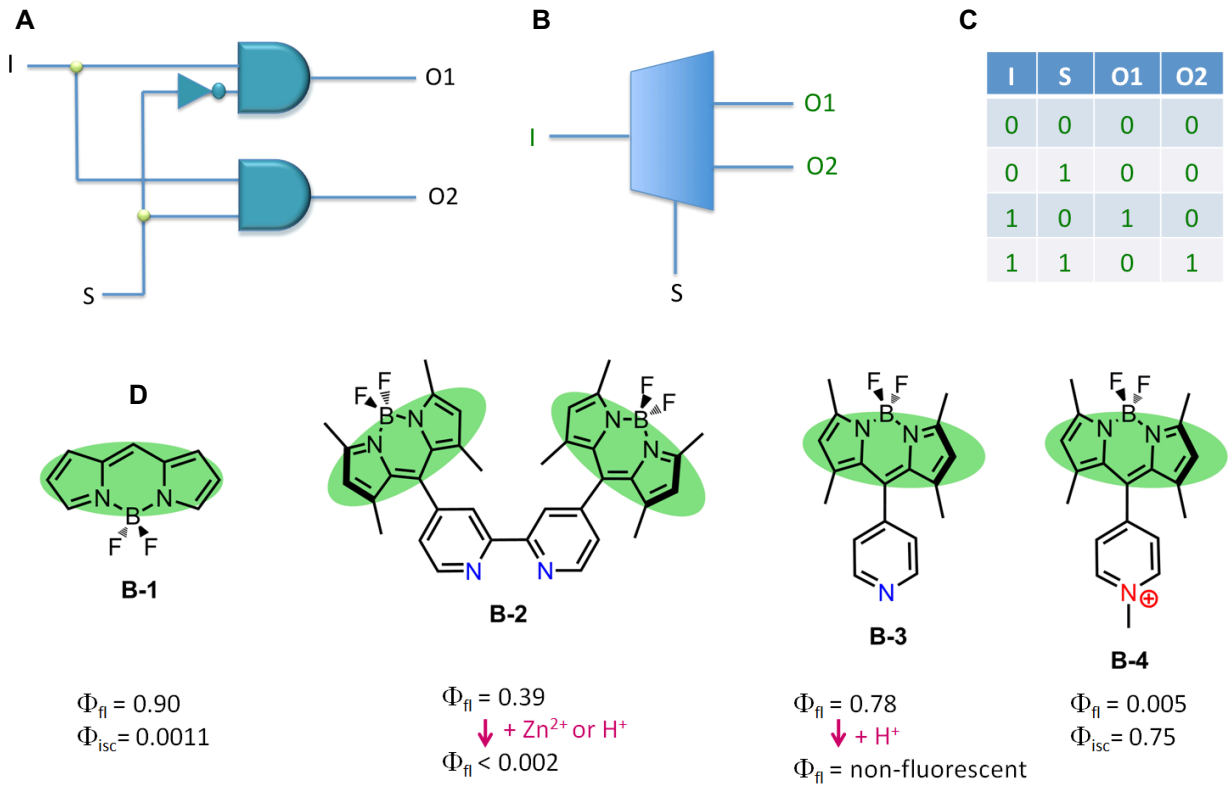

I	S	O1	O2
0	0	0	0
0	1	0	0
1	0	1	0
1	1	0	1

Figure 57. Two different representations and the truth table for the 1:2 DEMUX combinatorial circuit; and the structures of the parent Bodipy compound as well as its derivatives.

(**A)** DEMUX circuit with standard logic gate symbols. (**B)** Isosceles trapezoid is a common symbol for the MUX/DEMUX circuits. I is the data input, S is the "select" or "address" input, and O_1 and O_2 are two different outputs. **(C)** The truth table for a 1:2 DEMUX circuit is on the right. **(D)** Structures of the parent Bodipy compound **B-1**[143], and *meso*-pyridyl[144]/bipyridyl[103] substituted derivatives, together with their respective fluorescence and intersystem crossing quantum efficiencies are demonstrated. Protonation of both **B-2** and **B-3** result in the pyridinium cation, which switches on the intramolecular charge transfer process. Coordination of Zn^{2+} ions, or quaternization at the pyridine nitrogen (**B-4**) results in the same photophysical consequences.

Chemical implementation of this idea relies on the photophysics of the *meso*-pyridyl (or oligopyridyl) substituted Bodipy dyes (Figure 57D). Bodipy dyes are

exceptionally versatile and chemically malleable chromophores. The reference Bodipy chromophore (**B-1**) has high fluorescence quantum yield with a small Stokes' shift and on excitation, would have negligible access to the triplet manifold. This is also in part, the reason for higher chemical stability of this class of dyes under ambient conditions. In earlier investigations[103]aiming cation-responsive fluorophores (chemosensors), Baytekin et. al. observed a sharp decrease in the emission of bipyridyl-Bodipy compound (**B-2**) when an acid (TFA) or zinc perchlorate was added. Apparently, protonation of the ligand, or complexation with a +2 charged cation, transforms the ligand into a more easily reducible species, and photoinduced electron transfer from the excited Bodipy dye to the bipyridyl ligand becomes more efficient. Resulting charge transfer state (CTS) is responsible for the overall non-radiative relaxation (hence quenching). The orthogonal arrangement of the ligand and the chromophore is expected to facilitate intersystem crossing to the triplet state, as the charge recombination is typically accompanied with the population of the triplet excited state[145]. Thus, guided by the more recent studies on the photophysics of the similar Bodipy-pyridyl ligand systems[144], it is clear that such protonated pyridinium, or quaternized pyridinium substituted Bodipy dyes, and the Zn^{2+} complexes are more likely to be more efficient generators of singlet oxygen compared to the parent compounds from which they are derived, due to enhanced yield of the triplet state. Another useful aspect of this change is that it is chemically reversible; *i.e,* if the protonation is reversed, or charge on the Zn^{2+}

ion is neutralized (even partially), a return to the original state of affairs should be expected. Thus, the addition of phosphate to the **B-2**/Zn^{2+} complex, destabilizes the CT state, restores the fluorescence emission intensity (Figure 58).

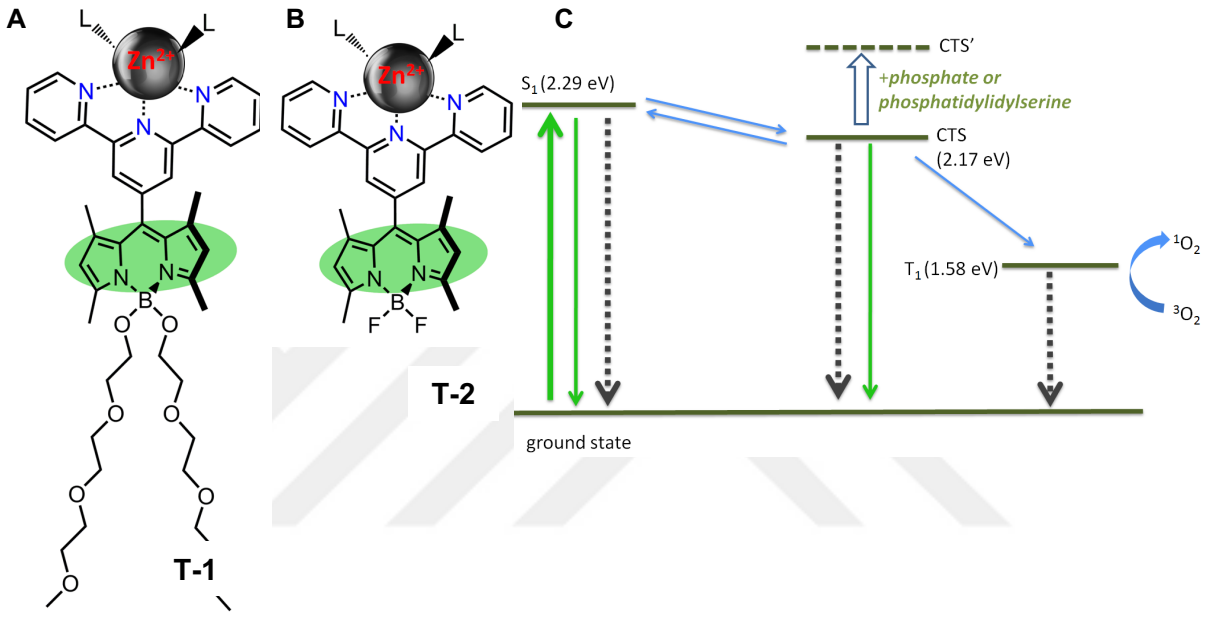

Figure 58. The structures of the Zinc(II) complexes of the terpyridyl-functionalized Bodipy compounds T-1 and T-2, and the modified Jablonski diagram depicting photophysical processes involved leading to DEMUX action.

(**A) (B)** L indicates solvent molecules as ligands, water or acetonitrile. Bodipy and the terpyridyl planes are orthogonal to each other due to the presence of 1,7-dimethyl substitution of the Bodipy chromophore. Double mTEG (methoxytriethyleneglycol) substitution at the boron center enhances water solubility. **(C)** Thicker green arrow is absorption, the other green arrows indicate radiative relaxations. Black-dashed arrows are non-radiative relaxation processes. Blue arrows indicate transitions between various excited states. CTS to T_1 transition is particularly enhanced because of the orthogonal geometry of the terpyridyl-Bodipy diad. Energy levels were experimentally estimated using the spectral data (S_1, CTS) in analogy to previous literature,[144]or based on the phosphorescence data[146] for similar Bodipy compounds (T_1).

4.3 Design of the Molecular Demultiplexer

In a demultiplexer design, the select input would determine the choice between the possible outputs. Searching for a candidate as the select input, we looked into the possibility of making use of structural changes taking place in the cell membranes during apoptosis. Fluorescence imaging of apoptosis relies on the loss of membrane asymmetry (ATP-dependent enzyme called flippase normally keeps phosphatidylserineinside the cell)[147, 148] as the negatively charged lipids and particularly phosphatidylserine is flipped to the extracellular side of the bilayer. The change is mediated by enzymes such as scramblase, which exposes phosphatidylserine on the cell's surface without consuming ATP.[147, 149]A selective probe for this event is the protein Annexin-V which selectively binds to phosphatidylserine. Since Annexin-V can be conveniently labelled with fluorescent dyes of different emission colours, it provides a set of useful tools for detecting apoptotic cells. There is also an interest in finding simpler, non-protein reporters of apoptosis, and in most of the reported examples,[150]the part which interacts with the phosphatidylserine unit is a Zn^{2+} complex where the metal ion which is held in place by pyridine-derived ligands, presenting coordination sites to the anionic groups of the phosphatidylserine.[151]

With these considerations, we targeted the compounds **T-1** and **T-2** for synthesis. Terpyridyl-Bodipy compounds **T-1** and **T-2** differ only in the groups attached to the boron bridge. A graphical representation of the operation of the automaton **T-1** is shown below (Figure 59).

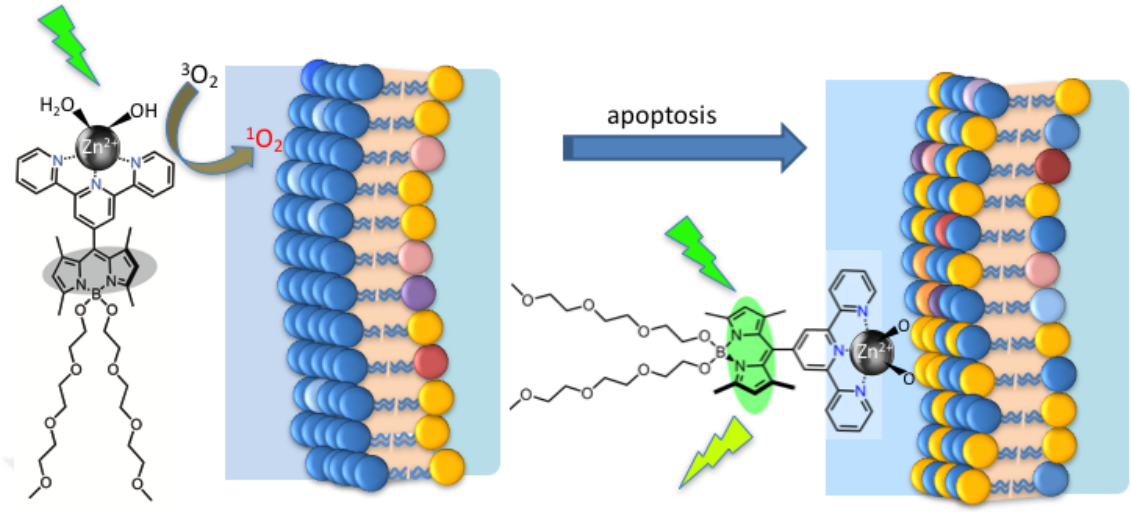

Figure 59. **T-1** induces apoptosis, then switches to diagnostic mode and fluorescently tags apoptotic cells. Blue polar heads represent phosphatidylcholine and sphingomyelins, whereas yellow, pink and purple heads represent phosphatidylserine, phosphatidylinositol and other negatively charged lipids. Apoptosis is accompanied by a loss of membrane asymmetry.

4.4 Results and Discussion

While compound **T-2** is appropriate for chemical characterization, compound **T-1** is better for biological media due to additional solubilizing oligoethyleneglycol units. The use of terpyridine instead of bipyridine ligand is favoured due to the stronger affinity of the former ligand to Zn^{2+} ions in aqueous media. The changes in emission was studied in acetonitrile. 2.0 µM solution of the model DEMUX **T-2** has an intense emission band (Φ_F = 0.34) with a maximum at 517 nm. Titration with Zn^{2+} ions in the form of perchlorate salt, results in sharp loss of emission intensity, with emission band moving to longer wavelengths, as the CT component in the emission becomes more prominent (Figure 60).

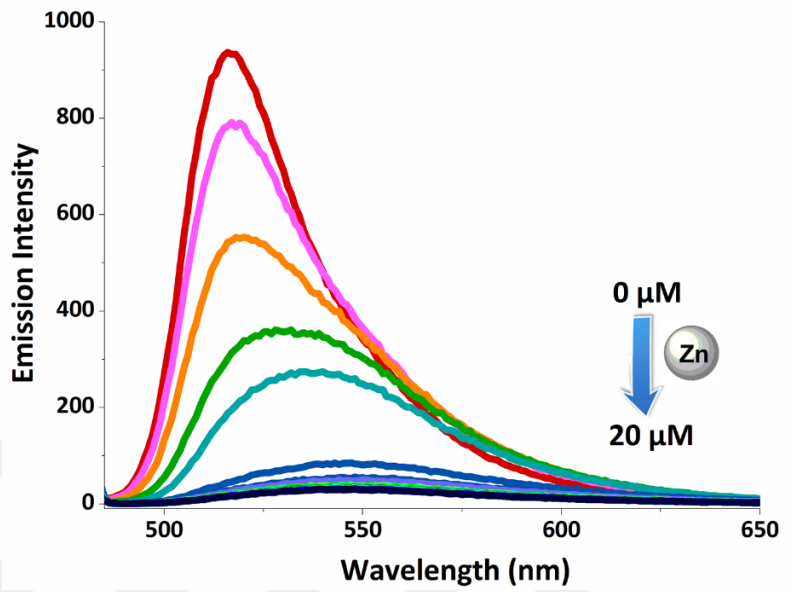

Figure 60. Fluorescence Emission Spectra of Bodipy **T-2** (2 µM) upon increased **Zn** concentrations (0-20 equiv.) in CH3CN (λex= 475 nm at 25 ^{o}C).

However, the addition of tetrabutylammonium phosphate completely reverses this change at 60 µM concentration in acetonitrile (Figure 61).

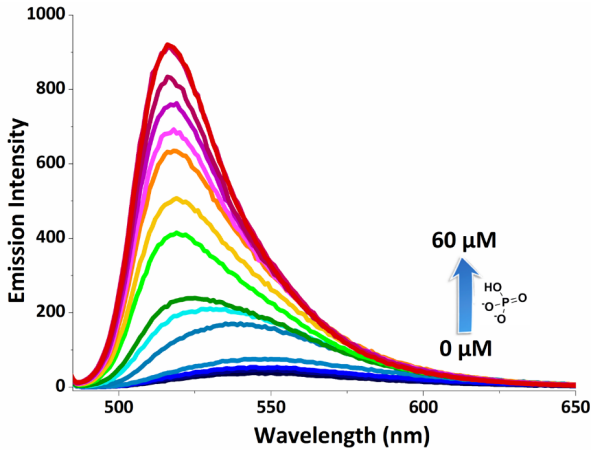

Figure 61. Fluorescence Emission Spectra of Bodipy **T-2** (2 µM)- ***Zn*** (5 equiv.) conjugate upon increasing concentrations of ***P*** (0 -30 equiv.) in CH_3CN (λ_{ex}= 475 nm at 25 ^{o}C).

In conclusion, figure 62 summarized the fluorescence emission spectra of **T-2**, (**T-2 -*Zn***) (5 equiv.), (**T-2 -*Zn-P*)** (15 equiv.), respectively**.**

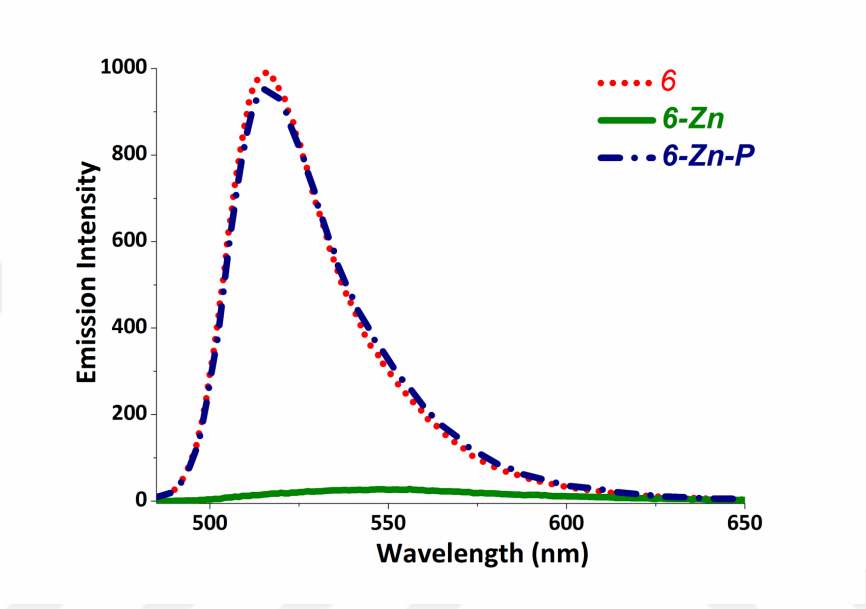

Figure 62. Normalized Fluorescence Emission Spectra of (**T-2**), (**T-2-Zn**), (**T-2-Zn-P**) in CH_3CN wherein concentrations are 2μM for **T-2**, 10 μM for ***Zn*** and 30 μM for ***P***.

The normalized absorbance graphics of **T-2**, (**T-2 -*Zn***), (**T-2 -*Zn-P*)** are shown in figure 62. **T-2** titration with Zn^{2+} ions in the form of perchlorate salt, results absorption band small shift to longer wavelengths. However, the addition of increased concentrations of tetrabutylammonium phosphate completely reverses this change in the absorption spectra.

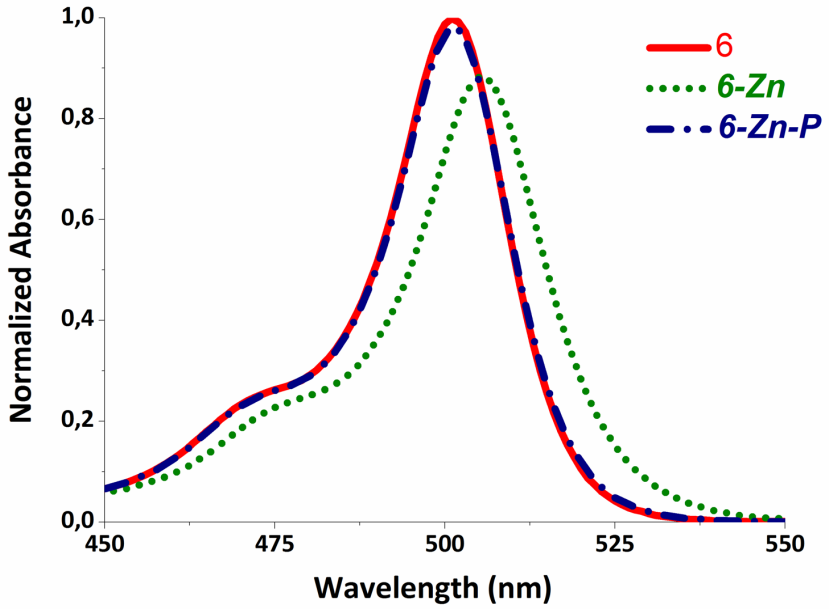

Figure 63. Normalized Electronic Absorption Spectra of $\mathbf{T_2}$, (**T-2** -***Zn***), (**T-2** -***Zn-P***) in CH_3CN wherein concentrations are 2µM for **T-2**, 10 µM for ***Zn*** and 30 µM for ***P***.

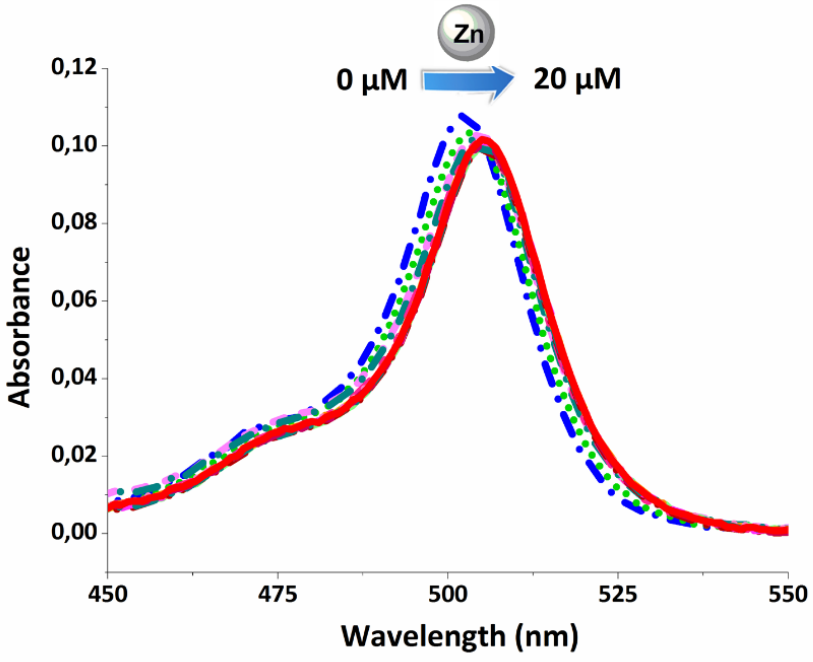

Figure 64. Electronic Absorption Spectra of Bodipy **T-2** (2µM) upon increased Zn concentrations (0-10equiv.) in CH_3CN.

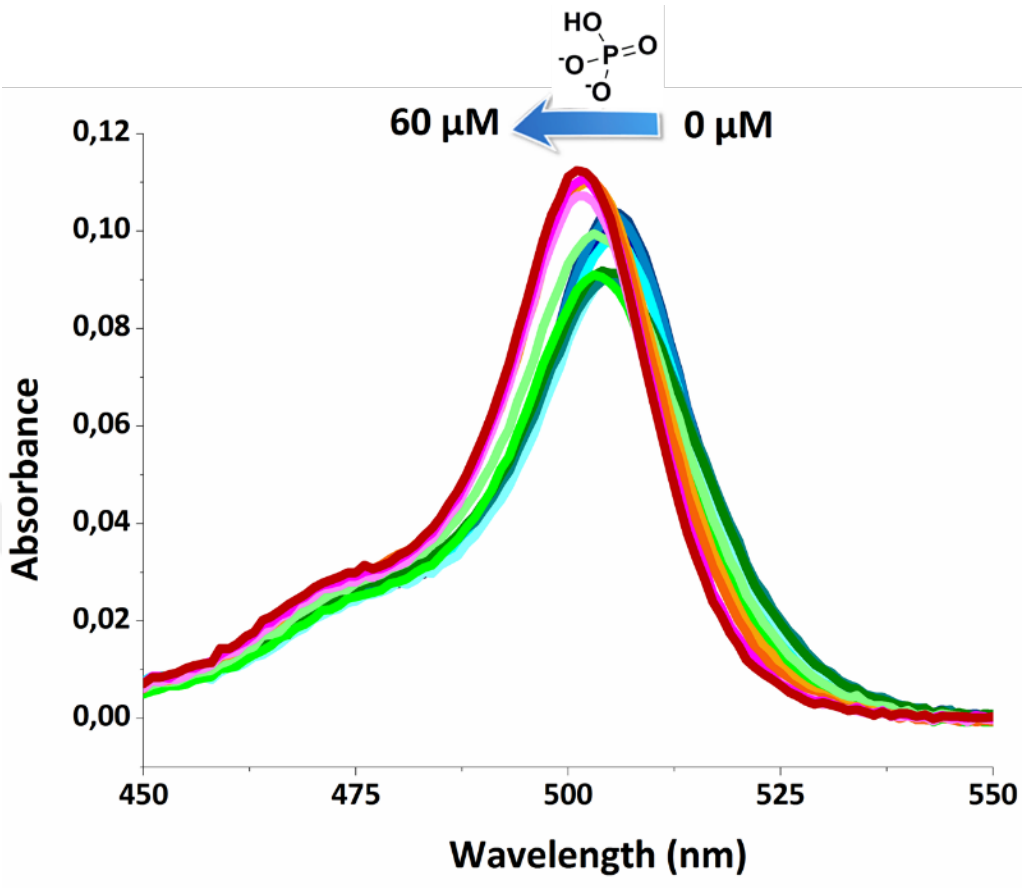

Figure 65. Electronic Absorption Spectra of Bodipy **T-2** (2µM) –**Zn** (5equiv.) conjugate upon increased concentrations of **P** (0-30equiv.) in CH3CN.

DEMUX **T-1** has an intense emission band (Φ_F = 0.49) with a maximum at 520 nm. Titration with Zn^{2+} ions in the form of perchlorate salt, results in sharp loss of emission intensity which gives similar result as **T-2**, with emission band moving to longer wavelengths, as the CT component in the emission becomes more prominent (Figure 66).

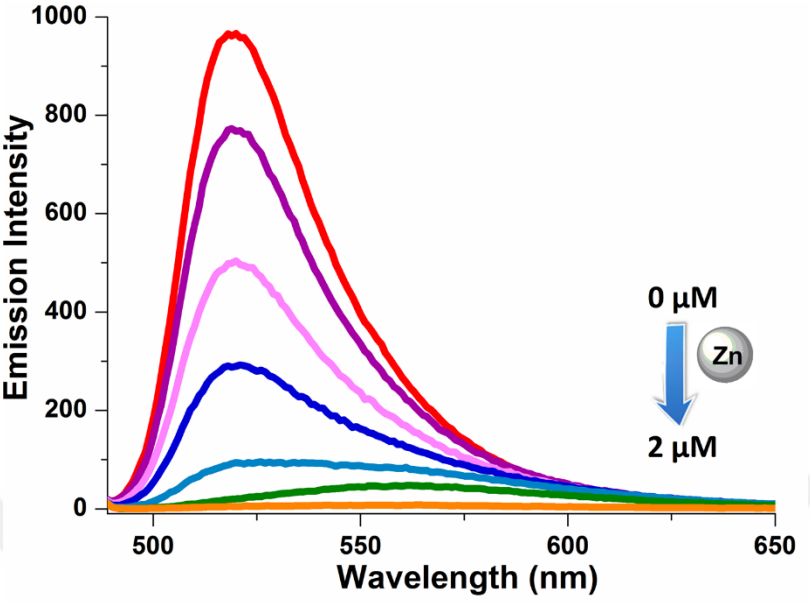

Figure 66. Fluorescence Emission Spectra of Bodipy **T-1** (1 µM) upon increased ***Zn*** concentrations (0-2 equiv.) in CH_3CN (λ_{ex}= 480 nm at 25 ^oC).

But, the addition of tetrabutylammonium phosphate completely reverses this change at 14 µM concentration in acetonitrile (Figure 67).

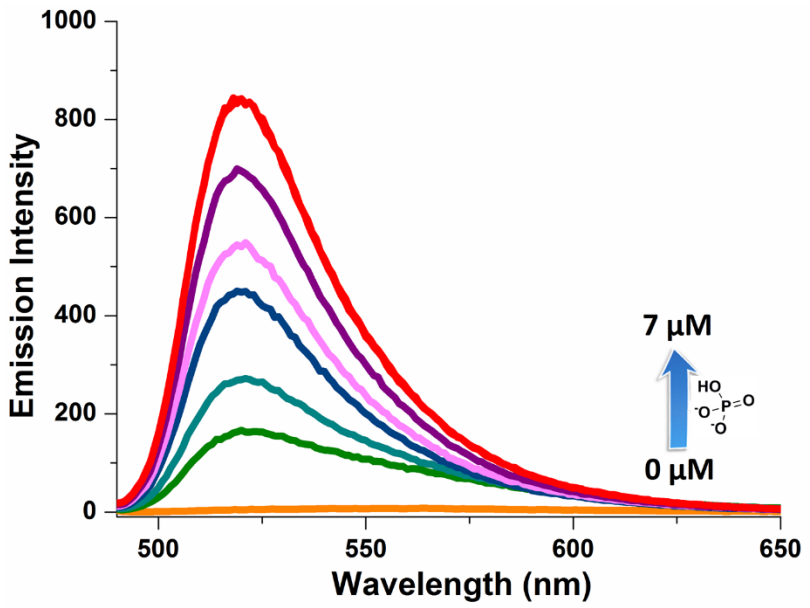

Figure 67. Fluorescence Emission Spectra of Bodipy **T-1** (1 µM)- ***Zn*** (2 equiv.) conjugate upon increasing concentrations of ***P*** (0 -7 equiv.) in CH_3CN (λ_{ex}= 480 nm at 25 ^oC) .

In summary, figure 68 concluded the fluorescence emission spectra of **T-1**, (**T-1 -*Zn***), (**T- -*Zn*-*P*).**

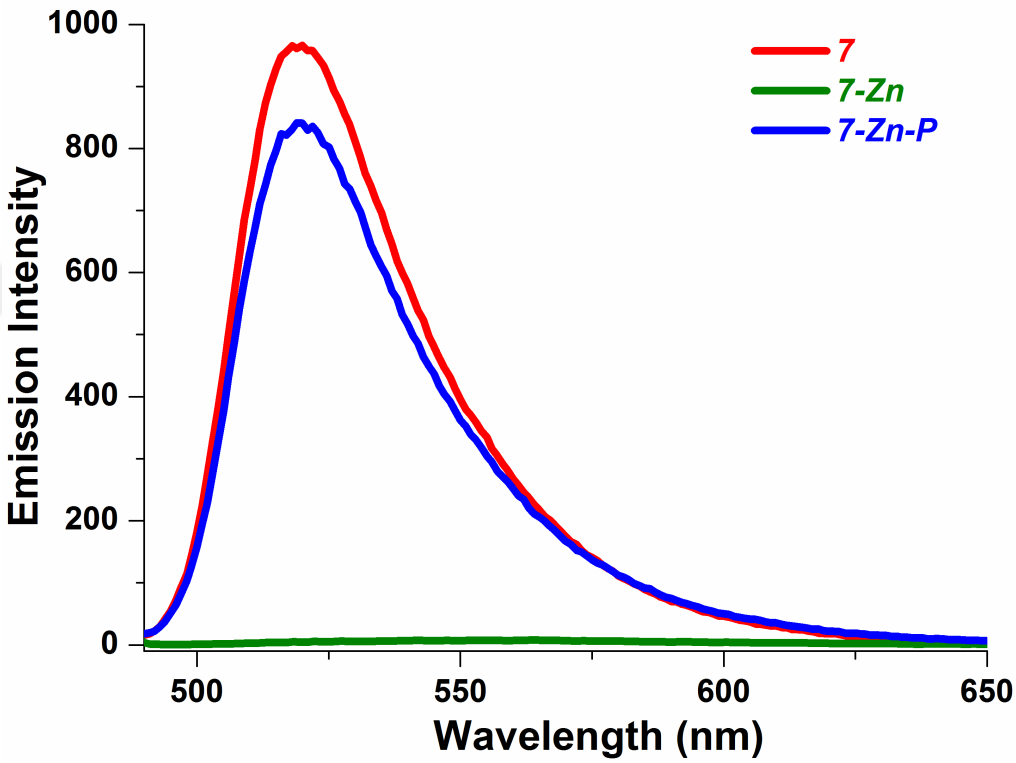

Figure 68. Normalized Fluorescence Emission Spectra of (**T-1**), (**T-1-Zn**), (**T-1-Zn-P**) in CH_3CN wherein concentrations are 1 µM for **T-1**, 2 µM for ***Zn*** and 7 µM for ***P***.

The normalized absorbance graphics of **T-1**, (**T-1 -*Zn***), (**T-1 -*Zn*-*P*)** are shown in figure 68. Similarly, **T-1** titration with Zn^{2+} ions in the form of perchlorate salt, results absorption band small shift to longer wavelengths. However, the addition of increased concentrations of tetrabutylammonium phosphate completely reverses this change in the absorption spectra.

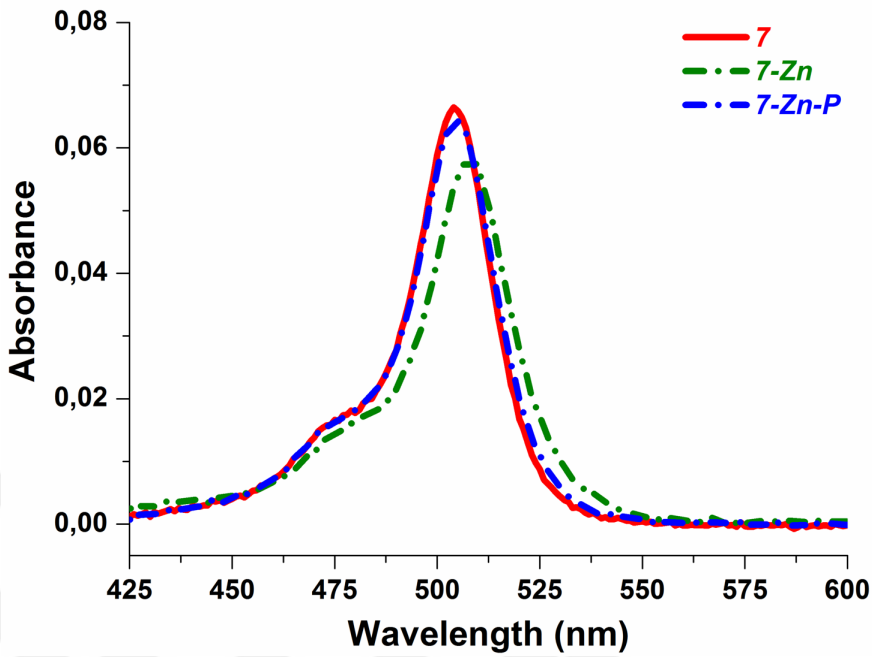

Figure 69. Normalized Electronic Absorption Spectra of (**T-1**), (**T-1 -Zn**), (**T-1 -Zn-P**) in CH_3CN wherein concentrations are 1 µM for **T-1**, 2 µM for ***Zn*** and 7 µM for ***P***.

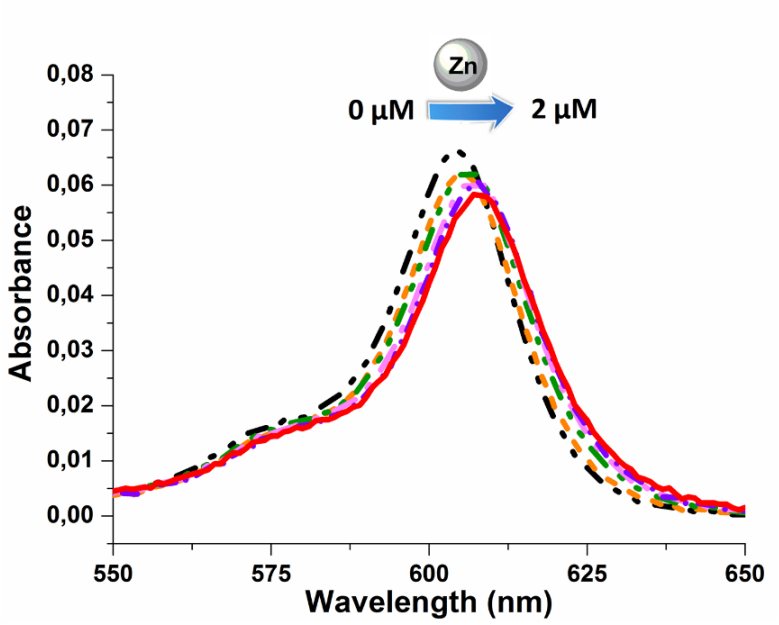

Figure 70. Electronic Absorption Spectra of Bodipy **T-1** (1 µM) upon increased ***Zn*** concentrations (0-2 equiv.) in CH_3CN.

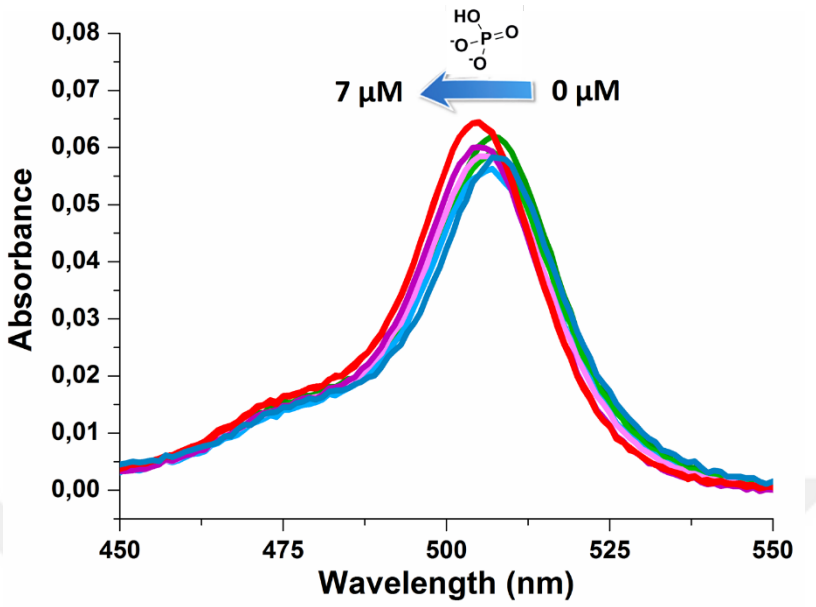

Figure 71. Electronic Absorption Spectra of Bodipy **T-2** (1 µM) –***Zn*** (2 equiv.) conjugate upon increased concentrations of ***P*** (0 -7 equiv.) in CH_3CN.

We then studied singlet oxygen generation rates under the same conditions for +/- phosphate: The singlet oxygen trap used is 1,3-diphenylisobenzofuran, its absorbance at 410 nm decreases due to a [4+2] cycloaddition with singlet oxygen, which is followed by decomposition.

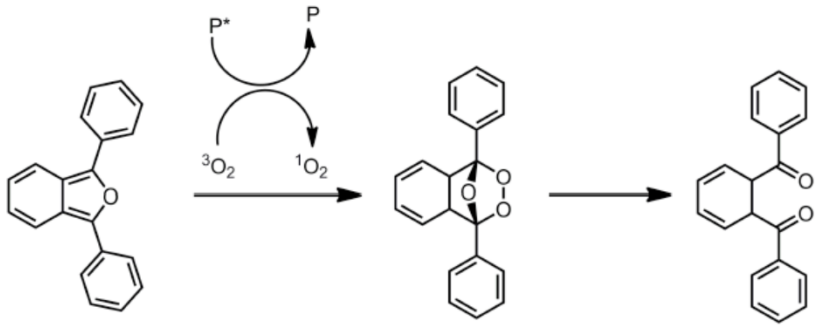

Figure 72. Reaction of singlet oxygen with 1,3-Diphenylisobenzofuran.

The fluorescence quantum yield (Φ_F) of the samples was calculated by using an equation (Equation 3);

$$\Phi_F = \Phi_F^0 \frac{I}{I_0} \frac{A}{A_0} \frac{n^2}{n_0^2} \qquad \textbf{Equation 3}$$

wherein ***I*** is the integrated fluorescence intensity, A is the absorbance at excitation wavelength, n is the refractive index of the solvent used, the subscript "0" stands for a reference compound. Rhodamine 6G was used as the reference compound (Φ_f=0.95 in water). Bodipy dyes (**T-1** and **T-2**) were dissolved in CH_3CN. Bodipy dyes and reference compound were prepared with the same absorbance (A_i) at the excitation wavelength (less than 0.05 in a 1.0 cm quartz cell). Reference compound and bodipy dyes (**T-1** and **T-2)** are excited at 488 nm. Calculated fluorescence quantum yields were given in the Table 5.

Compound[a]	λ_{abs}(nm)	λ_{ems}(nm)[b]	ε [c]	Φ_F[d]	τ (ns)
Bodipy T-2	501	517	67 000	0.34	1.62
T-2-*Zn*	505	547	59 200	0.048	-
T-2-Zn-P	501	517	65 800	0.37	1.56
Bodipy T-1	503	520	66 400	0.49	-
T-1-*Zn*	507	558	58 200	0.082	3.41
T-1-Zn-P	505	518	64200	0.48	-

Table 5. Photophysical data for (**T-2**), (**T-2-*Zn***), (**T-2-*Zn*-*P***), (**T-1**), (**T-1-*Zn***), (**T-1-*Zn*-*P***)

[a] Data acquired in CH_3CN.[b] λ_{exc}: 475 nm for Bodipy **T-2**, λ_{exc}: 480 nm for Bodipy **T-1**. [c] Unit: cm^{-1} M^{-1}. [d] Relative quantum yields. Reference dye: Rhodamine 6G in water (Φ_f=0.95).

In accordance with our design expectations, when irradiated with a λ=522 nm light-emitting diode array (at a 98.0 µmol.m^{-2}.s^{-1} photon flux), the Zinc complex is quite an effective photosensitizer. The singlet oxygen quantum yield (Φ_Δ) was determined in reference to Eosin Y, and found to be 0.11. However, the addition of 2.0 µM phosphate in the form of tetrabutylammonium phosphate, essentially stops singlet oxygen generation (Figure 73).

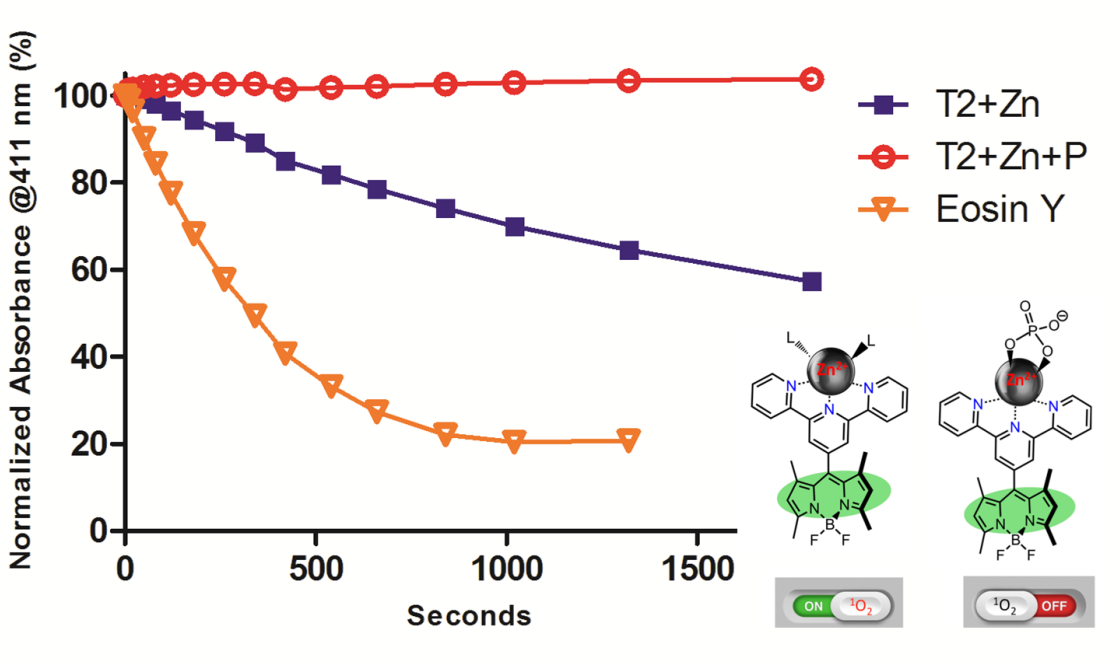

Figure 73. The decrease in the absorbance at 411 nm, in an oxygen saturated ethanol solution of selective singlet oxygen trap DPBF (50 µM) in the presence of 2.0 µM **T-2** and under irradiation with 522 nm green LED light source (solid blue squares). The singlet oxygen quantum yield (Φ_Δ) of **T-2** is

0.11. The addition of phosphate (red open circles) destabilizes the CTS state, blocking access to the triplet manifold. The absorbance data presented is the net absorbance values obtained by subtracting any background decrease in the probe absorbance due to light alone.

Thus, it is clear that fluorescence emission intensity and the singlet oxygen generation efficiency are inversely coupled, and the switch is the phosphate ions in solution. Operation of the molecular DEMUX circuit based on compound **T-2** was confirmed.

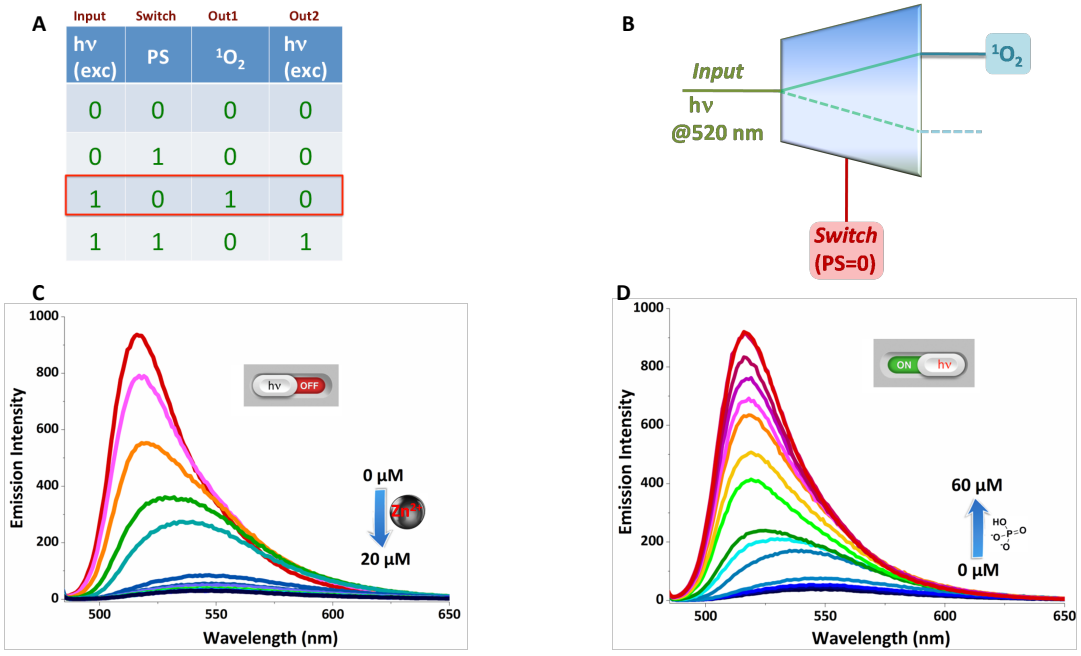

Figure 74. (A) The truth table with the data and switch inputs, and the corresponding outputs clearly identified, and the particular set of conditions valid under the light irradiation conditions on power-up were highlighted. **(B)** Switch input (no added phosphate in the model system or lack of phosphatidylserine(PS) in the external leaflet of the cell membrane in the cell cultures) selects singlet

oxygen as the primary output. **(C)** The model compound **T-2**, which is the Zn^{2+} complex of the *meso*-terpyridylbodipy compound, has a very low fluorescence emission intensity in acetonitrile. **(D)** The addition of phosphate ions results in a very sharp increase in emission intensity. The low emission intensity is due to the availability of a charge transfer state (CTS) resulting in enhanced intersystem crossing, which in turn leads to efficient generation of singlet oxygen.

Once the chemical validation was obtained, we ventured into cell culture experiments. Cell culture assays were performed with a human cancer suspension cell line-chronic myelogenous leukemia (K562). The cells were incubated with Dulbecco's Modified Eagle Medium (DMEM) supplemented with 20% FBS at the environmental conditions of 37 ^{o}C, 5% CO_2 and 60% humidity. Cells were treated with varying concentrations of the molecular automaton **T-1** (187.5 nM – 1.5 μM) and illuminated with a green light source (λ=522 nm light-emitting diode array, 98.0 $\mu mol.m^{-2}.s^{-1}$ photon flux) for a continuous duration of 12 hours. This 12-h period of illumination was followed by a 12-h incubation in the dark (total 24-h). The control group of the cells were incubated in the dark, for the exact duration of 24 hours under identical environmental conditions. The MTT assay was used in order to assess cell viability and cytotoxicity. Even the low doses of the automaton **T-1** seem to have resulted in a significant decrease of the cell viability (Figure 75, points and error bars designate means and standard deviations, respectively). The CC_{50} (50 % cytotoxic concentration) value of the **T-1** subjected to green light was estimated by fitting a model with non-linear regression (approximately 365 nM; the CC_{50} value of the compound in the dark

condition cannot be estimated since its projection is clearly out of the scale of the model fit).

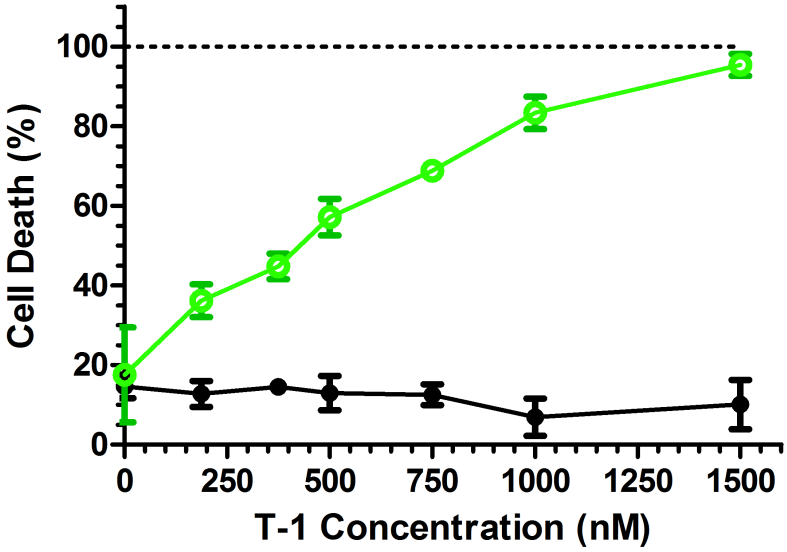

Figure 75. Powering up the automaton: Percent cell death as a function of increasing concentrations of the molecular terminator automaton **T-1**, quantified by MTT assays and phosphate, as the "switch" input, changing output from singlet oxygen to emission. Green open circles correspond to percent death of K562 cells under irradiation at 522 nm for 12 hours followed by continued incubation in dark for another 12 hours. Solid black circles correspond to cells kept under identical conditions of incubation with the agent, but in dark. Positive control (dashes at 100 % line) corresponds to cells incubated in DMSO-growth medium mixture (50/50, v/v).

In order to confirm the MTT assay results, and the switch from singlet oxygen generation to the emission/ signaling mode; Annexin V detection protocol for apoptosis was performed using flow cytometry. The percentage of fluorescent-labeled Annexin V (Phycoerythrin-PE) stained cells was much higher in the illuminated cell population compared with those incubated in the dark (73.7 %

vs. 18.0 %; Figure 76A, blue shaded areas represent the cells in the dark, green shaded areas represent the irradiated cells). In addition, 71.7 % of irradiated K562 cells (Figure 76B) were positive for **T-1** in contrast to 18.0 % of the cells incubated in the dark (Figure 76C), demonstrating that Annexin V and the automaton targets the same kind of cell membranes with outer leaflet enriched in phosphatidylserine, which are undergoing apoptosis. Cancer cells which are not killed or not undergoing apoptosis are not marked by the agent, but subject to cytotoxic singlet oxygen attack when the automaton is powered up by irradiation. Photocytotoxicity was further revealed in a 2-color analysis with PE-Annexin V in order to specifically target and identify apoptotic cells in conjunction with the **T-1** (Figure 76D). Approximately **70 %** of the illuminated cells were positive both for PE-Annexin V and **T-1** and about **16 %** of the cells were negative for both (area A++ and A-- in Figure 76D, respectively), confirming that the terminator automaton turns on the emission signal, only when the cells are undergoing apoptotic death process.

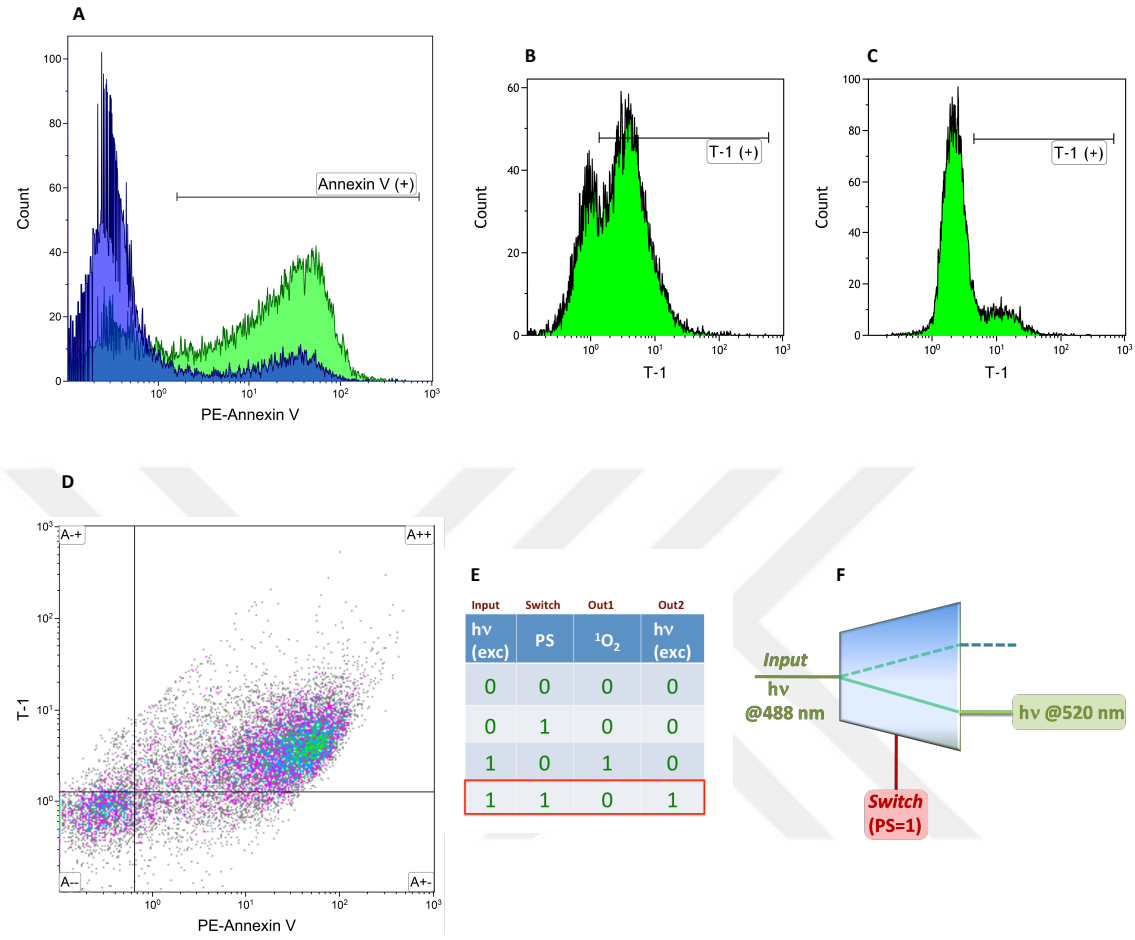

Figure 76. Kill confirmed: **T-1** signals apoptosis by switching to diagnostic mode. Flow cytometry data and confocal microscopy images for PE-Annexin V and molecular automaton **T-1**. **(A)** PE-Annexin labels most of the cells incubated with **T-1** under light irradiation (Annexin V (+) region of the green area). **(B)** Green channel: Cells incubated with **T-1** under irradiation. **(C)** Green channel: Cells incubated with **T-1** in the dark. **(D)** 2D plot for both green and red channels: **T-1** and PE-Annexin V (a specific apoptosis marker) stain the same kind of cells with a large (86%) agreement: 70% of the irradiated cells were co-stained with both **T-1** and PE-Annexin V, indicating only apoptotic cells are fluorescently labeled with **T-1. (E)** The truth table with input, the switch and the outputs clearly identified, and the particular set of conditions were highlighted. **(F)** Switch input (appearance of phosphatidylserine in the external leaflet of the cell membrane) selects fluorescence emission as the primary output.

Confocal microscopy provided further evidence corroborating the cytotoxicity results from MTT assays and flow cytometry, as well as the co-staining of PE-Annexin V and **T-1** in low cytometry analyses. The data demonstrate that just like PE-Annexin V, the automaton shows fluorescence signal only when attached to apoptotic cell membranes. Cellular membranes of the illuminated cells incubated with **T-1** were shown to be stained with both Annexin V and **T-1** (1.5 μM); in contrast to their counterparts incubated in the dark, which were not stained by either **T-1** (1.5 μM) or PE-Annexin V. Cell membranes of the illuminated cells in the presence of **T-1** appear bright green when excited at 488 nm and bright red when excited at 543 nm. However, their counterparts which had been incubated in the dark were negative for either green or red emission. Figure 77A-C panel shows the DIC, **T-1**, Annexin V and merged images, respectively.

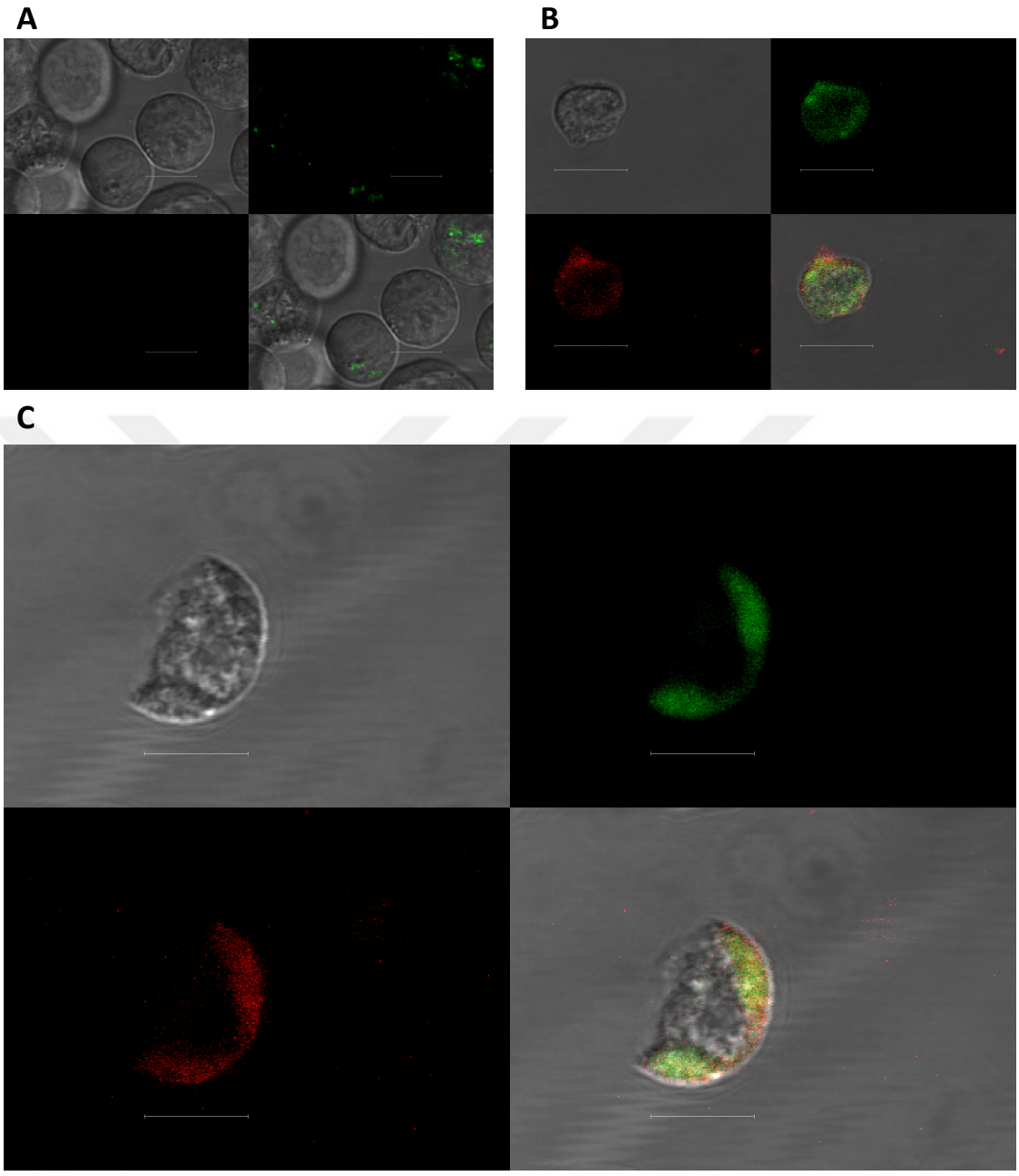

Figure 77. **(A)** Cells treated with PE-Annexin V and the **T-1,** and kept in dark, show no signs of morphological change, and the cellular membranes are not stained with either one of the agents (scale bar, 10 µm). **(B)** and **(C)** cells were incubated with **T-1**, irradiated with the LED light source, then treated with PE-Annexin V. The two agents (**T-1** and PE-Annexin V, green and red, respectively) label the same regions in the cells undergoing apoptosis (scale bar, 10 µm).

4.5 Experimental Details

4.5.1 General Experimental Procedures

^{1}H NMR and ^{13}C NMR spectra were recorded on Bruker Spectrospin Avance DPX 400 spectrometer using $CDCl_3$ as the solvent. Chemical shifts values are reported in ppm from tetramethylsilane as internal standard. Spin multiplicities are reported as the following: s (singlet), d (doublet), m (multiplet). Electronic absorption spectra in solution were acquired using a Varian Cary-100 spectrophotometer and a StellarNet BLACK Comet C-SR diode array miniature spectrophotometer connected to deuterium and halogen lamp by optical fiber using 1 cm matched quartz cuvettes at room temperature. Fluorescence spectra were determined on Varian Eclipse and Edinburgh Instruments FLS920 fluorospectrometer. Spectrophotometric grade solvents were used for spectroscopy experiments. Fluorescence lifetime of S1 state was measured by time-correlated single photon counting method (Edinburgh FLS920 spectrophotometer) with excitation at 507 nm by a portable diode laser (150 ps FWHM) and emission was monitored at 558 nm. The lifetime values were computed by the F900 software. All spectra were corrected for the sensitivity of the photo-multiplier tube. HRMS data were acquired on an Agilent Technologies 6530 Accurate-Mass Q-TOF LC/MS. Flash column chromatography (FCC) was performed by using glass columns with a flash grade silica gel (Merck Silica Gel 60

(40–63 μm)). Reactions were monitored by thin layer chromatography (TLC) using precoated silica gel plates (Merck Silica Gel PF-254), visualized by UV-Vis light. All organic extracts were dehydrated over anhydrous Na_2SO_4 and concentrated by using rotary evaporator before being subjected to FCC. In singlet oxygen measurements 1,3-Diphenylisobenzofuran was usedas a singlet oxygen trap in organic solvent measurements and was purchased from supplier. All other chemicals and solvents were supplied from commercial sources and used as received. Reference compound was synthesized based on the literature[30]. Titrations were performed by using ZnOAc as Zn source and tetrabutylammonium phosphate as phosphate source. ZnOAc is represented as Zn and phosphate source is represented as P in the graphs.

4.5.2 Synthetic Procedures

Synthetic Pathway:

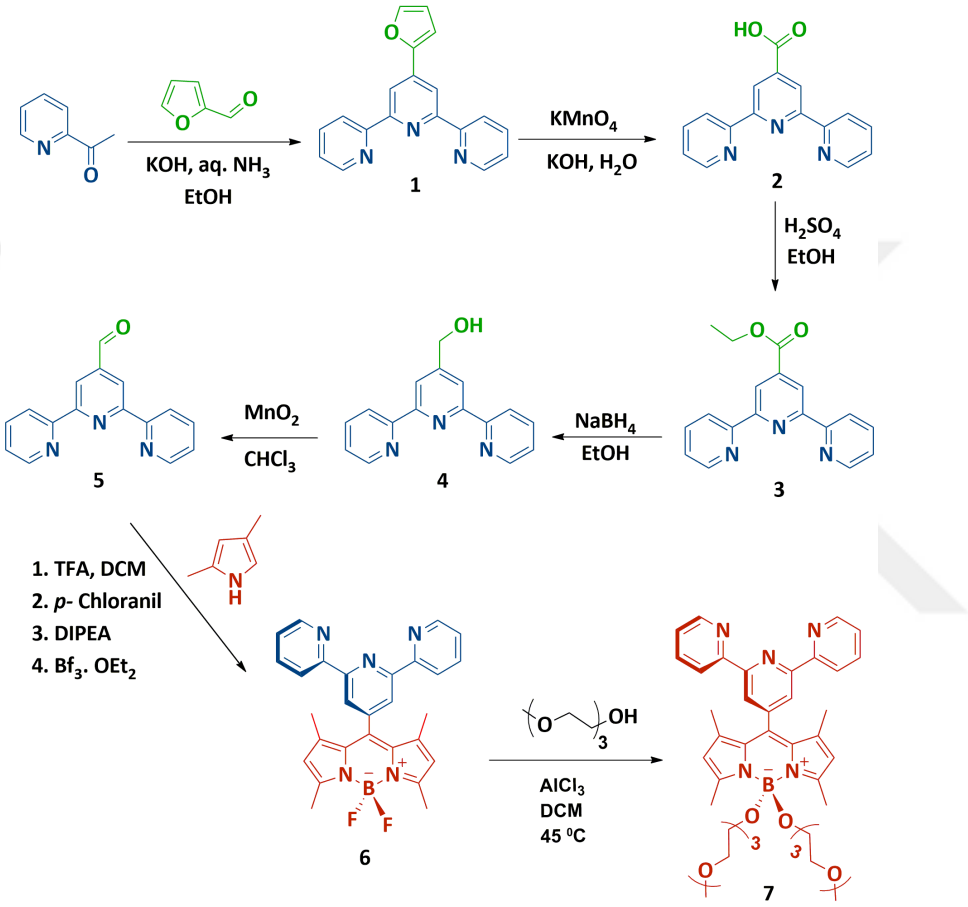

Figure 78. Total synthesis of **T-1** (**7**).

Synthesis of 4'-(2-furanyl)-2,2':6',2''-Terpyridine (**1**):

Furfuraldehyde (1.92 g, 20.0 mol) was added to the reaction mixture containing 2-acetylpyridine (4.48 g, 40.0 mmol) dissolved in ethanol (90.0 ml). KOH (3.08 g, 54.5 mmol) and 25% (wt/vol) aq. NH_3 (58.0 ml, 1.51 mmol) were added to reaction mixture which was left to stir at room temperature for 24 hours. Solids were filtered under vacuum onto a sintered funnel and washed with ice cold 50% (*v*/*v*) ethanol until the washings become colorless. Then, the solid was dried to obtain the compound **1** (2.24 g,56%).

^{1}H NMR (400 MHz, *d6*-DMSO): δ_H 8.76 (d, *J* = 4.8 Hz, 2H), 8.69 (s, 2H), 8.65 (d, *J*= 7.9 Hz, 2H), 8.04 (t, *J*= 7.7 Hz, 2H), 7.97 (s, 1H), 7.54 (dd, J= 4.8, 7.4 Hz, 2H),7.46 (d, J= 3.4 Hz, 1H), 6.75 (s, 1H).

^{13}C NMR (100 MHz, *d6*-DMSO): *δ* 156.2, 155.3, 151.2, 149.8, 145.5, 139.5, 137.9, 125.1, 121.3, 114.6, 113.2, 110.8 ppm.

MS (TOF- ESI): m/z: calculated: 300.11314, Found: 300.11265 $[M+ H]^+$, Δ= 1.56 ppm.

Synthesis of [2,2':6',2''-Terpyridine]-4'-carboxylic acid (**2**):

KOH pellets were added to demineralized water (120.0 ml) until the pH of the solution is adjusted to 10. Then, furyl-terpyridine **1** (2.24 g, 7.48 mmol) was added to the reaction mixture. After the addition of KMnO4 (4.72 g, 29.87 mmol), reaction mixture was refluxed for 3 hours. After cooling the reaction

medium to room temperature, reaction mixture was filtered through a pad of Celite which deposited on a sintered funnel and washed with demineralized water. The pH of the filtrate was adjusted to pH=5 by dropwise addition of concentrated HCl to afford white precipitate which was filtered via glass-sintered funnel and wash thoroughly with demineralized water till the washings become neutral. Then, the solid was dried to obtain the compound **2** (1.36 g, 66%).

^{1}H NMR (400 MHz, CH_3OD): δ_H 8.95 (s, 2H), 8.73 (d, *J* = 4.8 Hz, 2H), 8.68 (d, *J*= 7.9 Hz, 2H), 8.04 (td, *J*= 1.7, 7.8 Hz, 2H).

^{13}C NMR (100 MHz, CH_3OD) ***δ*** 156.4, 155.2, 148.9, 137.5, 124.4, 121.4, 120.1, 111.9 ppm.

MS (TOF- ESI): m/z: calculated: 278.0924, Found: 278.09255 $[M+ H]^+$, Δ= -0.53 ppm.

Synthesis of ethyl- [2,2':6',2''-Terpyridine]-4'-carboxylate (**3**):

[2,2':6',2''-Terpyridine]-4'-carboxylic acid 2 (1.36 g, 4.90 mmol) was dissolved in absolute ethanol (150.0 ml). After the addition of concentrated H_2SO_4 (1.0 ml), reaction mixture was refluxed for 72 hours. After the removal of ethanol under vacuum, the residue was dissolved in water (100.0 ml) and the pH of the solution was adjusted to 8.0 by portionwise addition of solid $NaHCO_3$. Aqueous

layer was extracted with dichloromethane, dried over Na_2SO_4 and concentrated under vacuum to isolate the compound **3** (1.20 g, 87%).

^{1}H NMR (400 MHz, $CDCl_3$): δ_H 9.02 (s, 2H), 8.78 (s, 2H), 8.65 (d, *J*= 7.9 Hz, 2H), 7.91 (t, *J*= 7.7 Hz, 2H),7.38-7.41 (m, 2H), 4.51 (q, *J*= 14.3 Hz, 2H), 1.49 (t, *J*= 7.1 Hz, 3H).

^{13}C NMR (100 MHz, $CDCl_3$) *δ* 156.6, 149.3, 16.9, 126.9, 124.1, 121.3, 120.4, 61.8, 14.4 ppm.

MS (TOF- ESI): m/z: calculated: 306.12370, Found: 306.12428 $[M+ H]^+$, Δ= -1.95 ppm.

Synthesis of [2,2':6',2''-Terpyridine]-4'-methanol (**4**):

Ethyl- [2,2':6',2''-Terpyridine]-4'-carboxylate (1.0 g, 3.28 mmol) was dissolved in ethanol (100.0 ml). After the addition of $NaBH_4$ (2.48 g, 65.6 mmol), reaction mixture was refluxed at 85°C. The progress of the reaction was followed by TLC (neutral Al_2O_3, DCM). When all the starting material was consumed, reaction medium was cooled to room temperature. Saturated $NaHCO_3$ solution was added to the reaction mixture in order to deactivate excess $NaBH_4$. After the removal of ethanol under vacuum, the residue was dissolved in water and extracted with ethyl acetate, dried over Na_2SO_4 and concentrated under vacuum to isolate the compound **4** (0.86 g, quantitative)[31].

^{1}H NMR (400 MHz, $CDCl_3$): δ_H 8.69 (s, 2H), 8.64 (d, *J*= 7.8 Hz, 2H), 8.41 (s, 2H), 8.02 (t, *J*= 7.7 Hz, 2H), 7.49 (t, *J*= 6.2 Hz, 2H), 4.86 (s, 2H).

^{13}C NMR (100 MHz, $CDCl_3$) *δ* 156.2, 155.6, 152.3, 149.1, 136.9, 123.8, 121.4, 118.5, 63.9 ppm.

MS (TOF- ESI): m/z: calculated: 264.11314, Found: 264.11434 $[M+ H]^+$, Δ=-4.55 ppm.

Synthesis of 4'-formyl-2,2':6',2''-Terpyridine (**5**):

[2,2':6',2''-Terpyridine]-4'-methanol (0.86 g, 3.27 mmol) was dissolved in $CHCl_3$. After the addition of MnO_2 (2.84 g, 32.7 mmol), the reaction mixture was refluxed until all the starting material was consumed. The progress of the reaction was followed by TLC (neutral Al_2O_3, DCM). When all the starting material was consumed, reaction medium was cooled to room temperature and filtered. The filtrate was concentrated under vacuum to isolate the compound **5** (0.85 g, quantitative).

^{1}H NMR (400 MHz, $CDCl_3$): δ_H 10.31 (s, 1H), 8.92 (s, 2H), 8.78 (s, 2H), 8.66 (d, *J*= 8.2 Hz, 2H), 7.93 (t, *J*= 7.8 Hz, 2H), 7.42 (t, *J*= 6.1 Hz, 2H).

^{13}C NMR (100 MHz, $CDCl_3$) *δ* 191.7, 157.1, 155.0, 149.3, 143.9, 136.9, 124.3, 121.2, 119.7 ppm.

MS (TOF- ESI): m/z: calculated: 262.09749, Found: 262.09824 $[M+ H]^+$, Δ= -2.87 ppm.

Synthesis of 4,4-difluoro-1,3,5,7-tetramethyl-8-(2,2':6',2''-Terpyridine)-4-bora-3a,4a-diaza-s-indacene(**6**):

Trifluoroacetic acid (TFA; 0.22 ml, 2.87 mmol) was added dropwise to a vigorously stirring solution of 4'-formyl-2,2':6',2''-Terpyridine (0.5 g, 1.91 mmol) and 2,4-dimethylpyrrole (0.473 ml, 4.58 mmol) in 500.0 mlargon deaerated dichloromethane (DCM). The resulting solution was left to stir at room temperature in the dark 1 day. *p*- Chloranil (0.47 g, 1.91 mmol) was added in one portion and reaction was left to stir for 2 hours. Diisopropylethylamine (8.0 ml) was added dropwise to this mixture over a period of 15 min, and the resulting dark brown solution was allowed to stir for an additional 30.0 min. $BF_3.OEt_2$ (8.0 ml) was then added dropwise over a period of 15 min and the resulting dark red solution was allowed to stir at room temperature in the dark for 1 day. The slurry reaction mixture was washed with water (3 × 300 ml) and dried over anhydrous Na_2SO_4. The solvent was evaporated and the residue was purified by using neutral Al_2O_3 using DCM: Hexane (1:1, *v*/*v*) as the eluent to afford compound **6** (0.37 g, 40%).

^{1}H NMR (400 MHz, $CDCl_3$): δ_H 8.70-8.73 (m, 4H), 8.57 (s, 2H), 7.92 (td, *J*= 1.9, 7.6 Hz, 2H), 7.37-7.40 (m, 2H), 6.01 (s, 2H), 2.60 (s, 6H), 1.56 (s,6H).

^{13}C NMR (100 MHz, $CDCl_3$) ***δ*** 156.4, 156.1, 155.3, 149.4, 145.3, 142.8, 138.8, 136.9, 130.5, 124.3, 121.6, 121.1, 120.6, 30.9, 15.2 ppm.

MS (TOF- ESI): m/z: calculated: 479.22019, Found: 479.22179 $[M+ H]^+$, Δ= -3.21 ppm.

Synthesis of 4,4-bis(2-(2-(2-methoxyethoxy)ethoxy)ethoxy)-1,3,5,7-tetramethyl-8-(2,2':6',2''-Terpyridine)-4-bora-3a,4a-diaza-s-indacene (**7**):

Bodipy ***6*** (0.05 g, 0.10 mmol) was dissolved in 3.0 ml DCM. Triethyleneglycol monomethyl ether (0.168 g, 1.0 mmol) was added to the reaction mixture which was stirred at 45°C. The reaction was started with the addition of $AlCl_3$ (0.031 g, 0.23 mmol). The progress of the reaction was followed by TLC (neutral Al_2O_3,DCM:MeOH [98:2, *v*/*v*]). When all the starting material was consumed, reaction medium was cooled to room temperature and filtered. The filtrate was concentrated under vacuum and the residue was purified by using neutral Al_2O_3 using DCM: MeOH (98:2) as the eluent to afford compound ***7*** (0.068 g, 88.%).

^{1}H NMR (400 MHz, $CDCl_3$): δ_H 8.75-8.70 (m, 4H), 8.54 (s, 2H), 7.95-7.90 (m, 2H), 7.41-7.37 (m, 2H), 5.95 (s, 2H), 3.66-3.54 (m, 24H), 3.39 (s, 6H), 2.59 (s, 6H), 1.52 (s, 6H).

^{13}C NMR (100 MHz, $CDCl_3$) δ 156.6, 156.2, 155.4, 149.3, 146.1, 144.5, 141.1, 140.7, 138.3, 137.0, 131.2, 124.3, 121.5, 121.2, 120.8, 96.4, 73.1, 72.3, 71.9, 70.7, 70.5, 70.4, 60.7, 59.0, 15.3, 14.9.

MS (TOF- ESI): m/z: calculated: 789.39940, Found: 789.40056 $[M+ H]^+$, Δ= -1.47 ppm.

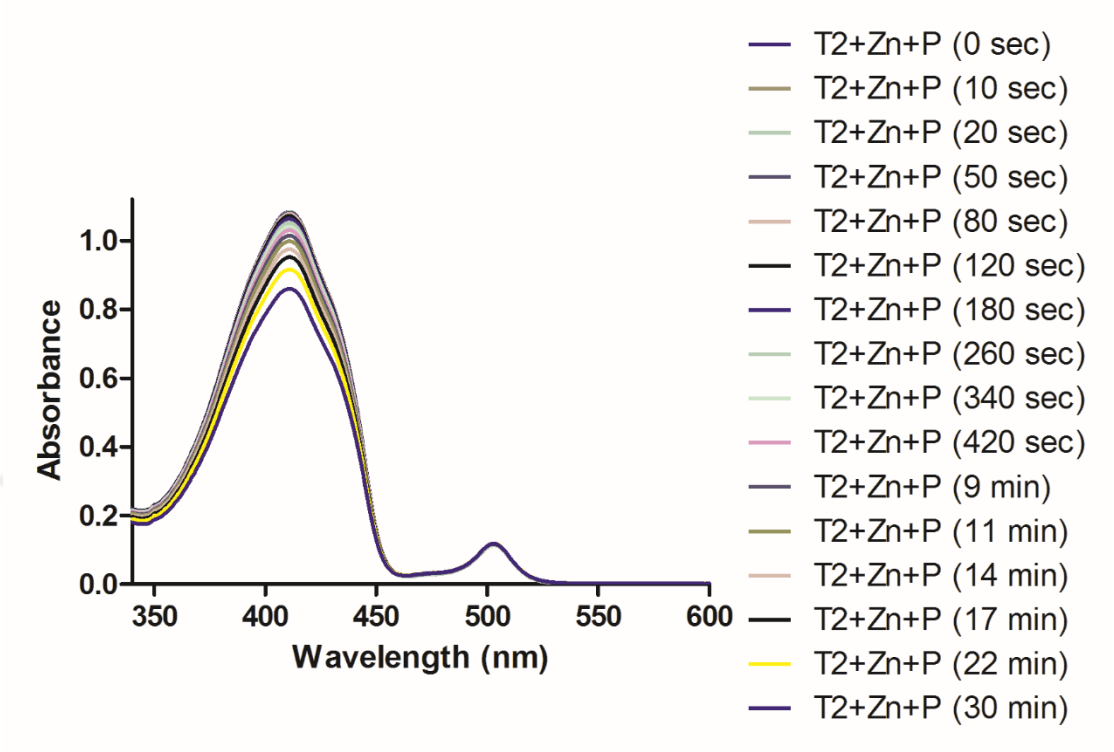

Figure 79. Raw data for the decrease in absorbance of DPBF in ethanol in the presence of **T2+Zn** and **phosphate** in medium. Singlet oxygen quantum yields were calculated as previously described using initial rate of decrease in the DPBF absorbance once any changes in absorbance of the DPBF without any agent added were subtracted[152]. In this particular case, the changes in absorbance is the same as the decrease in absorbance of DPBF alone, under irradiation.

4.5.3 Cell Culture and MTT Assay

K562 human chronic myelogenous leukemia suspension cells were cultured in 25 cm^2 culture flasks containing Dulbecco's Modified Eagle Medium (DMEM, Gibco, 11971-025) supplemented with 20 % fetal bovine serum in a cell culture incubator at 37°C, 5 % CO_2 and 60 % humidity. The main functional goals of the current

study are to study the cytotoxicity of **T-1** under illumination and its staining ability of the apoptotic cells. Since phosphate in the growth media can interfere with experimental results, we used DMEM w/o phosphate supplemented with 20 % fetal bovine serum that has been dialyzed extensively at 4^{o}C against isotonic saline (0.15 M NaCl) using dialysis tubing (Sigma-Aldrich, USA, (D7884)); since the viability of the cells cultured in such conditions is known to be not hampered for periods even more than 24-h[32]. This cell culture medium was also utilized for analyses with flow cytometry and confocal laser scanning microscopy to study cytotoxicity and cellular staining.

The compound was diluted in cell culture medium and assay concentrations were freshly prepared. Cell viability / death was evaluated by MTT (3-(4, 5-dimethylthiazolyl-2)-2,5-diphenyltetrazolium bromide) assay. Briefly, 50 µL cell suspensions in culture medium containing 3 x 10^4 K562 cells were plated in 96-well flat-bottom culture plates (Corning, MA, USA) and incubated for 12 hours to recover from handling. Varying concentrations of the chemical compound in cell culture medium was added into each well (the final concentrations were 187.5 nM – 1.5 µM) in quadruplicate. The experimental group of the cells were illuminated with a green light source (λ=522 nm light-emitting diode array, 98 µmol.m^{-2}.s^{-1} photon flux, distance between light source and cells: 10 cm) for a continuous duration of exactly 12 hours in a culture incubator (37^{o}C, 5 % CO_2, 60 % humidity). This 12-h period of illumination was followed by a 12-h incubation solely in the dark (total 24-h) also in the incubator. The control group of the cells

were incubated in the dark, for the exact duration of 24 hours under identical environmental conditions except illumination. According to the assay protocol, 25 µl of the MTT reagent (Sigma-Aldrich, MO, USA) was added to each well in order to assess cell viability (final concentration: 1 mg/ml) at the end of the 24-h incubation period. Following a 4-h incubation of the cells with the MTT reagent, the generated formazan precipitates were solubilized by the addition of the lysing buffer (80 µL, pH: 4.7), which is composed of 23% SDS (sodium dodecyl sulfate) dissolved in a solution of 45% DMF (N,N-Dimethylformamide). After an overnight incubation at 37^{o}C, the absorbance values (of each well) were measured at 570 nm in a microtiter plate reader (Spectramax Plus, Molecular Devices, CA, USA) at 25^{o}C. Cells incubated in culture medium only (without the compound) served as the control for cell viability both for the illuminated plates and for the ones kept in the dark; whereas DMSO (50 %, v/v) was used to observe maximum cell death (positive control). Cell death (%) was assessed with the normalization of the values calculated by the formula "optical density (OD) of control cells – OD of treated cells". The CC_{50} values of the compound in the illuminated condition was estimated by fitting a model with non-linear regression.

4.5.4 Flow Cytometry

Illuminated and control K562 cells (in the dark) were stained with PE-Annexin V, as described in the technical data sheet (BioLegend, USA), and were analyzed by FACS Aria II (equipped with 488 nm and 635 nm lasers) using FACS Diva software.

4.5.5 Confocal Laser Scanning Microscopy

Illuminated and control (dark) K562 cells were analyzed under a confocal laser scanning microscope (Zeiss LSM 510 META, Germany) at the excitation wavelengths of 488 or 543 nm to view the green (**T-1**) and red (PE-Annexin V) fluorescence, respectively in order to investigate the correlation of staining of the cells with **T-1** and Annexin V; operating in the sequential (multitrack) excitation/recording mode to eliminate a possible cross-talk between the channels with recording the fluorescence signal in the green (BP 505–530 nm) or red (LP 560) channel. Annexin V serves as a sensitive marker for detection of cells that are undergoing apoptosis. Images were captured at a magnification of 63×, 1.4 numerical aperture objective and a scan speed of 400 Hz.

4.6 Conclusion

It appears judiciously designed molecular logic devices can carry out critical information processing in or around the cells. Widely speculated “nanorobots” are not expected to be miniaturized versions of their macroscopic counterparts, but as illustrated here, most likely to be developed by careful control of photophysics and chemical reactivity at the individual molecule level, resulting in molecular entities with intelligent responses and actions. The zinc complex of the terpyridyl-bodipy, **T-1**, is approximately 3 nm at the longest dimension, yet it is capable of killing cancer cells when powered up by light, and then autonomously switching to a signaling mode in response to changing membrane characteristics, thus confirming apoptosis by a strong emission signal.

Equally important, is the fact that singlet oxygen generation is turned off once the cells show signs of apoptosis, which is very valuable in containing unintended damage by singlet oxygen. This clearly qualifies **T-1** as a molecular terminator automaton, or an example of a functional molecular robot. While most nano-sized robotics work is at present focussed on mobility, it is interesting to note that mobility is far from being the number one issue for a functional, molecule-sized robot. Most infectious microorganisms, cells fighting against these agents, and drug molecules are efficiently carried passively *via* the circulatory system to any part of the body. It is the intelligent autonomous operation that provides the most crucial challenge, and the terminator automaton **T-1** demonstrates one way of moving ahead to meet that challenge.

REFERENCES

1. Khan, A.U. and M. Kasha, *Red Chemiluminescence of Molecular Oxygen in Aqueous Solution.* The Journal of Chemical Physics, 1963. **39**(8): p. 2105-2106.
2. Lang, K., J. Mosinger, and D.M. Wagnerová, *Photophysical properties of porphyrinoid sensitizers non-covalently bound to host molecules; models for photodynamic therapy.* Coordination Chemistry Reviews, 2004. **248**(3-4): p. 321-350.
3. Pryor, W.A., *The Role of Free Radical Reactions in Biological Systems*, in *Free Radicals in Biology*, W.A. Pryor, Editor. 1976, Academic Press. p. 1-49.
4. Gorman, A.A., *The Bimolecular Reactivity of Singlet Molecular Oxygen*, in *Advances in Photochemistry*. 2007. p. 217-274.
5. Dougherty, T.J., *Photochemistry in the Treatment of Cancer*, in *Advances in Photochemistry*. 2007. p. 275-311.
6. Ali, H. and J.E. van Lier, *Metal Complexes as Photo- and Radiosensitizers.* Chemical Reviews, 1999. **99**(9): p. 2379-2450.
7. Boyle, R.W. and D. Dolphin, *Structure and biodistribution relationships of photodynamic sensitizers.* Photochem Photobiol, 1996. **64**(3): p. 469-85.
8. Warner W., B.R.S., *Hund's rule.* Nature, 1985. **313**.
9. DeRosa, M.C. and R.J. Crutchley, *Photosensitized singlet oxygen and its applications.* Coordination Chemistry Reviews, 2002. **233-234**: p. 351-371.
10. Korycka-Dahl, M.B. and T. Richardson, *Activated oxygen species and oxidation of food constituents.* CRC Crit Rev Food Sci Nutr, 1978. **10**(3): p. 209-41.
11. Wilkinson, F., W.P. Helman, and A.B. Ross, *Rate Constants for the Decay and Reactions of the Lowest Electronically Excited Singlet State of Molecular Oxygen in Solution. An Expanded and Revised Compilation.* Journal of Physical and Chemical Reference Data, 1995. **24**(2): p. 663-677.
12. Kochevar, I.E. and R.W. Redmond, *[2] Photosensitized production of singlet oxygen*, in *Methods in Enzymology*. 2000, Academic Press. p. 20-28.
13. Kearns, D.R., *Physical and chemical properties of singlet molecular oxygen.* Chemical Reviews, 1971. **71**(4): p. 395-427.
14. Li, B., et al., *Photosensitized singlet oxygen generation and detection: Recent advances and future perspectives in cancer photodynamic therapy.* J Biophotonics, 2016. **9**(11-12): p. 1314-1325.

15. Chuit, P., et al., *Recherches dans la série de l'acide undécylénique et de ses homologues (II).* Helvetica Chimica Acta, 1927. **10**(1): p. 113-131.
16. Nilsson, R. and D.R. Kearns, *Role of singlet oxygen in some chemiluminescence and enzyme oxidation reactions.* J Phys Chem, 1974. **78**(17): p. 1681-3.
17. Khan, A.U. and M. Kasha, *Singlet molecular oxygen evolution upon simple acidification of aqueous hypochlorite: application to studies on the deleterious health effects of chlorinated drinking water.* Proceedings of the National Academy of Sciences, 1994. **91**(26): p. 12362.
18. Arnhold, J., et al., *Chemiluminescence intensities and spectra of luminol oxidation by sodium hypochlorite in the presence of hydrogen peroxide.* Journal of Bioluminescence and Chemiluminescence, 1991. **6**(3): p. 189-192.
19. Foote, C.S., et al., *Chemistry of singlet oxygen. IV. Oxygenations with hypochlorite-hydrogen peroxide.* Journal of the American Chemical Society, 1968. **90**(4): p. 975-981.
20. Murray, R.W. and M. Kaplan, *Singlet oxygen sources in ozone chemistry.* Journal of the American Chemical Society, 1968. **90**(2): p. 537-538.
21. Wasserman, H.H. and J.R. Scheffer, *Singlet oxygen reactions from photoperoxides.* Journal of the American Chemical Society, 1967. **89**(12): p. 3073-3075.
22. Wasserman, H.H., J.R. Scheffer, and J.L. Cooper, *Singlet oxygen reactions with 9,10-diphenylanthracene peroxide.* Journal of the American Chemical Society, 1972. **94**(14): p. 4991-4996.
23. Bobrowski, M., et al., *CAS MCSCF/CAS MCQDPT2 Study of the Mechanism of Singlet Oxygen Addition to 1,3-Butadiene and Benzene.* Journal of the American Chemical Society, 2000. **122**(34): p. 8112-8119.
24. Martinez-Fernandez, L., et al., *Time-resolved insight into the photosensitized generation of singlet oxygen in endoperoxides.* J Chem Theory Comput, 2015. **11**(2): p. 406-14.
25. Wasserman, H.H., et al., *Photooxidation of methylnaphthalenes.* J Org Chem, 2005. **70**(1): p. 105-9.
26. Pierlot, C., et al., *Water-soluble naphthalene derivatives as singlet oxygen (1O2, 1Δg) carriers for biological media.* Journal of Photochemistry and Photobiology B: Biology, 1996. **36**(1): p. 31-39.

27. Turro, N.J. and M.F. Chow, *Mechanism of thermolysis of endoperoxides of aromatic compounds. Activation parameters, magnetic field, and magnetic isotope effects.* Journal of the American Chemical Society, 1981. **103**(24): p. 7218-7224.
28. Stolik, S., et al., *Measurement of the penetration depths of red and near infrared light in human "ex vivo" tissues.* Journal of Photochemistry and Photobiology B: Biology, 2000. **57**(2-3): p. 90-93.
29. Xiao, Z., et al., *Fractionated versus standard continuous light delivery in interstitial photodynamic therapy of dunning prostate carcinomas.* Clin Cancer Res, 2007. **13**(24): p. 7496-505.
30. Benz, S., et al., *Controlled oxygen release from pyridone endoperoxides promotes cell survival under anoxic conditions.* J Med Chem, 2013. **56**(24): p. 10171-82.
31. Turan, I.S., et al., *A Bifunctional Photosensitizer for Enhanced Fractional Photodynamic Therapy: Singlet Oxygen Generation in the Presence and Absence of Light.* Angew Chem Int Ed Engl, 2016. **55**(8): p. 2875-8.
32. Otsu, K., et al., *An abortive apoptotic pathway induced by singlet oxygen is due to the suppression of caspase activation.* Biochem J, 2005. **389**(Pt 1): p. 197-206.
33. Otsu, K., et al., *Impaired activation of caspase cascade during cell death induced by newly synthesized singlet oxygen generator, 1-buthylnaphthalene-4-propionate endoperoxide.* Cell Biol Int, 2008. **32**(11): p. 1380-7.
34. Kolemen, S., et al., *Remote-Controlled Release of Singlet Oxygen by the Plasmonic Heating of Endoperoxide-Modified Gold Nanorods: Towards a Paradigm Change in Photodynamic Therapy.* Angew Chem Int Ed Engl, 2016. **55**(11): p. 3606-10.
35. Castano, A.P., P. Mroz, and M.R. Hamblin, *Photodynamic therapy and anti-tumour immunity.* Nat Rev Cancer, 2006. **6**(7): p. 535-45.
36. Korbelik, M., *PDT-associated host response and its role in the therapy outcome.* Lasers Surg Med, 2006. **38**(5): p. 500-8.
37. Buytaert, E., M. Dewaele, and P. Agostinis, *Molecular effectors of multiple cell death pathways initiated by photodynamic therapy.* Biochim Biophys Acta, 2007. **1776**(1): p. 86-107.
38. Danial, N.N. and S.J. Korsmeyer, *Cell death: critical control points.* Cell, 2004. **116**(2): p. 205-19.

39. Suliman, A., et al., *Intracellular mechanisms of TRAIL: apoptosis through mitochondrial-dependent and -independent pathways.* Oncogene, 2001. **20**(17): p. 2122-33.
40. Ashkenazi, A. and V.M. Dixit, *Death receptors: signaling and modulation.* Science, 1998. **281**(5381): p. 1305-8.
41. Nakagawa, T., et al., *Caspase-12 mediates endoplasmic-reticulum-specific apoptosis and cytotoxicity by amyloid-beta.* Nature, 2000. **403**(6765): p. 98-103.
42. Li, L.Y., X. Luo, and X. Wang, *Endonuclease G is an apoptotic DNase when released from mitochondria.* Nature, 2001. **412**(6842): p. 95-9.
43. Susin, S.A., et al., *Two distinct pathways leading to nuclear apoptosis.* J Exp Med, 2000. **192**(4): p. 571-80.
44. Kessel, D. and N.L. Oleinick, *Chapter 1 Initiation of Autophagy by Photodynamic Therapy*, in *Autophagy in Disease and Clinical Applications, Part C*. 2009, Academic Press. p. 1-16.
45. Glick, D., S. Barth, and K.F. Macleod, *Autophagy: cellular and molecular mechanisms.* J Pathol, 2010. **221**(1): p. 3-12.
46. Dewaele, M., et al., *Autophagy pathways activated in response to PDT contribute to cell resistance against ROS damage.* J Cell Mol Med, 2011. **15**(6): p. 1402-14.
47. Dini, L., et al., *Rose bengal acetate photodynamic therapy-induced autophagy.* Cancer Biol Ther, 2010. **10**(10): p. 1048-55.
48. Panzarini, E., V. Inguscio, and L. Dini, *Timing the multiple cell death pathways initiated by Rose Bengal acetate photodynamic therapy.* Cell Death Dis, 2011. **2**: p. e169.
49. Riethmuller, M., N. Burger, and G. Bauer, *Singlet oxygen treatment of tumor cells triggers extracellular singlet oxygen generation, catalase inactivation and reactivation of intercellular apoptosis-inducing signaling.* Redox Biol, 2015. **6**: p. 157-168.
50. Bauer, G., *The Antitumor Effect of Singlet Oxygen.* Anticancer Res, 2016. **36**(11): p. 5649-5663.
51. Harrison, L.B., et al., *Impact of tumor hypoxia and anemia on radiation therapy outcomes.* Oncologist, 2002. **7**(6): p. 492-508.
52. Wouters, A., et al., *Review: implications of in vitro research on the effect of radiotherapy and chemotherapy under hypoxic conditions.* Oncologist, 2007. **12**(6): p. 690-712.

53. Melillo, G., *Targeting hypoxia cell signaling for cancer therapy.* Cancer Metastasis Rev, 2007. **26**(2): p. 341-52.
54. Heijmen, L., et al., *Monitoring hypoxia and vasculature during bevacizumab treatment in a murine colorectal cancer model.* Contrast Media Mol Imaging, 2014. **9**(3): p. 237-45.
55. Mehta, S., et al., *Assessing early therapeutic response to bevacizumab in primary breast cancer using magnetic resonance imaging and gene expression profiles.* J Natl Cancer Inst Monogr, 2011. **2011**(43): p. 71-4.
56. Wilson, W.R. and M.P. Hay, *Targeting hypoxia in cancer therapy.* Nat Rev Cancer, 2011. **11**(6): p. 393-410.
57. Meng, F., et al., *Molecular and cellular pharmacology of the hypoxia-activated prodrug TH-302.* Mol Cancer Ther, 2012. **11**(3): p. 740-51.
58. Dolmans, D.E., D. Fukumura, and R.K. Jain, *Photodynamic therapy for cancer.* Nat Rev Cancer, 2003. **3**(5): p. 380-7.
59. Wen, X., Y. Li, and M.R. Hamblin, *Photodynamic therapy in dermatology beyond non-melanoma cancer: An update.* Photodiagnosis Photodyn Ther, 2017. **19**: p. 140-152.
60. Pottier, R. *Past, Present and Future of Photosensitizers*. in *Photosensitisation*. 1988. Berlin, Heidelberg: Springer Berlin Heidelberg.
61. Li, X., et al., *Activatable Photosensitizers: Agents for Selective Photodynamic Therapy.* Advanced Functional Materials, 2017. **27**(5): p. 1604053.
62. Li, X., S. Lee, and J. Yoon, *Supramolecular photosensitizers rejuvenate photodynamic therapy.* Chem Soc Rev, 2018. **47**(4): p. 1174-1188.
63. Li, X., et al., *Innovative Strategies for Hypoxic-Tumor Photodynamic Therapy.* Angew Chem Int Ed Engl, 2018. **57**(36): p. 11522-11531.
64. Li, M., et al., *Near-Infrared Light-Initiated Molecular Superoxide Radical Generator: Rejuvenating Photodynamic Therapy against Hypoxic Tumors.* J Am Chem Soc, 2018. **140**(44): p. 14851-14859.
65. Turan, I.S., et al., *Molecular demultiplexer as a terminator automaton.* Nat Commun, 2018. **9**(1): p. 805.
66. Callaghan, S. and M.O. Senge, *The good, the bad, and the ugly - controlling singlet oxygen through design of photosensitizers and delivery systems for photodynamic therapy.* Photochem Photobiol Sci, 2018. **17**(11): p. 1490-1514.

67. Yuan, Z., et al., *Near-infrared light triggered photothermal and photodynamic therapy with an oxygen-shuttle endoperoxide of anthracene against tumor hypoxia.* Polymer Chemistry, 2018. **9**(16): p. 2124-2133.
68. Ozdemir, T., et al., *Generation of Singlet Oxygen by Persistent Luminescent Nanoparticle-Photosensitizer Conjugates: A Proof of Principle for Photodynamic Therapy without Light.* ChemPhotoChem, 2017. **1**(5): p. 183-187.
69. Matsumoto, M., M. Yamada, and N. Watanabe, *Reversible 1,4-cycloaddition of singlet oxygen to N-substituted 2-pyridones: 1,4-endoperoxide as a versatile chemical source of singlet oxygen.* Chem Commun (Camb), 2005(4): p. 483-5.
70. Phillips, R.M., *Targeting the hypoxic fraction of tumours using hypoxia-activated prodrugs.* Cancer Chemother Pharmacol, 2016. **77**(3): p. 441-57.
71. Luo, S., et al., *A Probe for the Detection of Hypoxic Cancer Cells.* ACS Sens, 2017. **2**(8): p. 1139-1145.
72. Cui, L., et al., *A new prodrug-derived ratiometric fluorescent probe for hypoxia: high selectivity of nitroreductase and imaging in tumor cell.* Org Lett, 2011. **13**(5): p. 928-31.
73. Yan, J., et al., *Self-immolative colorimetric, fluorescent and chemiluminescent chemosensors.* Chem Soc Rev, 2018. **47**(18): p. 6900-6916.
74. Wu, D. and P. Yotnda, *Induction and testing of hypoxia in cell culture.* J Vis Exp, 2011(54).
75. Ke, N., et al., *The xCELLigence System for Real-Time and Label-Free Monitoring of Cell Viability*, in *Mammalian Cell Viability: Methods and Protocols*, M.J. Stoddart, Editor. 2011, Humana Press: Switzerland. p. 33-43.
76. *Structural Effects on Fluorescence Emission*, in *Molecular Fluorescence*. 2012. p. 75-107.
77. Lakowicz, J.R., *Principles of fluorescence spectroscopy*. 1999: Second edition. New York : Kluwer Academic/Plenum, [1999] ©1999.
78. Song, L., et al., *Photobleaching kinetics of fluorescein in quantitative fluorescence microscopy.* Biophys J, 1995. **68**(6): p. 2588-600.
79. Deshpande, S.S., *Principles and applications of luminescence spectroscopy.* Crit Rev Food Sci Nutr, 2001. **41**(3): p. 155-224.

80. Isacsson, U. and G. Wettermark, *Chemiluminescence in analytical chemistry.* Analytica Chimica Acta, 1974. **68**(2): p. 339-362.
81. Li, X., et al., *Design strategies for water-soluble small molecular chromogenic and fluorogenic probes.* Chem Rev, 2014. **114**(1): p. 590-659.
82. Baeyer, A., *Ueber eine neue Klasse von Farbstoffen.* Berichte der deutschen chemischen Gesellschaft, 1871. **4**(2): p. 555-558.
83. Beija, M., C.A. Afonso, and J.M. Martinho, *Synthesis and applications of Rhodamine derivatives as fluorescent probes.* Chem Soc Rev, 2009. **38**(8): p. 2410-33.
84. Cosa, G., et al., *Photophysical properties of fluorescent DNA-dyes bound to single- and double-stranded DNA in aqueous buffered solution.* Photochem Photobiol, 2001. **73**(6): p. 585-99.
85. Soh, N. and T. Ueda, *Perylene bisimide as a versatile fluorescent tool for environmental and biological analysis: a review.* Talanta, 2011. **85**(3): p. 1233-7.
86. Boens, N., V. Leen, and W. Dehaen, *Fluorescent indicators based on BODIPY.* Chem Soc Rev, 2012. **41**(3): p. 1130-72.
87. Nakata, E., et al., *Synthesis and photophysical properties of new SNARF derivatives as dual emission pH sensors.* Bioorg Med Chem Lett, 2011. **21**(6): p. 1663-6.
88. Best, Q.A., et al., *Design and investigation of a series of rhodamine-based fluorescent probes for optical measurements of pH.* Org Lett, 2010. **12**(14): p. 3219-21.
89. Zhu, H., et al., *Imaging of lysosomal pH changes with a fluorescent sensor containing a novel lysosome-locating group.* Chem Commun (Camb), 2012. **48**(96): p. 11766-8.
90. Jokic, T., et al., *Highly photostable near-infrared fluorescent pH indicators and sensors based on BF2-chelated tetraarylazadipyrromethene dyes.* Anal Chem, 2012. **84**(15): p. 6723-30.
91. Gareis, T., et al., *Phenol/phenolate-dependent on/off switching of the luminescence of 4,4-difluoro-4-bora-3a,4a-diaza-s-indacenes.* Chemical Communications, 1997(18): p. 1717-1718.
92. Baruah, M., et al., *BODIPY-based hydroxyaryl derivatives as fluorescent pH probes.* J Org Chem, 2005. **70**(10): p. 4152-7.
93. Murtagh, J., D.O. Frimannsson, and D.F. O'Shea, *Azide conjugatable and pH responsive near-infrared fluorescent imaging probes.* Org Lett, 2009. **11**(23): p. 5386-9.

94. Yu, F., et al., *Development of reversible fluorescence probes based on redox oxoammonium cation for hypobromous acid detection in living cells.* Chem Commun (Camb), 2012. **48**(62): p. 7735-7.

95. Tang, B., et al., *A near-infrared neutral pH fluorescent probe for monitoring minor pH changes: imaging in living HepG2 and HL-7702 cells.* J Am Chem Soc, 2009. **131**(8): p. 3016-23.

96. Tang, B., et al., *A dual near-infrared pH fluorescent probe and its application in imaging of HepG2 cells.* Chem Commun (Camb), 2007(36): p. 3726-8.

97. Lee, K.S., et al., *Fluorescent chemodosimeter for selective detection of cyanide in water.* Org Lett, 2008. **10**(1): p. 49-51.

98. Gee, K.R., et al., *Detection and imaging of zinc secretion from pancreatic beta-cells using a new fluorescent zinc indicator.* J Am Chem Soc, 2002. **124**(5): p. 776-8.

99. Valeur, B., *Design principles of fluorescent molecular sensors for cation recognition.* Coordination Chemistry Reviews, 2000. **205**(1): p. 3-40.

100. Baki, C.N. and E.U. Akkaya, *Boradiazaindacene-appended calix[4]arene: fluorescence sensing of pH near neutrality.* J Org Chem, 2001. **66**(4): p. 1512-3.

101. Fabbrizzi, L. and A. Poggi, *Sensors and switches from supramolecular chemistry.* Chemical Society Reviews, 1995. **24**(3): p. 197-202.

102. De Silva, A., T.S. Moody, and G.D. Wright, *Fluorescent PET (Photoinduced Electron Transfer) Sensors as Potent Analytical Tools.* The Analyst, 2009. **134**(12): p. 2385-2393.

103. Turfan, B. and E.U. Akkaya, *Modulation of boradiazaindacene emission by cation-mediated oxidative PET.* Org Lett, 2002. **4**(17): p. 2857-9.

104. Brown, S.B., E.A. Brown, and I. Walker, *The present and future role of photodynamic therapy in cancer treatment.* Lancet Oncol, 2004. **5**(8): p. 497-508.

105. O'Connor, A.E., W.M. Gallagher, and A.T. Byrne, *Porphyrin and nonporphyrin photosensitizers in oncology: preclinical and clinical advances in photodynamic therapy.* Photochem Photobiol, 2009. **85**(5): p. 1053-74.

106. Daniell, M.D. and J.S. Hill, *A history of photodynamic therapy.* Aust N Z J Surg, 1991. **61**(5): p. 340-8.

107. Dougherty, T.J., et al., *Photodynamic therapy.* J Natl Cancer Inst, 1998. **90**(12): p. 889-905.

108. Sivaprasad, S. and P. Hykin, *The role of photodynamic therapy in ophthalmology.* Br J Hosp Med (Lond), 2006. **67**(12): p. 647-50.

109. Rockson, S.G., et al., *Photoangioplasty: An emerging clinical cardiovascular role for photodynamic therapy.* Circulation, 2000. **102**(5): p. 591-6.

110. Chen, S., et al., *Mechanism-based tumor-targeting drug delivery system. Validation of efficient vitamin receptor-mediated endocytosis and drug release.* Bioconjug Chem, 2010. **21**(5): p. 979-87.

111. Vander Heiden, M.G., *Targeting cancer metabolism: a therapeutic window opens.* Nat Rev Drug Discov, 2011. **10**(9): p. 671-84.

112. Wood, T.E. and A. Thompson, *Advances in the chemistry of dipyrrins and their complexes.* Chem Rev, 2007. **107**(5): p. 1831-61.

113. Boole, G., *The mathematical analysis of logic*. 1847: Philosophical Library.

114. Millman, J. and A. Grabel, *Microelectronics, 2nd ed*. 1987: McGraw-Hill, Inc.

115. de Silva, P.A., N.H.Q. Gunaratne, and C.P. McCoy, *A molecular photoionic AND gate based on fluorescent signalling.* Nature, 1993. **364**(6432): p. 42-44.

116. de Silva, A.P., et al., *Signaling Recognition Events with Fluorescent Sensors and Switches.* Chem Rev, 1997. **97**(5): p. 1515-1566.

117. Guliyev, R., et al., *From virtual to physical: integration of chemical logic gates.* Angew Chem Int Ed Engl, 2011. **50**(42): p. 9826-31.

118. de Silva, A.P., H.Q.N. Gunaratne, and G.E.M. Maguire, *'Off–on' fluorescent sensors for physiological levels of magnesium ions based on photoinduced electron transfer (PET), which also behave as photoionic OR logic gates.* J. Chem. Soc., Chem. Commun., 1994. **0**(10): p. 1213-1214.

119. Privman, M., et al., *Switchable electrode controlled by enzyme logic network system: approaching physiologically regulated bioelectronics.* J Am Chem Soc, 2009. **131**(3): p. 1314-21.

120. Erbas-Cakmak, S. and E.U. Akkaya, *Cascading of molecular logic gates for advanced functions: a self-reporting, activatable photosensitizer.* Angew Chem Int Ed Engl, 2013. **52**(43): p. 11364-8.

121. Erbas-Cakmak, S., et al., *Selective photosensitization through an AND logic response: optimization of the pH and glutathione response of activatable photosensitizers.* Chem Commun (Camb), 2015. **51**(61): p. 12258-61.

122. Amir, R.J., et al., *Prodrug activation gated by a molecular "OR" logic trigger.* Angew Chem Int Ed Engl, 2005. **44**(28): p. 4378-81.

123. Erbas-Cakmak, S., et al., *Proof of principle for a molecular 1 : 2 demultiplexer to function as an autonomously switching theranostic device.* Chem. Sci., 2013. **4**(2): p. 858-862.

124. Brown, M. and C. Wittwer, *Flow cytometry: principles and clinical applications in hematology.* Clin Chem, 2000. **46**(8 Pt 2): p. 1221-9.

125. Logue, S.E., M. Elgendy, and S.J. Martin, *Expression, purification and use of recombinant annexin V for the detection of apoptotic cells.* Nat Protoc, 2009. **4**(9): p. 1383-95.

126. Zhang, G., et al., *Early detection of apoptosis using a fluorescent conjugate of annexin V.* Biotechniques, 1997. **23**(3): p. 525-31.

127. Koopman, G., et al., *Annexin V for flow cytometric detection of phosphatidylserine expression on B cells undergoing apoptosis.* Blood, 1994. **84**(5): p. 1415-20.

128. de Silva, A.P. and S. Uchiyama, *Molecular logic and computing.* Nat Nanotechnol, 2007. **2**(7): p. 399-410.

129. Ozlem, S. and E.U. Akkaya, *Thinking outside the silicon box: molecular and logic as an additional layer of selectivity in singlet oxygen generation for photodynamic therapy.* J Am Chem Soc, 2009. **131**(1): p. 48-9.

130. Pischel, U., et al., *Information processing with molecules--Quo vadis?* Chemphyschem, 2013. **14**(1): p. 28-46.

131. Andreasson, J. and U. Pischel, *Molecules with a sense of logic: a progress report.* Chem Soc Rev, 2015. **44**(5): p. 1053-69.

132. de Silva, A.P., *Molecular logic gate arrays.* Chem Asian J, 2011. **6**(3): p. 750-66.

133. Margulies, D., G. Melman, and A. Shanzer, *A molecular full-adder and full-subtractor, an additional step toward a moleculator.* J Am Chem Soc, 2006. **128**(14): p. 4865-71.

134. de Ruiter, G., et al., *Sequential logic operations with surface-confined polypyridyl complexes displaying molecular random access memory features.* Angew Chem Int Ed Engl, 2010. **49**(1): p. 169-72.

135. Credi, A., et al., *Logic Operations at the Molecular Level. An XOR Gate Based on a Molecular Machine.* Journal of the American Chemical Society, 1997. **119**(11): p. 2679-2681.

136. Baytekin, H.T. and E.U. Akkaya, *A molecular NAND gate based on Watson-Crick base pairing.* Org Lett, 2000. **2**(12): p. 1725-7.
137. Ball, P., *Chemistry meets computing.* Nature, 2000. **406**(6792): p. 118-20.
138. *"Killer App"*, in *Merriam-Webster*. https://www.merriam-webster.com/dictionary/killer%20app.
139. Agostinis, P., et al., *Photodynamic therapy of cancer: an update.* CA Cancer J Clin, 2011. **61**(4): p. 250-81.
140. Kochevar, I.E., et al., *Singlet Oxygen, but not Oxidizing Radicals, Induces Apoptosis in HL-60 Cells¶.* Photochemistry and Photobiology, 2007. **72**(4): p. 548-553.
141. Agarwal, R., et al., *Apoptosis is an Early Event During Phthalocyanine Photodynamic Therapy-Induced Ablation of Chemically Induced Squamous Papillomas in Mouse Skin.* Photochemistry and Photobiology, 1996. **63**(4): p. 547-552.
142. Amelia, M., M. Baroncini, and A. Credi, *A simple unimolecular multiplexer/demultiplexer.* Angew Chem Int Ed Engl, 2008. **47**(33): p. 6240-3.
143. Schmitt, A., et al., *Synthesis of the core compound of the BODIPY dye class: 4,4'-difluoro-4-bora-(3a,4a)-diaza-s-indacene.* J Fluoresc, 2009. **19**(4): p. 755-8.
144. Harriman, A., et al., *Rapid intersystem crossing in closely-spaced but orthogonal molecular dyads.* Chemphyschem, 2007. **8**(8): p. 1207-14.
145. Okada, T., et al., *Ultrafast intersystem crossing in some intramolecular heteroexcimers.* The Journal of Physical Chemistry, 1981. **85**(26): p. 3957-3960.
146. Wu, W., et al., *Long-lived room-temperature near-IR phosphorescence of BODIPY in a visible-light-harvesting N^C^N Pt(II)-acetylide complex with a directly metalated BODIPY chromophore.* Chemistry, 2012. **18**(7): p. 1961-8.
147. Nagata, S., et al., *Exposure of phosphatidylserine on the cell surface.* Cell Death Differ, 2016. **23**(6): p. 952-61.
148. Daleke, D.L., *Phospholipid flippases.* J Biol Chem, 2007. **282**(2): p. 821-5.
149. van Meer, G., D.R. Voelker, and G.W. Feigenson, *Membrane lipids: where they are and how they behave.* Nat Rev Mol Cell Biol, 2008. **9**(2): p. 112-124.
150. Hanshaw, R.G., et al., *Fluorescent detection of apoptotic cells by using zinc coordination complexes with a selective affinity for membrane surfaces enriched with phosphatidylserine.* Chembiochem, 2005. **6**(12): p. 2214-20.

151. Lakshmi, C., R.G. Hanshaw, and B.D. Smith, *Fluorophore-linked zinc(II)dipicolylamine coordination complexes as sensors for phosphatidylserine-containing membranes.* Tetrahedron, 2004. **60**(49): p. 11307-11315.

152. Cakmak, Y., et al., *Designing excited states: theory-guided access to efficient photosensitizers for photodynamic action.* Angew Chem Int Ed Engl, 2011. **50**(50): p. 11937-41.

APPENDİX A

NMR Spectra

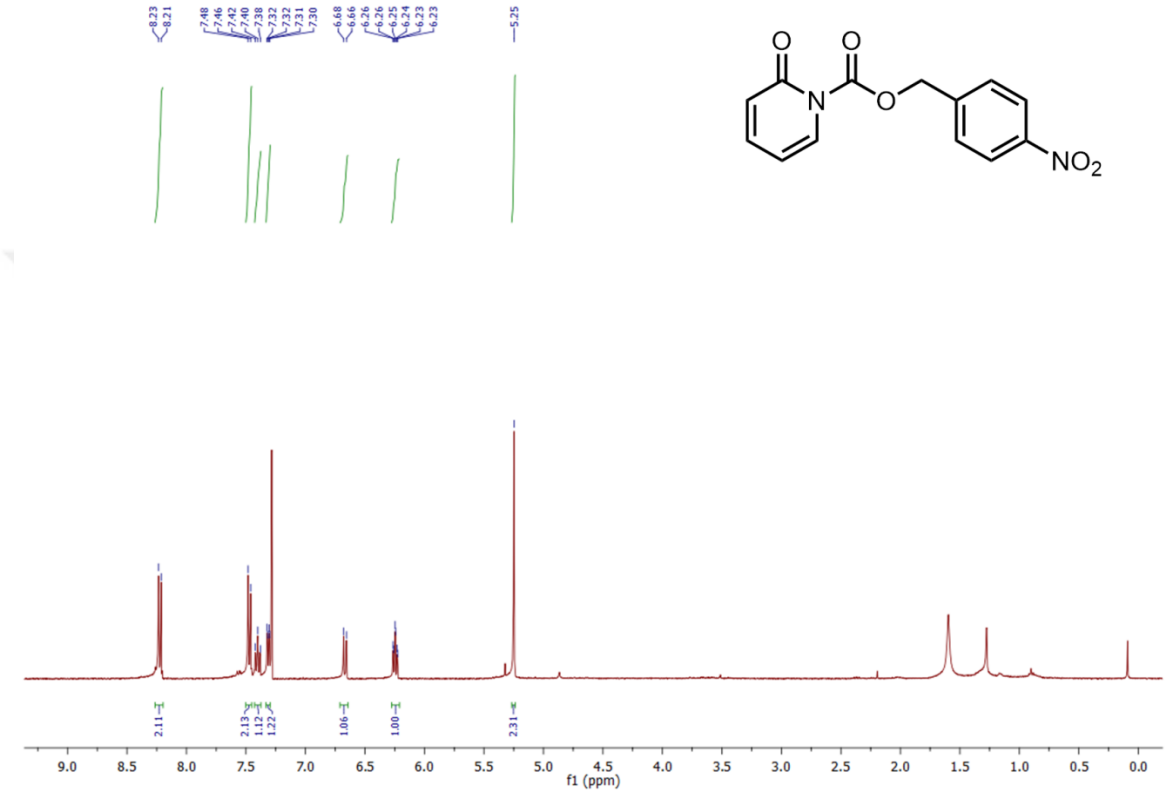

^{1}H-NMR Spectrum of Compound **3** in $CDCl_3$.

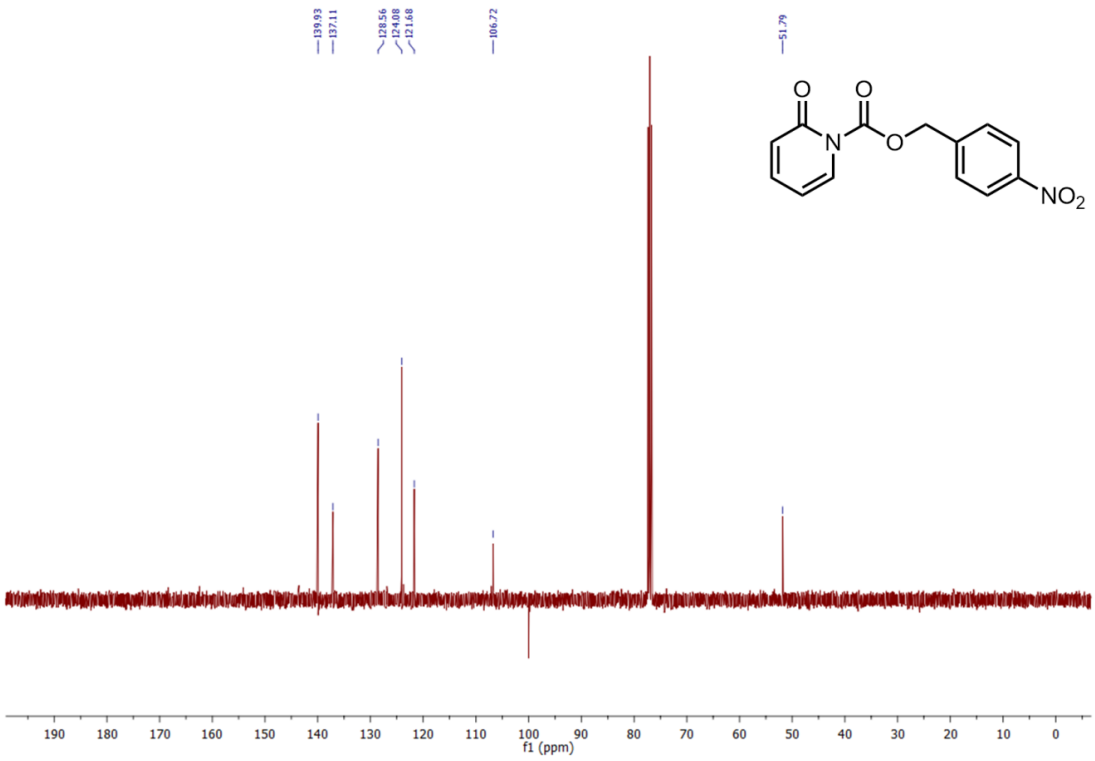

^{13}C-NMR Spectrum of Compound **3** in $CDCl_3$.

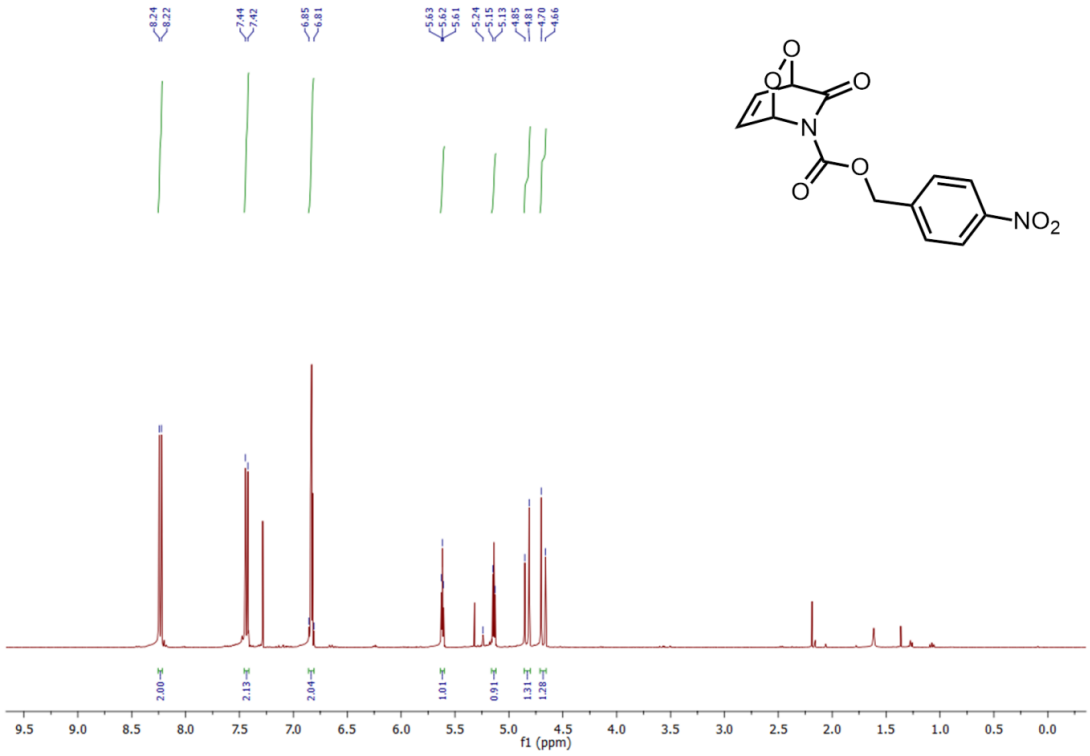

^{1}H-NMR Spectrum of Endoperoxide **1** in $CDCl_3$.

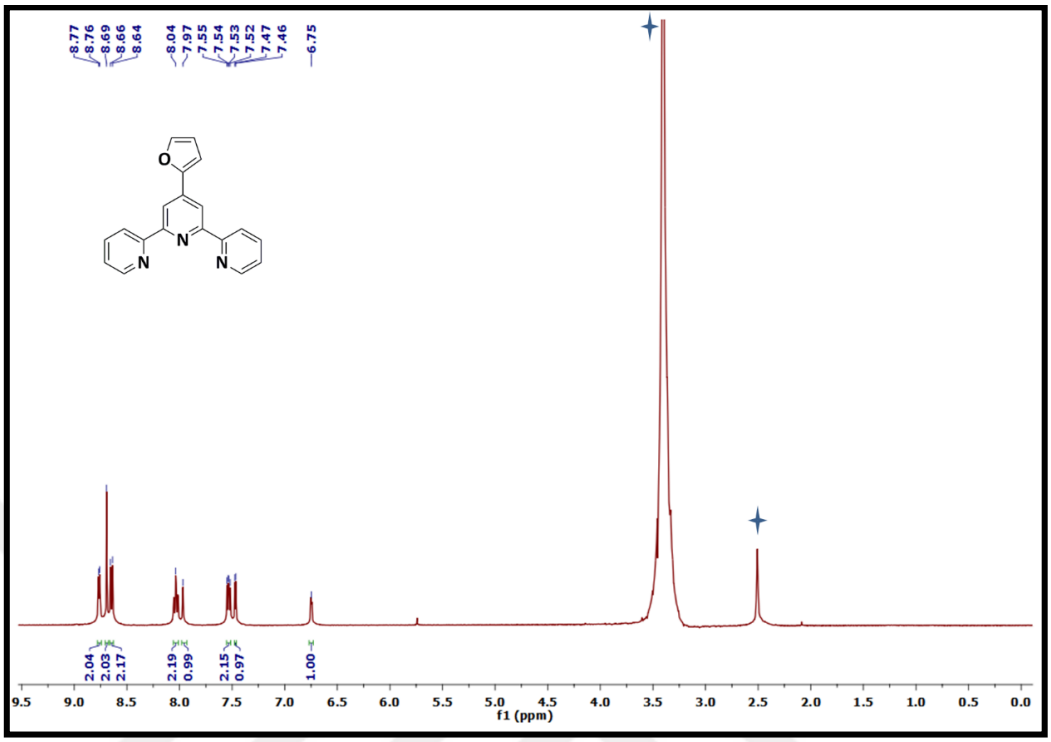

^{1}H-NMR Spectrum of Compound **1** in DMSO-d_6.

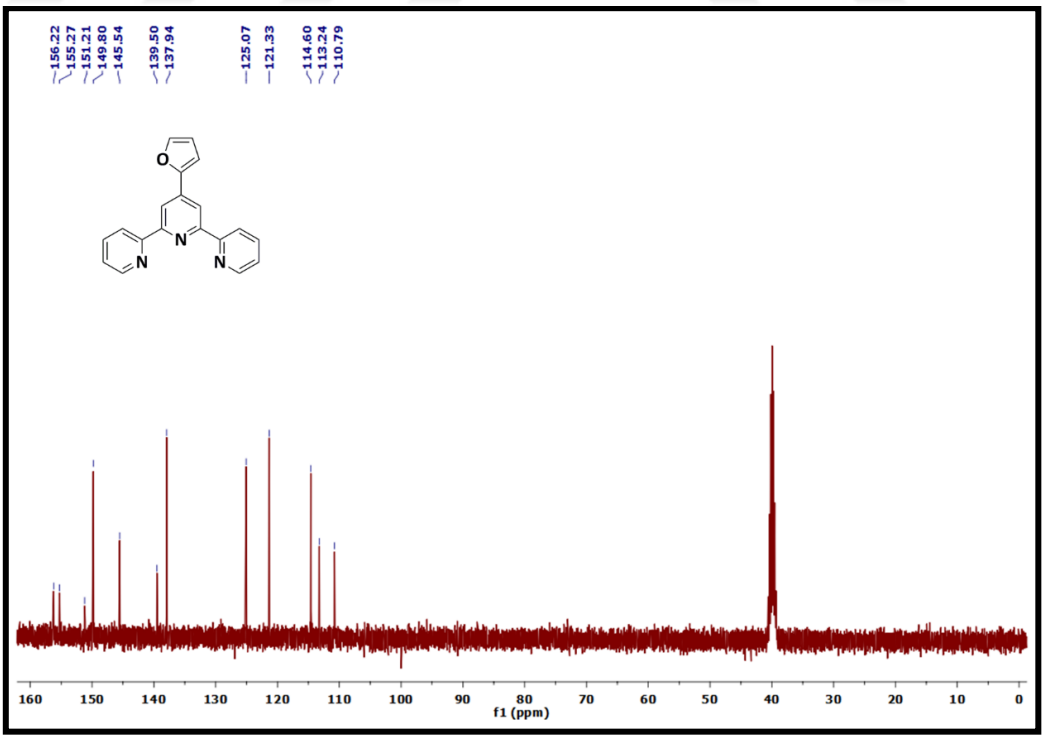

^{13}C-NMR Spectrum of Compound **1** in DMSO-d_6.

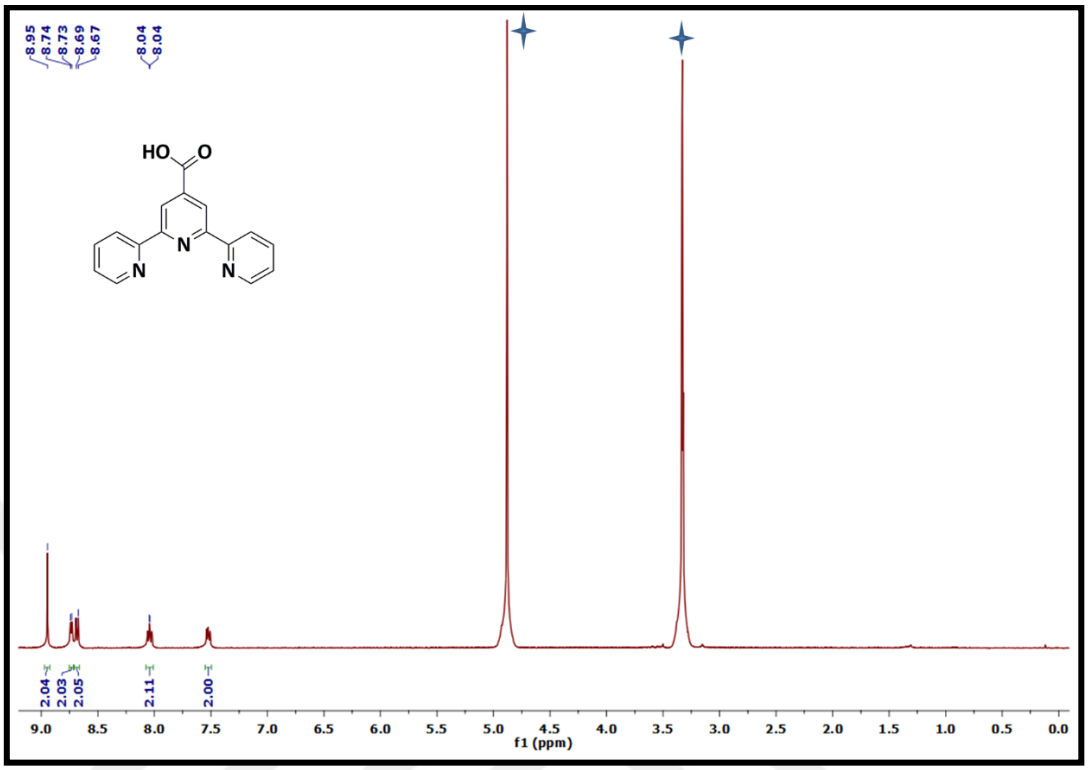

^{1}H-NMR Spectrum of Compound **2** in CD_3OD.

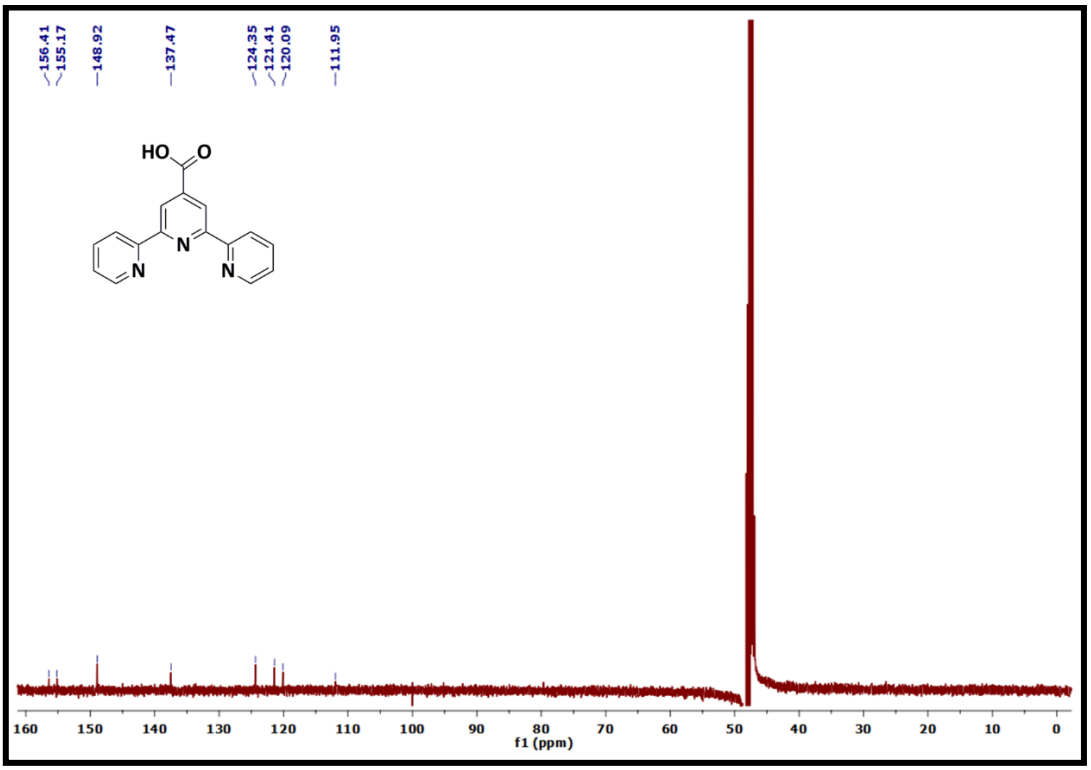

^{13}C-NMR Spectrum of Compound **2** in CD_3OD.

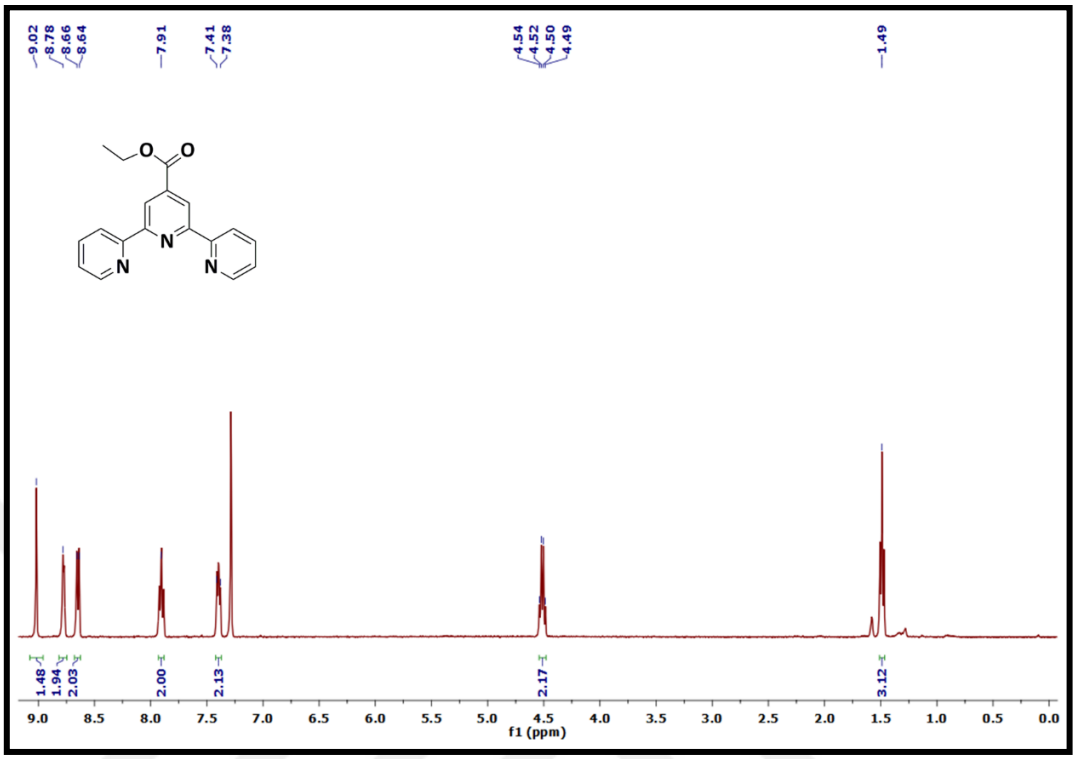

^{1}H-NMR Spectrum of Compound **3** in $CDCl_3$.

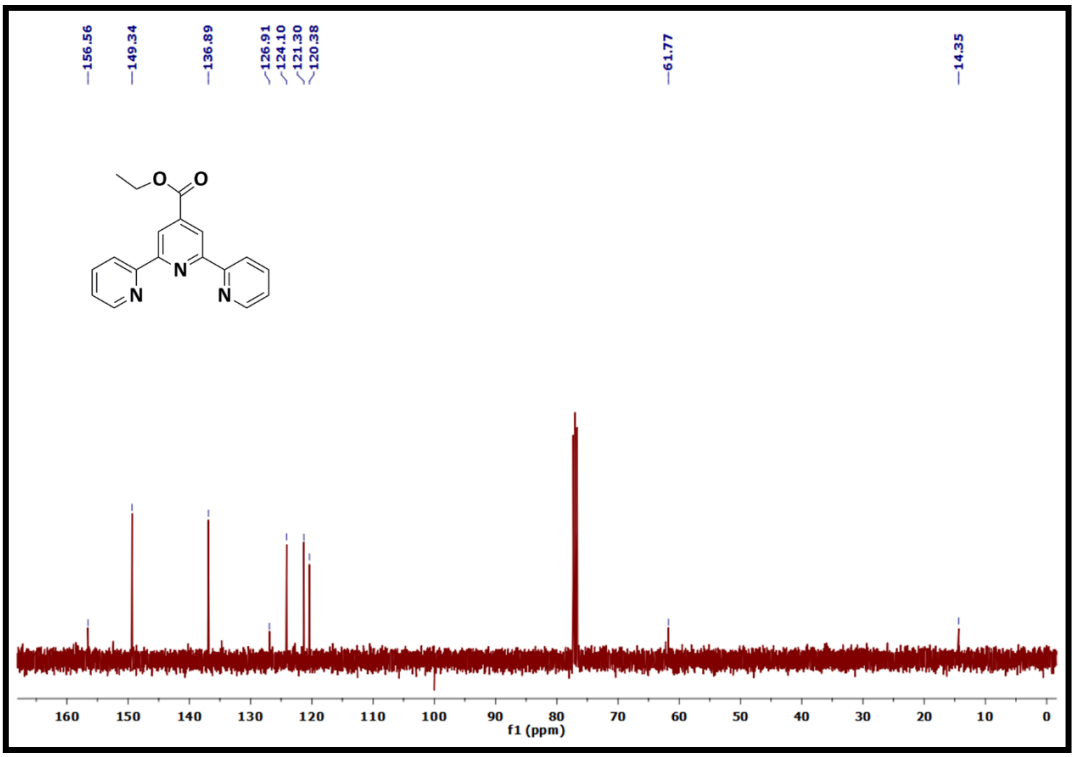

^{13}C-NMR Spectrum of Compound **3** in $CDCl_3$.

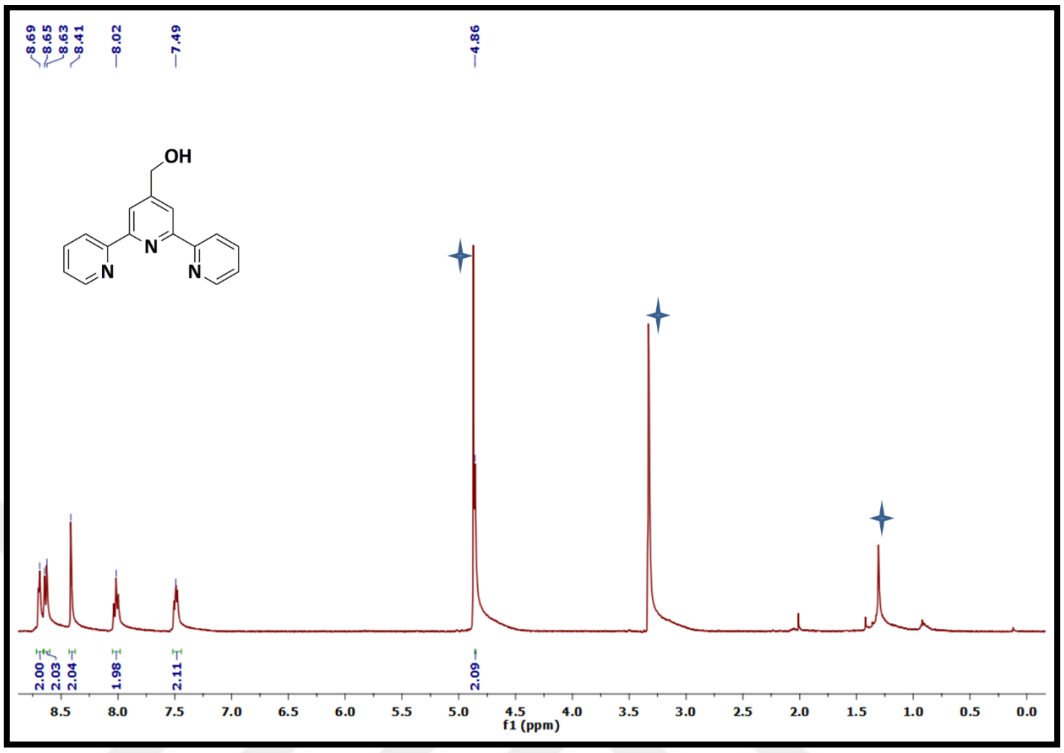

^{1}H-NMR Spectrum of Compound **4** in $CDCl_3$.

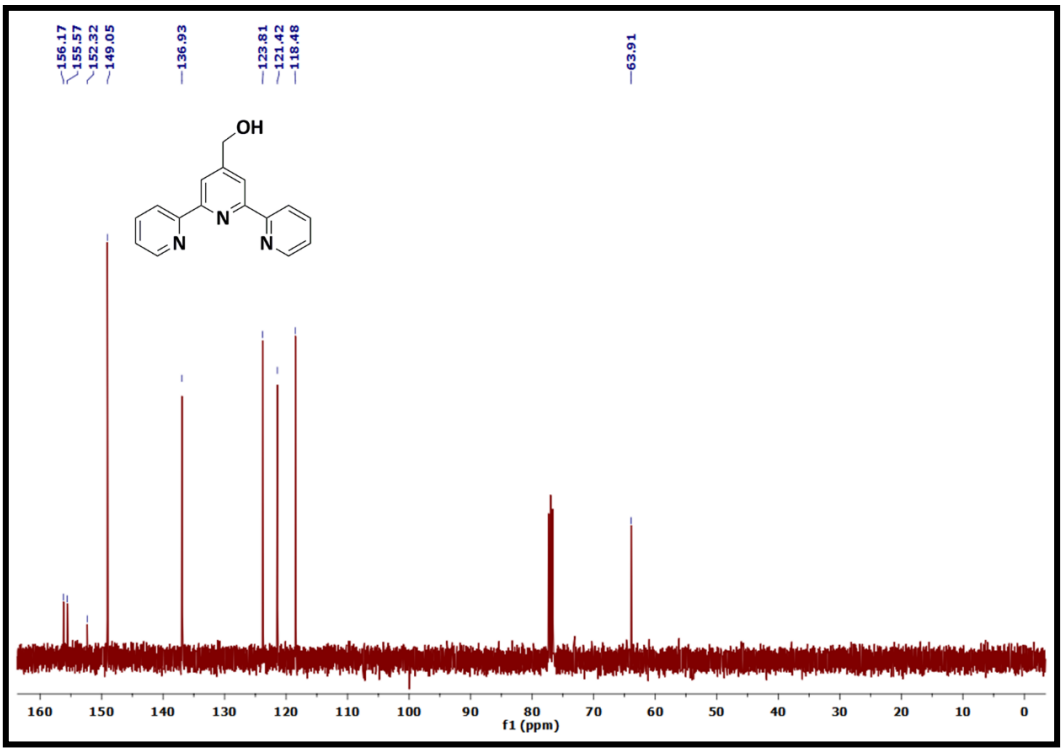

^{13}C-NMR Spectrum of Compound **4** in $CDCl_3$.

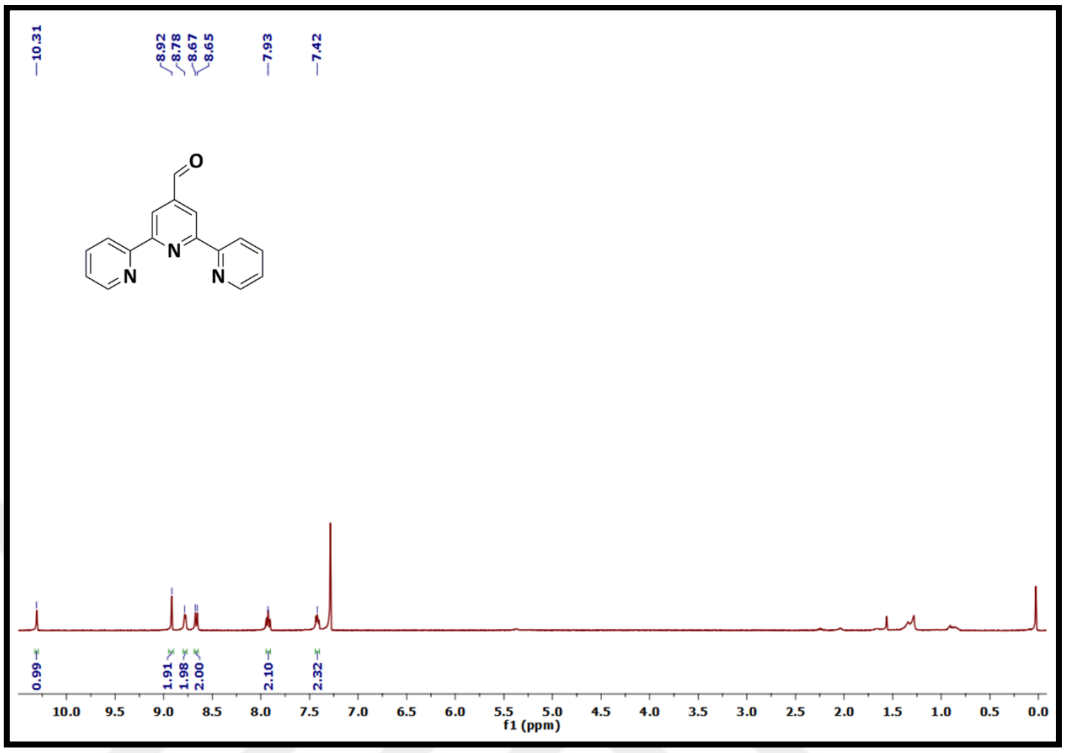

^{1}H-NMR Spectrum of Compound **5** in $CDCl_3$.

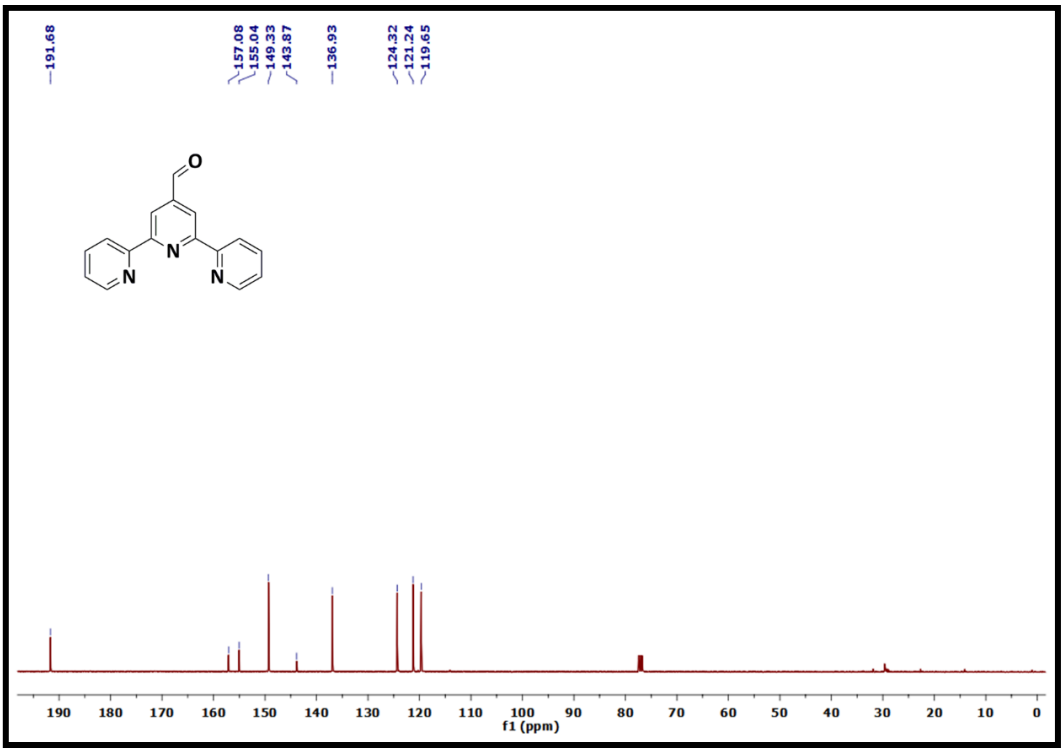

^{13}C-NMR Spectrum of Compound **5** in $CDCl_3$.

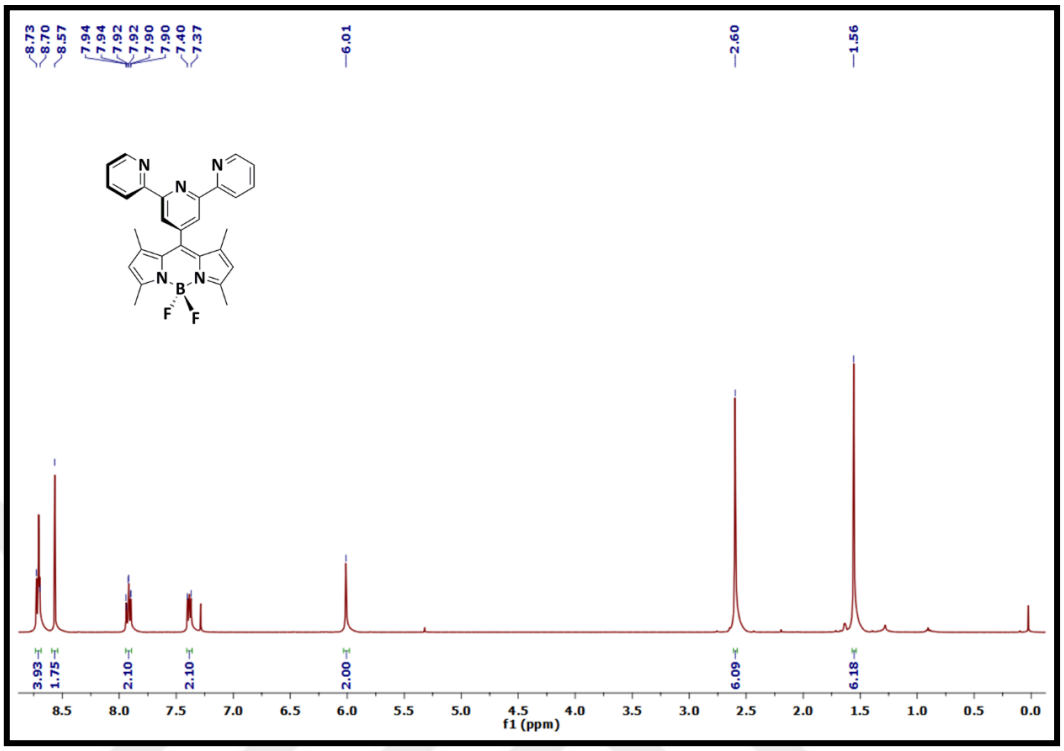

^{1}H-NMR Spectrum of Compound **6** in $CDCl_3$.

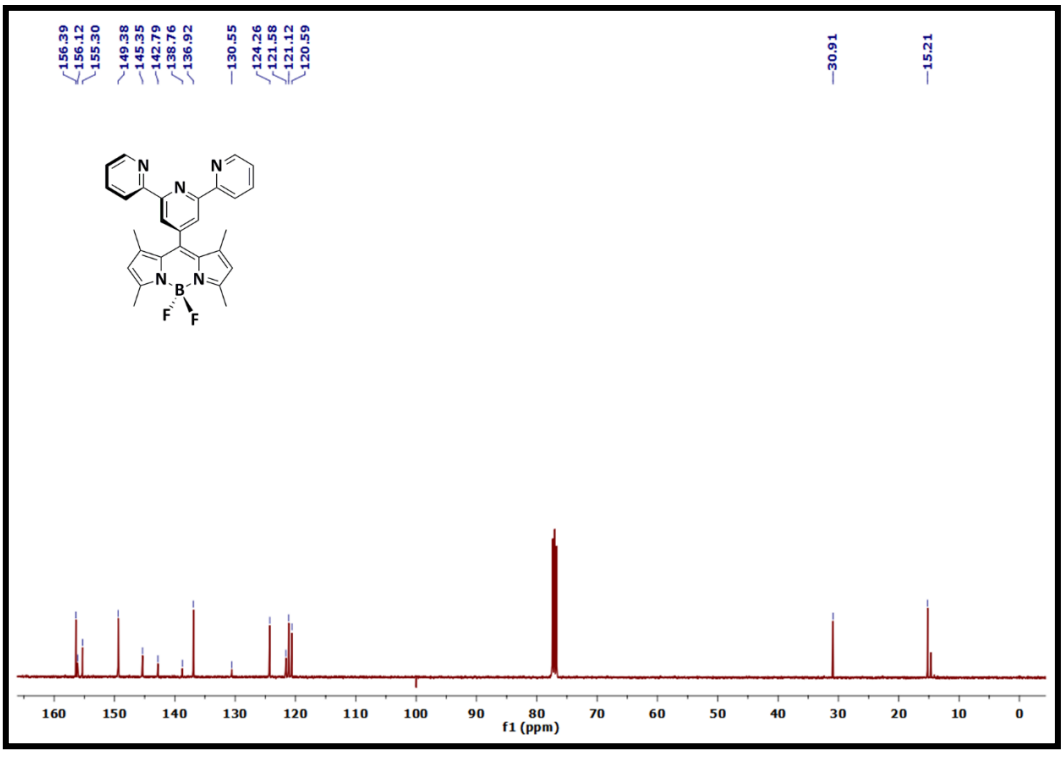

^{13}C-NMR Spectrum of Compound **6** in $CDCl_3$.

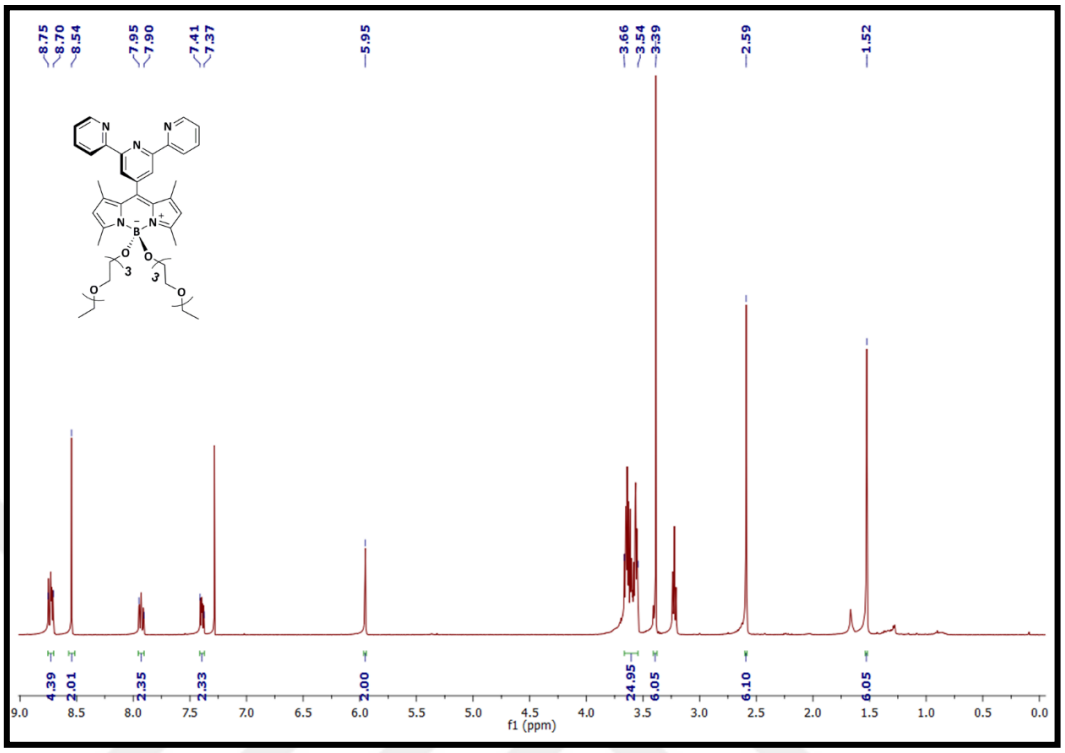

^{1}H-NMR Spectrum of Compound **7** in $CDCl_3$.

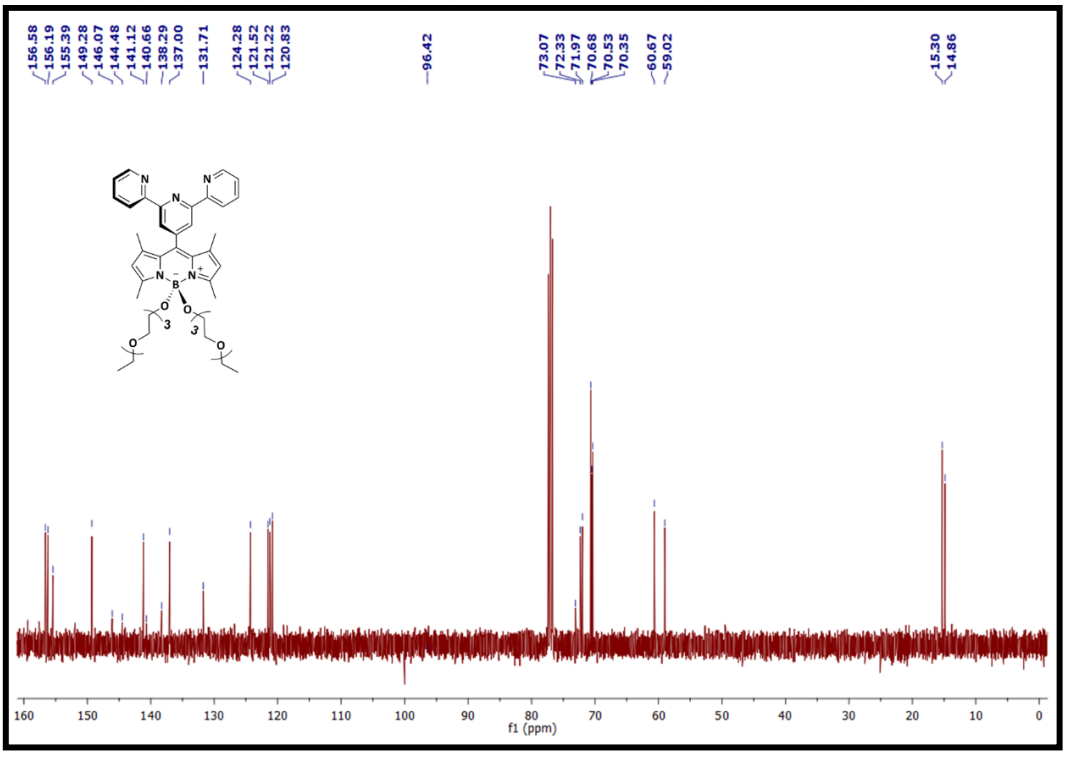

^{13}C-NMR Spectrum of Compound **7** in $CDCl_3$.

APPENDİX B

Mass spectra

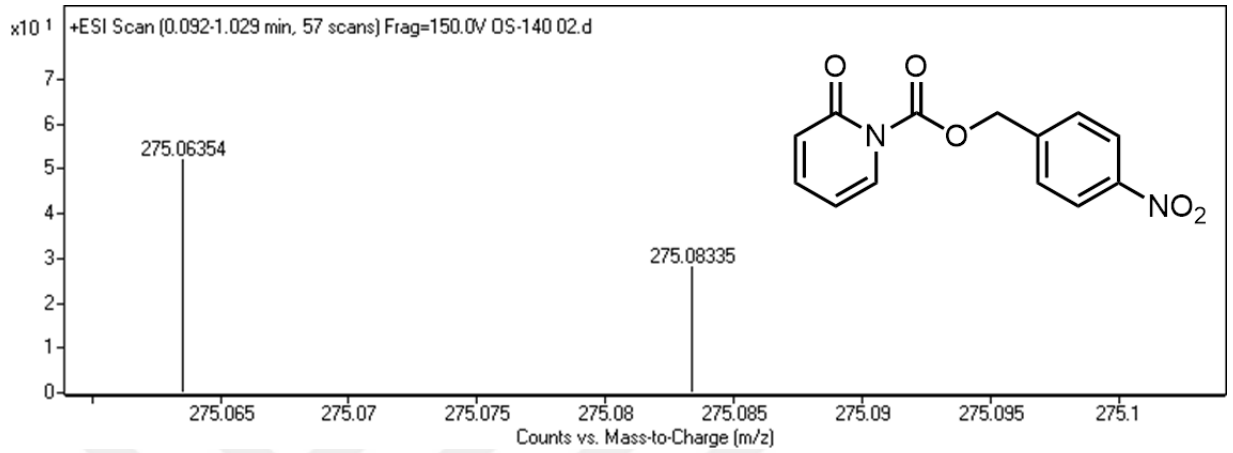

HRMS Spectrum of Compound **3**.

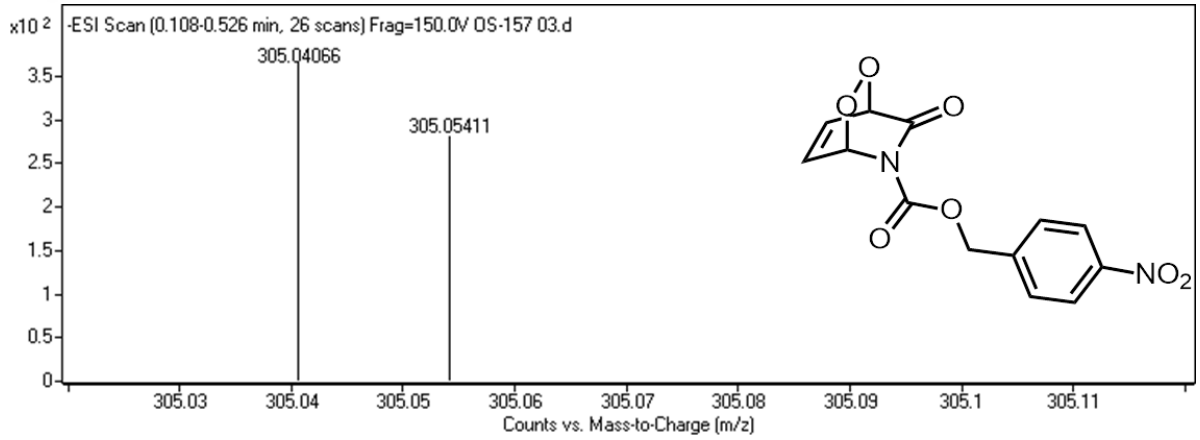

HRMS Spectrum of Endoperoxide **1**.

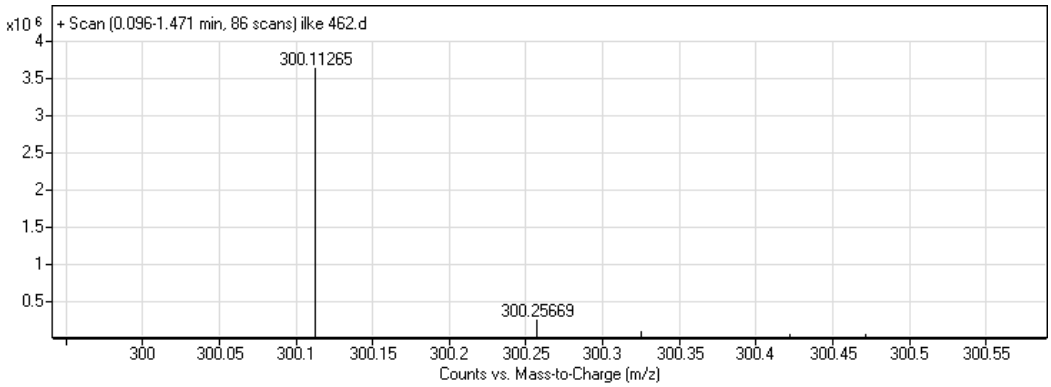

HRMs Spectrum of Compound **1**.

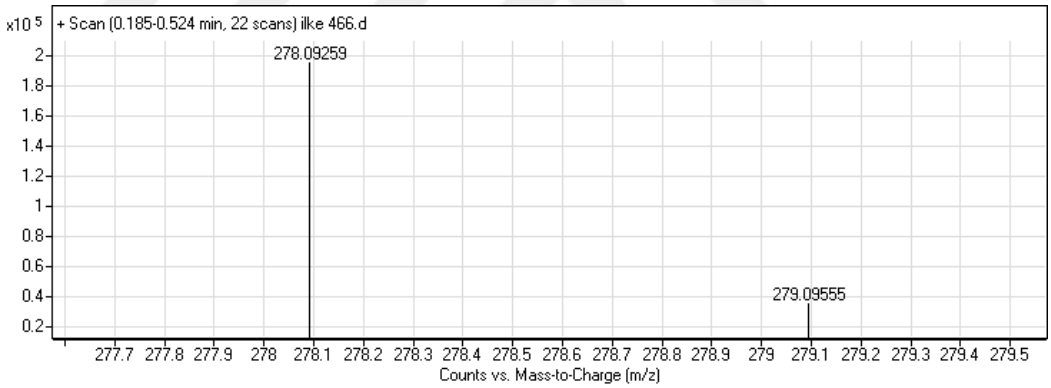

HRMs Spectrum of Compound **2**.

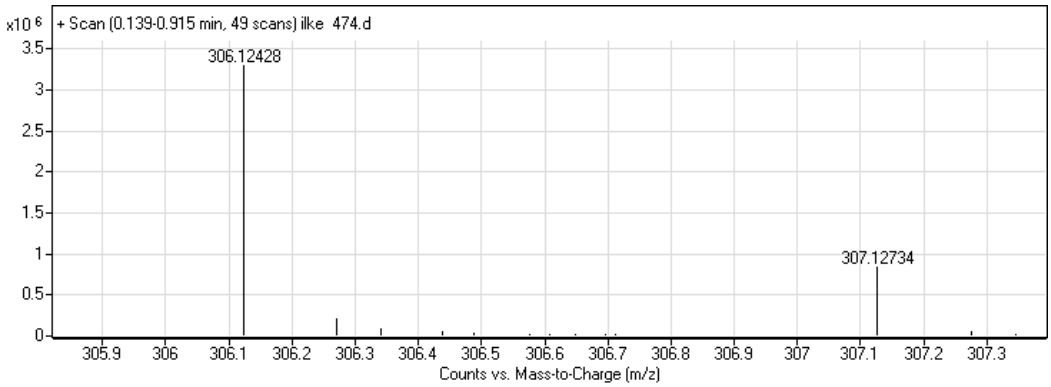

HRMs Spectrum of Compound **3**.

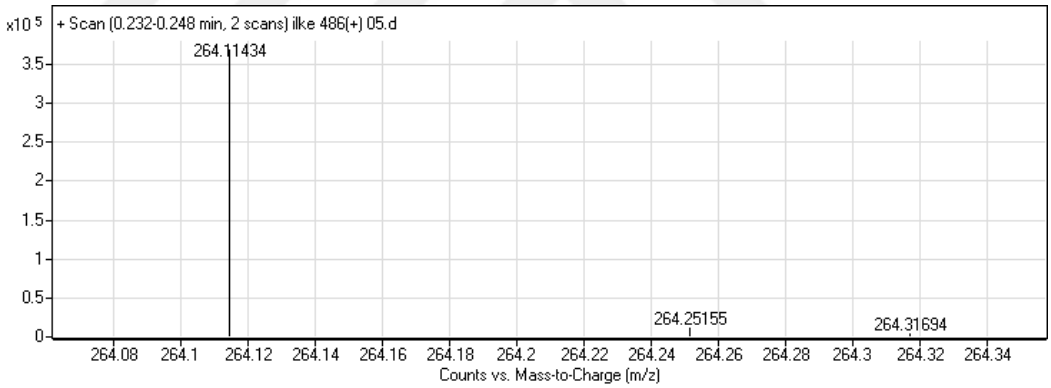

HRMs Spectrum of Compound **4**.

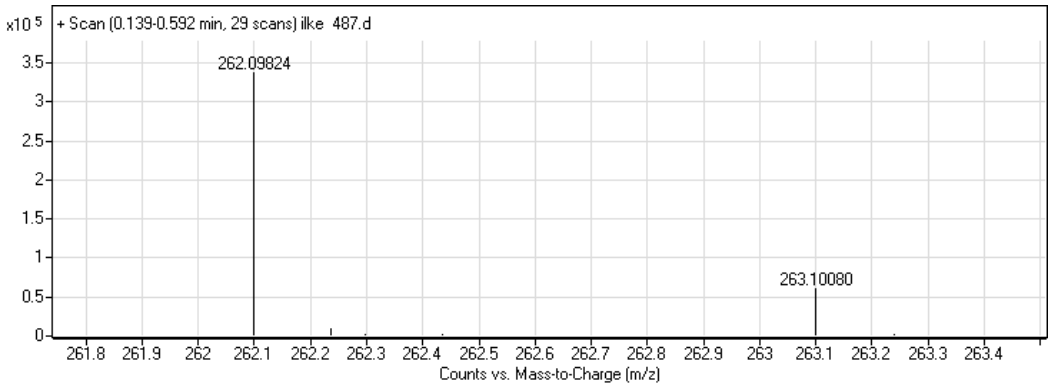

HRMs Spectrum of Compound **5**.

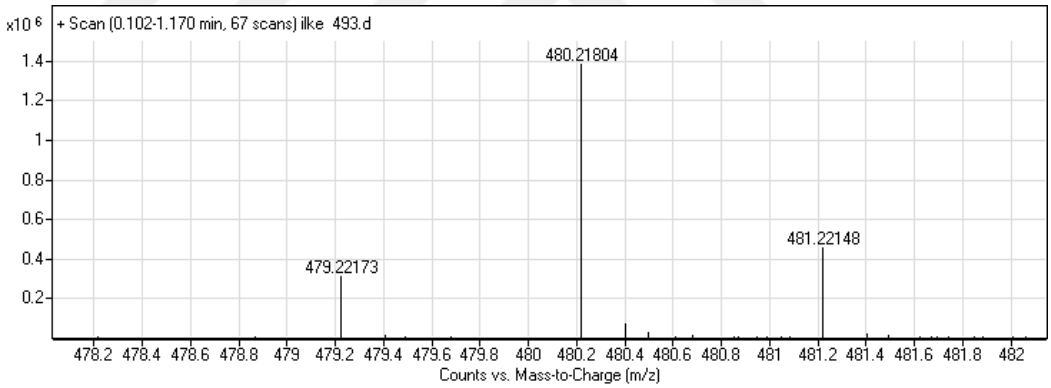

HRMs Spectrum of compound **6**.

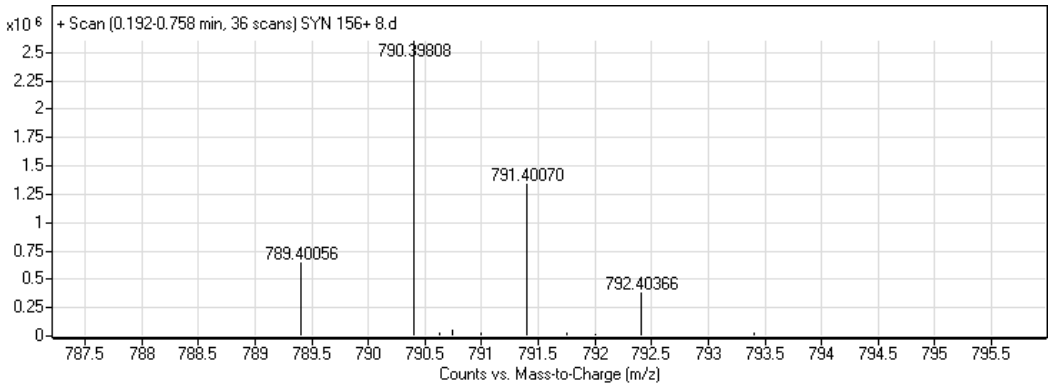

HRMs Spectrum of compound **7**.